Source Localization with MIMO Systems

Parth Raj Singh

UNIVERSITE BRETAGNE LOIRE

UNIVERSITÉ DE NANTES

Thèse de Doctorat

Parth Raj SINGH

Mémoire présenté en vue de l'obtention du
grade de Docteur de l'Université de Nantes
sous le sceau de l'Université Bretagne Loire

École doctorale : Sciences et technologies de l'information, et mathématiques (STIM-503)

Discipline : Électronique
Spécialité : Communications numériques
Unité de recherche : IETR UMR CNRS 6164

Soutenue le 12 October 2017

Source Localization with MIMO Systems

JURY

Président :	**M. Jean-Pierre CANCES**, Professeur, Université de Limoges
Rapporteurs :	**M. Rémy BOYER**, Maître de conférences/HDR, CentraleSupélec
	M. Salah BOURENNANE, Professeur, École Centrale Marseille
Directeur de thèse :	**M. Yide WANG**, Professeur, Université de Nantes
Co-directeur de thèse :	**M. Pascal CHARGÉ**, Professeur, Université de Nantes

Remerciements

During this three-year research work at Institute of Electronics and Telecommunication of Rennes (IETR), Polytech Nantes, I have been academically and psychologically supported by many people to whom I am very grateful.

First of all, I would like to convey my sincere gratitude to the director of my thesis, Professor Yide Wang, for offering me the opportunity to pursue PhD (Master as well) under his supervision. I am also very grateful to the co-director of my thesis, Professor Pascal Chargé for his useful remarks and encouragement during this period. I am very thankful for their precious time, motivation, expert guidance, understanding, and patience for the last four years. Without their well-designed research plan and clear goals, I couldn't have completed my PhD.

I would like to express my appreciation to the committee members, Professor Jean-Pierre Cances, Professor Salah Bourennane, and Professor Rémy Boyer, for accepting the request to validate my thesis and participate in my oral defense. I am also thankful for their insightful comments and positive suggestions.

I would like to thank Mrs. Sandrine Charlier for establishing a solid foundation for our academic life and handling all the administrative affairs, which has greatly facilitated my research. I would also like to thank Mr. Marc Brunet and Mr. Guillaume Lirzin for their technical support and activeness in organizing social events. Along with them, IETR is blessed with many professors like Professor Jean-François Diouris, Professor Tchanguiz Razban, Professor Christophe Bourlier, Professor Safwan El Assad and so on who are always ready to provide academic assistance.

My colleagues have also played a significant role during my PhD by sharing their knowledge and experience. They are Dušan Cvetković, Mohammed Abutaha, Nabil Zaraneh, Christophe Bouguet, Ons Jallouli, Ali Mohydeen, Jingjing Pan, Meng Sun, Randa Jaouadi, Taoufik Bouguera, Simei Yang, Jinze Du, Irfan Ali Tunio, Yunniel Arencibia Noa, Julien Weckbrodt and few more. Specially, I would like to express additional gratitude to Jingjing Pan and Ali Mohydeen for their useful academic discussions.

Moreover, I feel honored to have Amit Karel, Bhanu Pratap Singh Jadav, and Shubham Maheshwari as my best friends for their unconditional friendship and moral support during my PhD. A special thank also goes to Marion Giraud, Mr. Jean Marie Barth, Erwan Quemere, Armand Bax, and Armand Fuchs for introducing me to the

French culture and cuisine. They have greatly enriched my life in France.

Finally, from the bottom of my heart I would like to thank my mother Heeramani, my father Nanku Ram, and my little sister Divya Shail for their endless love, support and encouragement throughout my endeavors.

Résumé

La localisation des cibles est présente dans notre vie quotidienne. La plupart des animaux et les humains sont équipés de certains types de systèmes de localisation. Le fait d'avoir deux oreilles est la première preuve. Avoir deux oreilles aide les animaux à localiser la direction de la source sonore. En outre, les chauves-souris utilisent des ondes ultrasonores pour naviguer dans l'obscurité. Inspiré de la nature, le traitement des signaux électromagnétiques et acoustiques a été étudié pendant de nombreuses décennies pour localiser les sources radio et acoustiques, respectivement. La localisation de sources est utilisée dans le radar, le sonar et même les télécommunications. Cependant, grâce à la capacité à se propager dans l'espace, à grande vitesse et à une petite longueur d'onde des ondes radio, les radars ont de nombreux avantages par rapport au sonar, tels qu'une résolution élevée, une réponse rapide, et une capacité de localiser les sources aussi bien à l'intérieur d'une structure que dans l'espace.

Le radar a attiré l'attention pendant la Seconde Guerre mondiale lorsqu'il a surpassé les capacités visuelles des humains pour détecter les avions et les navires. Le radar a de nombreuses applications civiles et militaires qui nous permettent de l'utiliser directement ou indirectement. Il joue un rôle dominant dans la navigation des transports comme les avions, les bateaux, les navires et les voitures intelligentes. Les radars sont également utilisés dans les prévisions météorologiques, le suivi de météorites, la surveillance pour des raisons de sécurité, les contrôles de la circulation, les recherches scientifiques et bien d'autres domaines. Un radar est distingué en fonction de ses applications, du type de forme d'onde utilisé et de ses principales caractéristiques. En conséquence, il existe de nombreuses façons de classer un système radar. Une de ces classifications consiste à distinguer les radars passifs et actifs. Un système radar passif est composé uniquement d'antennes réceptrices. Il s'appuie sur les signaux émis par les sources ou par une antenne de transmission non-coopérative qui illumine les sources. D'autre part, le système radar actif contient des éléments transmetteurs et récepteurs. En raison des antennes de transmission dédiées, nous connaissons les formes d'onde émises qui nous permettent d'extraire plus d'informations sur les cibles des échos reçus. Initialement, des antennes directives ont été montées sur une configuration mécanique rotative pour scruter la région d'intérêt. Plus tard, cette configuration est remplacée par un réseau de déphaseurs qui peut diriger le faisceau à grande vitesse

dans la région d'intérêt. Nous pouvons trouver une énorme quantité de travail sur les techniques de la localisation de sources en utilisant des radars passifs et actifs avec des antennes multiples. La formation de voies, MVDR, MUSIC, ESPRIT, etc. sont des méthodes d'estimation de DOA les plus célèbres.

Depuis le début, le radar a connu de nombreuses évolutions. Récemment, la technique de communication basée sur MIMO a inspiré le développement du radar MIMO. L'amélioration des composantes hyperfréquences et des architectures de processeurs rapides a également joué un rôle très important dans le développement d'un radar MIMO. Un radar MIMO se compose de plusieurs antennes d'émission et de réception comme un radar à balayage de faisceaux classique. Cependant, les antennes d'émission dans un radar MIMO transmettent des signaux linéairement indépendants qui peuvent être facilement identifiés par les filtres adaptés au niveau du récepteur. Lors de l'interaction des signaux orthogonaux transmis avec les cibles, chaque signal transmis possède individuellement des informations sur les cibles. Après les filtrages adaptés des signaux reçus, les informations sur les cibles sont traitées afin d'extraire les distances, les DOAs, les DODs, les vitesses, les tailles, etc. de ces cibles. Le radar MIMO fournit une haute résolution angulaire, une grande diversité spatiale et une excellente identifiabilité des paramètres. Dans un sens large, un système de radar MIMO peut être classé comme statistique ou cohérent. Un radar MIMO statistique a des antennes largement séparées alors qu'un radar MIMO cohérent a plutôt des antennes co-localisées. Cette thèse est consacrée aux systèmes radar MIMO avec des antennes co-localisées, précisément, un système MIMO bistatique dont les réseaux d'émission et de réception avec antennes co-localisées sont séparés d'une grande distance.

En fonction de la distance d'une cible par rapport au centre du réseau d'antennes, la cible peut être considérée comme située en champ proche ou en champ lointain de ce réseau. En champ lointain, le front d'onde sphérique d'une onde est approximé comme planaire. La plupart des méthodes de localisation de sources existantes sont consacrées à la situation du champ lointain. Cependant, la localisation de cibles en champ proche est également importante en raison de ses nombreuses applications, notamment à l'intérieur des bâtiments. Dans la zone du champ proche d'un réseau, le front d'onde sphérique d'un signal source ne peut plus être considéré comme planaire. Afin de réduire la non-linéarité du modèle exact du signal basé sur le front d'onde sphérique et de simplifier les algorithmes de localisation, le front d'onde sphérique est souvent approximé en quadrique (surface quadratique) en utilisant les termes de deux premiers ordres de l'expansion de Taylor (appelé aussi approximation de Fresnel).

Dans cette thèse, nous avons proposé une nouvelle méthode pour localiser des cibles en champ proche d'un système MIMO bistatique en utilisant l'approximation de Fresnel. Dans le cas du MIMO bistatique en champ proche, nous devons estimer quatre paramètres pour chaque cible, à savoir, la direction du départ par rapport au

réseau d'antennes d'émission (DOD) ; la direction d'arrivée par rapport au réseau d'antennes de réception (DOA) ; la distance entre la cible et le point de référence du réseau d'émission et la distance entre la cible et le point de référence du réseau de réception. Dans cette méthode, qui est basée sur le modèle approximé des signaux reçus, nous estimons d'abord les DODs et les DOAs en utilisant la méthode 1D RARE. Ensuite, la distance entre la cible et le réseau d'antenne d'émission est estimée en utilisant les DODs estimés auparavant. Enfin, à partir de la distance cible-réseau d'émission et DOD, nous estimons la distance cible-réseau de réception et en même temps que nous réalisons l'appariement des DOAs estimés en utilisant la technique 2D MUSIC. Cette méthode proposée est comparée à une méthode existante basée sur les sous-matrices de la matrice de covariance. À partir de la comparaison des résultats de simulation, on peut observer que la méthode proposée surpasse largement la méthode existante en termes de RMSE et du nombre maximal de cibles localisables. Il convient de signaler que, la méthode proposée et la méthode existante utilisent toutes les deux, des antennes linéaires uniformes symétriques ayant une distance inter-élément égale au quart de longueur d'onde.

Comme mentionné précédemment, dans l'approximation de Fresnel, le vrai front d'onde sphérique est approximé comme front d'onde quadrique. Cette approximation introduit une erreur dans le modèle du signal reçu résultant une erreur systématique sur les paramètres de localisation estimés (biais d'estimation). Ces biais dégradent la précision des techniques d'estimation. Il existe deux approches permettant de réduire, voire éliminer ces bais d'estimation dus à l'approximation de Fresnel. La première méthode consiste à réduire l'effet de l'approximation de Fresnel sur les paramètres de localisation estimés en utilisant une méthode de correction. La deuxième approche est d'éviter l'utilisation de l'approximation de Fresnel et de travailler directement avec le modèle exact des signaux reçus qui est basé sur le front d'onde sphérique.

La première approche vise à réduire l'effet de l'approximation de Fresnel. Nous avons proposé deux nouvelles méthodes pour corriger les paramètres de localisation estimés par des méthodes basées sur le modèle approximé.

- La première méthode de correction utilise deux LUTs correspondant aux réseaux d'émission et de réception respectivement. Les deux LUTs représentent la correspondance entre les vrais paramètres de localisation et les paramètres biaisés calculés à l'aide du modèle approximé de signal reçu. La région du champ proche étant délimitée par les limites inférieure et supérieure de la région de Fresnel, pour créer un LUT correspondant à l'émission et à la réception, la région du champ proche est d'abord discrétisée. Ensuite, pour chaque position discrétisée (donc les vrais paramètres de localisation), les paramètres de localisation biaisés correspondants sont calculés en utilisant une méthode des moindres carrés pour résoudre un système surdéterminé d'équations linéaires. Il peut y avoir plusieurs

méthodes permettant d'obtenir les paramètres de localisation biaisés. Chaque méthode utilise une approche différente qui mène une erreur différente pour les mêmes vrais paramètres de localisation. Ainsi, nous choisissons la méthode la moins dépendante de l'angle directionnel. Parce que l'erreur d'approximation de Fresnel devrait idéalement diminuer lorsque la cible s'éloigne du réseau d'antennes, il ne devrait pas avoir de dépendance critique sur l'angle directionnel. Les paramètres de localisation biaisés peuvent être obtenus en utilisant une méthode basée sur le modèle approximé appliquée aux signaux générés avec un modèle exacte. Les LUT étant discrets, les paramètres de localisation estimés ne correspondent pas nécessairement à une des entrées de LUT. Par conséquent, nous cherchons les quatre entrées de LUT les plus proches des paramètres estimés et interpolons en utilisant une technique d'interpolation de faible complexité pour obtenir les paramètres de localisation corrigés. Deux LUTs sont construits, l'un servant à la correction des paramètres liés au réseau d'antennes d'émission et l'autre pour la réception.

- La méthode de correction basée sur LUT peut prendre un peu de temps car elle nécessite de chercher les quatre paramètres de localisation biaisés les plus proches des paramètres estimés. Ainsi, nous proposons une autre méthode de correction qui estime directement les longueurs de chemin relatives à partir des paramètres biaisés de localisation estimés en utilisant le modèle de signal approché. Une longueur de parcours relative d'une antenne d'un réseau est simplement la différence entre la distance d'une cible à cette antenne et celle de la même cible à l'antenne de référence de ce réseau. Cette méthode de correction utilise le fait que les longueurs relatives d'une cible sont mieux estimées que les paramètres (distances et angles) par les méthodes basées sur un modèle approximé. En d'autres termes, si une méthode basée sur le modèle approximé est appliquée sur un signal en champ proche, elle va générer des erreurs sur les paramètres DOA, DOD et les distances, mais les erreurs sur les longueurs relatives (ou bien sur le vrai vecteur directionnel) sont beaucoup plus petites. Une fois que nous avons des estimations des longueurs relatives des chemins, nous pouvons obtenir un système surdéterminé d'équations linéaires en utilisant le modèle exacte basé sur le front d'onde sphérique. Nous pouvons le résoudre en utilisant l'estimateur des moindres carrés pour obtenir les paramètres de localisation corrigés.

La comparaison en termes des RMSE des paramètres de localisation avant et après la correction montre que les méthodes de correction peuvent réduire considérablement le biais pour des SNR élevés où les erreurs dominantes sont celles liées à l'approximation du modèle. Les performances de correction des méthodes proposées dépendent également de la performance de la méthode basée sur le modèle approximé utilisée pour

estimer les paramètres de localisation.

En plus des deux méthodes de correction, nous avons aussi proposé deux nouvelles méthodes qui peuvent traiter directement le modèle exacte des signaux basé sur le front d'onde sphérique.

- La première méthode proposée basée sur le modèle exacte s'inspire d'une méthode basée sur le modèle approximé existante pour localiser les cibles en champ proche d'un radar MIMO bistatique. L'idée principale de travailler avec le modèle exact du signal, est d'estimer d'abord directement les vecteurs directionnels, puis d'en extraire les paramètres de localisation. Par conséquent, la méthode proposée basée sur le modèle exacte utilise une technique s'appuyant sur les sous-espaces pour estimer les vecteurs directionnels. À partir des vecteurs directionnels estimés, nous pouvons alors extraire les longueurs relatives des chemins. Elles peuvent être utilisées pour obtenir un système surdéterminé d'équations linéaires qui peut être résolu par un estimateur des moindres carrés pour obtenir les paramètres de localisation. L'extraction des longueurs de chemin relatives à partir du vecteur directionnel nécessite un déroulement (phase unwrapping) et une correction du décalage de phase. Le déroulement de phase est nécessaire car les composants des vecteurs directionnels sont complexes et leurs phases ne peuvent être récupérées que dans leur domaine principal, tandis que les longueurs des chemins relatives sont directement proportionnelles aux phases réelles des composants complexes des vecteurs directionnels. Le déroulement fournit habituellement des phases décalées qui peuvent être corrigées à partir du fait que la phase de la composante de référence devrait être nulle. Ainsi, en soustrayant la phase du composant de référence des phases restantes, on obtient les estimations des longueurs de trajets relatives. Les longueurs de parcours estimées peuvent être utilisées pour estimer les paramètres de localisation en utilisant la procédure utilisée par la deuxième méthode de correction proposée.
- La deuxième méthode basée sur le modèle exacte utilise la décomposition des tenseurs pour estimer les vecteurs directionnels. Les signaux reçus d'un système MIMO bistatique peuvent être représentés pas un tenseur d'ordre trois qui peut être décomposé en vecteurs directionnels par PARAFAC. Une fois que les estimations des vecteurs directionnels sont disponibles, la même approche, qui est utilisée dans la méthode proposé ci-dessus, peut être utilisée pour obtenir les paramètres de localisation.

La comparaison entre les deux méthodes proposées basées sur le modèle exacte révèle que la méthode basée sur PARAFAC a des performances légèrement meilleures, notamment parce que la première méthode n'utilise pas la totalité de l'information disponible. Les méthodes basées sur le modèle exacte n'ont pas de contrainte sur la

distance inter-élément du réseau d'antennes, donc elles sont applicables aux réseaux d'antennes avec un espacement entre éléments à demi-longueur d'onde.

En conclusion, dans cette thèse, nous avons proposé deux méthodes de localisation de sources basées sur le modèle exact, une méthode basée sur le modèle approximé et deux méthodes de correction pour la localisation de sources en champ proche d'un système MIMO bistatique.

Contents

List of Figures

List of Algorithms

List of Acronyms

CANDECOMP CANonical DECOMPosition

COMFAC COMplex parallel FACtor

CRLB Cramér–Rao Lower Bound

DOA Direction Of Arrival

DOD Direction Of Departure

DTLD Direct TriLinear Decomposition

EM ElectroMagnetic

ESPRIT Estimation of Signal Parameters via Rotational Invariance Techniques

GRAM Generalized Rank Annihilation Method

LS Least Squares

LUT Look Up Table

MATLAB MATrix LABoratory

MIMO Multiple Input Multiple Output

ML Maximum Likelihood

MSE Mean Square Error

MUSIC MUltiple SIgnal Classification

MVDR Minimum Variance Distortionless Response

PARAFAC PARAllel FACtor

PARAFAC2 Parallel factor for cross-product matrices

PARATUCK PARAFAC–TUCKER

PM Propagator Method

RADAR RAdio Detection And Ranging

RARE RAnk REduction

RCS Radar Cross Section

RD-PARAFAC Reduced Dimensional PARAllel FACtor

RMSE Root Mean Square Error

SNR Signal-to-Noise Ratio

SVD Singular Value Decomposition

TALS Trilinear Alternating Least Squares

TLS Total Least Squares

ULA Uniform Linear Array

Notations

a, α, A	Scalar
$\boldsymbol{a}, \boldsymbol{\alpha}$	Vector
$\boldsymbol{A}$	Matrix
$\boldsymbol{\mathcal{A}}$	3-way tensor
$[\cdot]^T$	Transpose
$[\cdot]^*$	Conjugate
$[\cdot]^H$	Hermitian transpose (conjugate transpose)
$[\cdot]^\dagger$	Left pseudo inverse
$[\cdot]^{-1}$	Inverse of a square matrix
$\mathrm{E}\{\cdot\}$	Expectation
$\|\cdot\|_F$	Frobenius norm
j	$\sqrt{-1}$
$\Re\{a\}$	Real part of a
$\Im\{a\}$	Imaginary part of a
$\|a\|$	Absolute value of a
$\arg\{a\}$	Argument of a
$\angle\{a\}$	Principal value of a
$\boldsymbol{I}_N$	$N \times N$ identity matrix
$\boldsymbol{J}_N$	$N \times N$ exchange matrix
$\boldsymbol{0}_N$	$N \times 1$ zeros vector
$\underline{\boldsymbol{0}}_N$	$N \times N$ zeros matrix
$\underline{\boldsymbol{1}}_N$	$N \times N$ ones matrix
$\underline{\boldsymbol{1}}_{M\times N}$	$M \times N$ ones matrix
$\mathbb{N}_1$	Set of all natural numbers without zero
$\mathbb{Z}$	Set of all integers
$\mathbb{R}$	Set of all real numbers
$\mathbb{C}$	Set of all complex numbers
$\mathrm{card}(\cdot)$	Cardinal number of a set
$\odot$	Hadamard product
$\otimes$	Kronecker product
$\boxdot$	Khatri-Rao product (column wise Kronecker product)

$\text{diag}\{\boldsymbol{a}\}$	Diagonal matrix with the elements of $\boldsymbol{a}$ as its diagonal elements
$\text{diag}\{\boldsymbol{A}\}$	Column vector containing the diagonal elements of $\boldsymbol{A}$
$\text{rank}\{\boldsymbol{A}\}$	Rank of $\boldsymbol{A}$
$\text{tr}\{\boldsymbol{A}\}$	Trace of $\boldsymbol{A}$
$\det\{\boldsymbol{A}\}$	Determinant of $\boldsymbol{A}$
$[\boldsymbol{a}]_i$	ith component of $\boldsymbol{a}$
$\mathcal{N}_c(\mu, \sigma^2)$	Complex circular Gaussian distribution with mean μ and variance σ^2

Introduction

RAdio Detection And Ranging (RADAR) has been an important research topic since many decades. Even now, its development is continuing with a steady pace. To begin, we summarize the transition of radar technology from conventional to Multiple Input Multiple Output (MIMO) system with its applications, classifications, and advantages. MIMO system based radars are the recent kinds of radar systems which have shown better performance as compared to the conventional radar systems. Consequently, the radar systems with MIMO technology are currently a hot topic of research. The development of signal processing techniques linked to the MIMO radar systems is discussed under the state of the art. And at last, the organization of this dissertation is provided, followed by the list of related publications.

1 Radar

Radar is a localization system which analyses the received ElectroMagnetic (EM) signals to detect, locate, and track the objects in its range. It is because, when an EM wave interacts with an object, the property of the wave changes based on the characteristics of the objects like distance, velocity, shape, and size. By analyzing the echoed signal, we can extract the information regarding the characteristics of that object. According to the historical records, it all started in 1886, when Heinrich Rudolf Hertz decided to practically test the EM theory developed by James Clerk Maxwell. He further studied the reflection of the radio waves by different dielectric substances. The frequency of a radio wave may vary from 3 kHz to 300 GHz. However, the preferred frequency range in radar is 25 MHz to 70 GHz. Inspired by the work of Hertz, many researchers worked on the radar systems which were less attractive field at that time. Many successful experiments like radio telegraphy, detection of ships and aircrafts, radar based altimeter, range finding, etc. were already performed using continuous and pulsed waveforms. However, the radar development only accelerated in World War II for military applications. After the war, the research bent towards the civilian applications. Since then, it has gone through a lot of improvements and it is still an active field of research. Parallel researches on the electronics and microwave devices like processors, magnetrons, klystrons, traveling-wave tubes, mixers, filters, etc. have

played a significantly important role in the development of radar [4,5].

1.1 Applications

The primary objective of inventing the radar was to locate the aircrafts and ships in World War II. However, after the end of the war the radar is also developed for the civilian applications. It is now used for navigation. Modern aircrafts are equipped with altimeter and weather radars to increase safety. Altimeter radar can also be used to map the ground from air. Weather radar provides a large resource for the weather forecast. Radar is very useful in navigation when optical visibility is poor. Doppler radars are used in road safety by detecting speedy vehicles. Radar can also be used for surveillance to secure the public places like airports, museums, concerts, politically sensitive conferences, metro trains, etc. Radar is still used by the military to detect, track, and guide missiles for national security. During the world wars, many land mines were buried underground which can still be active. Ground penetration radar can be used to detect those land mines in order to disable them. Not only the land mines, the ground penetration radar can also be used to explore ancient ruins without physically exploiting them. Radar also contributes in the researches related to astronomy, civil engineering, medicines, etc. [4–6].

1.2 Passive and Active Radar Systems

A radar is distinguished based on its applications, type of waveform used, and its significant feature. As a result, there are many ways in which a radar system can be classified. Consequently, here we only discuss the classification concerning the passive and active radar systems which are shown in Figure 1.

Passive radar system only contains receiver. It simply listens to the EM signals emitted or reflected by the targets. Since it has no dedicated transmitter, the targets which do not emit their own signals can not be detected in the absence of any EM wave broadcasting source. However, this drawback makes it nearly undetectable to the surveillance radar.

On the other hand, active radar system contains transmitter along with the receiver. To locate a target, the receiver processes the reflections of the known signal broadcast by its dedicated transmitter. Since, we know the waveform of the transmitted signal, we can extract more information about the target from the echo of transmitted known signals. MIMO systems fall under active radar [7].

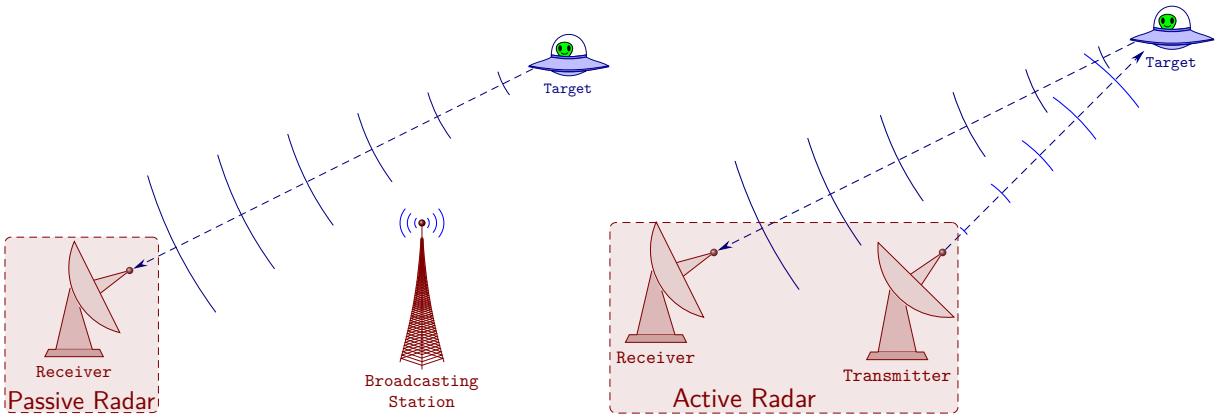

(a) Passive Radar System (b) Active Radar System

Figure 1 – Passive and active radar systems schematic.

1.3 Array Based Radar

Initial radar systems were using mechanical setup to rotate a single antenna with directivity to scan the region of interest. Later phased array got attention which can electrically steer the beam along the region of interest. The main advantage of electrical steering is the scanning speed. To steer the beam, each antenna of the array is fed with different weighted signal waveform. The main purpose of these weights is to induce different phase delays in the transmitted waveforms corresponding to the different antennas. However, sometimes amplitude is also modified to get some specific beam shapes. Finding the location of a target is one of the main objectives of the arrays based radar.

In 1969, J. Capon proposed a high resolution direction finding algorithm using phased array for seismic application [8]. This method is also known as Minimum Variance Distortionless Response (MVDR) beamformer, which signifies its working principle [9]. More than a decade later, inspired by a frequency estimation technique known as Pisarenko harmonic decomposition [10], spectral MUltiple SIgnal Classification (MUSIC) technique was developed which is based on the orthogonality between the signal and noise subspaces [11, 12]. It has higher resolution capability than MVDR and can provide unbiased estimates of the number of sources, Direction Of Arrivals (DOAs), and polarizations [12]. For a standard linear array, the cost function in the spectral MUSIC technique can be transformed into a polynomial. If there are P sources, then the P roots of this polynomial which are inside and closest to the unit circle provide the DOAs of the P sources [13]. Because of the involvement with the polynomial roots, this method is often called as root MUSIC. Beside it, a high resolution low computational complexity subspace based method, referred to as Estimation of Signal Parameters via Rotational Invariance Techniques (ESPRIT), was proposed in 1986 which uses two identical arrays with displacement invariance [14–16]. The com-

putation complexity of this method is close to the root MUSIC, however lower than the spectral MUSIC. Mean Square Error (MSE) of the DOAs estimated by root MUSIC is lower than that by ESPRIT [17]. In [16], the authors have claimed that ESPRIT has more robustness with imperfect array than MUSIC method. Subspace based methods like MUSIC and ESPRIT usually use eigendecomposition which adds high computational complexity to these techniques. Propagator Method (PM) is a subspace based method that doesn't use eigendecomposition, however provides satisfactory performance as compared to the MUSIC techniques [18]. RAnk REduction (RARE) is another subspace based method which shows performance comparable to the other subspace based methods [19]. There are many other localization methods such as minimum-norm, linear prediction, etc. for DOA estimation [20–22]. Almost all of the above mentioned methods focus on the far field region of a standard linear array. However, they were also developed further to deal with other array geometries and situations. As a result, there exist many variations of these methods in the literature concerning sources localization.

Because of the influence of the military applications on the initial development of the radar, near field sources localization had received less attention as compared to the far field. However, the technological upgrades in the human civilization have driven the development of near field sources localization from last few decades along with the far field sources localization. The wavefront received at the array from a far field source is often considered as planar whereas the wavefront is approximated as quadric (quadratic surface) for a near field source. However, the wavefront of a point like source is always spherical in practical situation [23, 24]. The mathematical expression of the spherical wavefront has high nonlinearity. Thus, to reduce the nonlinearity of this expression only first order term of the Taylor expansion of this expression is used to express the planar wavefront and the first and second orders terms are used for a near field source that model a quadric wavefront. When an array of antennas is used, the range and DOA of each near field source are estimated. However, in case of a far field source only its DOA is usually estimated. The approximation of the spherical wavefront adds bias to the estimated location parameters (range and DOA). The biases in the location parameters due to the wavefront approximation decrease with the increase in range [23]. Consequently in the far field situation, the bais due to the wavefront approximation is significantly small as compared to the wavelength of the source carrier signal. However, this bias can't be ignored in the near field case, if precision is our prime concern. Regardless of that there exist many near field sources localization techniques which use quadric wavefront based model [2, 3, 23–28]. And these techniques are usually analyzed using the received signals generated with the quadric wavefront based model which can not be considered as a fair testing of their performance concerning the estimation error in the location parameters.

2 MIMO Radar

The idea of MIMO communication [29–31] was stretched out to MIMO radar [32, 33]. A MIMO system consists of multiple transmitting and receiving antennas. These antennas may be placed in distributed or colocated manner. Each transmitting antenna emits a waveform orthogonal to the waveform transmitted by the remaining transmitting antennas. This orthogonality may exist in the signal space, time domain, or frequency domain [34]. The receiving array receives the superposition of the echoes of the transmitted signals after their interaction with the targets. The acquired signal at each receiving antenna is then passed through the matched filters. The orthogonality between the transmitted signal allows the matched filters to identify the known transmitted signals in the received signal at each receiving antenna [35, 36]. Consequently, we collect the number of transmitting antennas times the number of receiving antennas data points at a time instance. Because of the advancements in the computation capabilities, we can apply complicated signal processing techniques on the data collected at the receiver of a MIMO radar [37]. A MIMO radar can also be considered as an upgrade to the active phased array radars. The major difference between the two is that a phased array radar transmits weighted versions of the same signal waveform whereas in a MIMO radar each transmitting antenna emits linearly independent waveforms [38].

2.1 Advantages

A MIMO radar is an active radar therefore it inherits the merits and demerits of an active radar. Multiple paths in a channel may cause fading of the signals. Due to the multiple transmitting and receiving antennas, this fading phenomenon can be minimized to a great extent [37, 39]. The ability to uniquely identify the targets is known as parameter identifiability. Due to the use of linearly independent transmitted signals, MIMO radar has waveform diversity which provides high parameter identifiability as compared to a phased array radar with same number of transmitting and receiving antennas [40]. In other words, a MIMO radar can unambiguously identify more targets than a phased array radar.

2.2 Classification of MIMO Radar Systems

In a broad sense, a MIMO radar system is categorized as statistical and coherent [34, 41]. In a statistical MIMO radar, the transmitting and receiving antennas are widely separated from each other. Due to the spare array, statistical MIMO radar can view a target from many directions and gather more information about that target [42]. Some targets may have small Radar Cross Section (RCS) for some locations however large

RCS at the other locations. These spatially diverse targets can not easily hide from a MIMO radar with widely separated antennas.

In a coherent MIMO radar, the transmitting and receiving antennas are colocated. Based on the number of colocated antennas arrays and the separation between the transmitting and receiving arrays, a coherent MIMO radar can be classified as a monostatic, bistatic, or multistatic. In monostatic MIMO radar, the transmitting and receiving arrays overlap. Therefore, the DOA and Direction Of Departure (DOD) for a target are same. If the surface of target facing the radar has small RCS, the monostatic radar may not detect it. This situation can be overcome by using a bistatic MIMO radar in which the transmitting array is placed far from the receiving array [37]. Because of the large separation between the transmitting and receiving arrays, a bistatic MIMO radar has more degrees of freedom than a monostatic MIMO radar [37]. In a monostatic MIMO radar, DOA is equal to DOD, therefore the signal model is simple as compared to a bistatic MIMO radar and as a result, a monostatic MIMO radar requires estimating only one direction for each target [43–48]. A multistatic MIMO radar contains many transmitting and receiving arrays. The antennas in these arrays are locally colocated however the arrays are widely separated. This increases the spatial diversity of the mutistatic MIMO radar. It can also be considered as a combination of the statistical and coherent MIMO radars. The colocated antennas in these radar provide high angular resolution and detection sensitivity [32, 49]. The work in this thesis only deals with a bistatic MIMO radar which has more spatial diversity than a monostatic MIMO radar and less complexity than a multistatic MIMO radar.

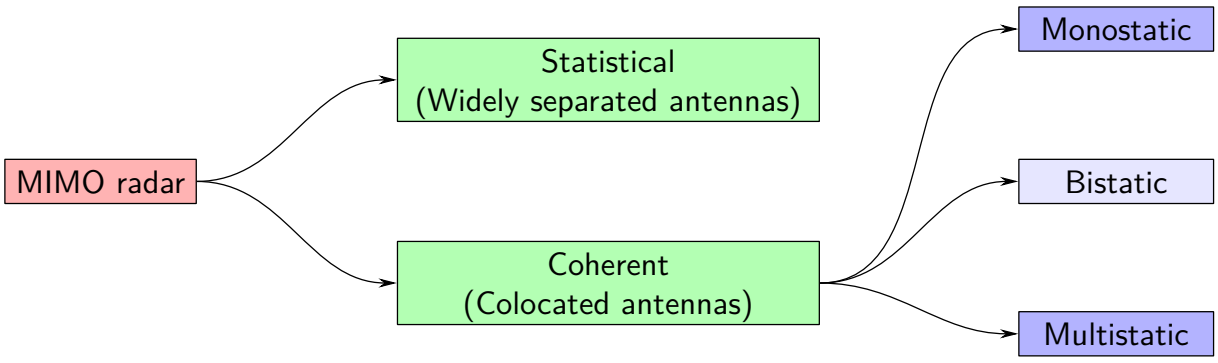

Figure 2 – Types of MIMO radar.

3 State of the Art

In a passive radar with standard linear array, we only need to estimate DOA which often requires one parameter estimation technique [8, 9, 11–22]. However in a bistatic MIMO radar with standard linear arrays, we need to estimate the DODs along with the DOAs of targets because it is an active radar. To estimate two parameters, we can

use a two-dimensional estimator or use two one-dimensional estimators. Maximum Likelihood (ML) is a usual approach to estimate unknown parameters. However, it is computationally expensive. As a result, in 2006, a 2D unitary ESPRIT based technique was proposed to jointly estimate the DODs and DOAs that has less computational complexity than a ML based approach [9, 50]. A two-dimensional estimation method is generally slower than two one-dimensional estimation methods. Thus, multiple one-dimensional estimation methods are preferred over one multiple-dimensional estimation method. A drawback of using two one-dimensional estimation methods is that the DODs and DOAs of the targets are not paired. This lack of pairing can be observed in [51] which uses two 1D ESPRIT to estimate the DODs and DOAs of targets followed by an additional process to pair them. The pairing process adds additional computation burden to the whole localization procedure. Furthermore, at low Signal-to-Noise Ratio (SNR), the paring may not be correct. Keeping these things in mind, soon after [51], a method was proposed which achieved automatic pairing between the DODs and DOAs using two 1D ESPRIT with a little modified approach [52]. Another study in 2009, achieved automatic pairing using ESPRIT for a signal with colored noise [53]. However the method was limited to three transmitters. The limitations on the number of transmitters in [53] were overcame by using Singular Value Decomposition (SVD) along with ESPRIT in [54]. In 2010, Reduced dimension MUSIC algorithm was proposed, in which 2D-MUSIC problem was divided into two 1-D MUSIC problems [55]. Automatic paring of DOD and DOA, can also be achieved using polynomial rooting technique [56]. In this, polynomial root-MUSIC was compared to 2-D MUSIC pseudo-spectrum and double 1-D MUSIC pseudo-spectrum and found to be more efficient than the other two methods. The computation time of root-MUSIC is higher than ESPRIT. Therefore, a combined solution was proposed [57]. In this method DOD was estimated by using ESPRIT and their corresponding DOA was estimated by using root-MUSIC. The performance of the method proposed in [57] was good enough to extend this method for the polarimetric bistatic MIMO radar [58, 59].

Beside the subspaces based methods, there are factor analysis methods to estimate DOD, DOA and Doppler shift. Uniqueness and rotation of factors analysis were discussed in [60–62]. Using factor analysis, Tucker decomposition was proposed to decompose a three dimensional tensor into three matrices (2-D tensors) and one 3-D tensor factors [63]. In 1969, an attempt was made to define the rank of tensors by taking the rank of matrices as a reference [64]. In 1970, PARAllel FACtor (PARAFAC) and CANonical DECOMPosition (CANDECOMP) trilinear decompostions were introduced independently in [65] and [66] respectively. In 1972, Harshman introduced Parallel factor for cross-product matrices (PARAFAC2) [67]. In this, he also discussed about the algorithm and uniqueness of PARAFAC2 model. J. B. Kruskul extended the matrix rank to the rank of multi-way array and provided a relation between the

uniqueness and the rank of 3-way array for PARAFAC [68–70]. In [71], Harshman and Lundy reviewed on direct and indirect fitting of PARAFAC, PARAFAC2 and PARAFAC–TUCKER (PARATUCK) models. In 1997, Rasmus Bro published tutorial and applications of PARAFAC under Chemometrics and Intelligent Laboratory Systems [72]. In this, he discussed about the uniqueness and rank of multi-way arrays. He also summarized Trilinear Alternating Least Squares (TALS) and three different ways to speed it up. He used chemometric examples to show his finding. He further elaborated multi-way analysis for food industry in his PhD thesis [73]. His team also proposed a direct fitting algorithm for PARAFAC2 [74] and used it in fluorescence spectroscopy [75]. Sensor array processing became an application of PARAFAC [76, 77]. In 1999, COMplex parallel FACtor (COMFAC) was introduced which dealt with PARAFAC for trilinear complex valued data [78]. University of Copenhagen, has provided free N-way toolbox for MATrix LABoratory (MATLAB) [79]. This toolbox contains the updated versions of useful functions, algorithms and documents. To avoid confusions, [80] proposed standard notations for the tensors and operations on it. Uniqueness, being an important characteristics of tensor decomposition, was extended from trilinear to multilinear case [81]. The multi-way analysis has became a part of multilinear (tensor) algebra [82, 83]. The tensor algebra can be considered as a super set of linear algebra [84, 85].

Many fitting algorithms were proposed for PARAFAC to decompose tensor. However, among those TALS was found to have better performance [86]. TALS sometime converges very slowly between initial and final state. Since, TALS convergences time depends upon the size of tensor, therefore some techniques were proposed using Tucker method to compress its size [87, 88]. In TALS, the initialization also plays a significant role in convergence and avoiding local minima. Few initialization method like Generalized Rank Annihilation Method (GRAM), Direct TriLinear Decomposition (DTLD) were also helpful to accelerate the convergences [89–92]. Another solution to speed up the convergence of TALS is line search. Line search was initially used in [65] with a constant step size (1.25). Later, another iteration dependent step size (cube root of iteration) was proposed which performed better than constant step size [73]. In 2008, enhanced line search algorithm for real valued tensors was proposed in which step size was a factor that minimizes the cost function [93]. Following this research work, the algorithm was extended to complex valued tensors [94]. The above mentioned methods have greatly improved TALS performance. However, due to the increase in the area of applications, fast TALS was proposed for multi-way tensors which achieved memory and time benefits over previous TALS algorithms [95].

The localization using MIMO radar can be considered as a trilinear algebra problem which was the most common data structure in tensor decomposition research. In case of bistatic MIMO radar, the performance of PARAFAC was proved much bet-

ter in terms of computation time and estimation error as compared to 2-D spectral Capon [96]. In mutistatic and bistatic case, the performance of PARAFAC was found better than 2-D spectral subspace techniques with considerable resolution [97]. Due to trilinear decomposition, DOA, DOD and Doppler frequency were estimated jointly for a bistatic MIMO radar using PARAFAC [98]. In 2014, PARAFAC-MUSIC was proposed in which the estimated Doppler frequencies were fed again to the matched filters bank to cancel the effect of Doppler shift and estimated DOA (monostatic) using filtered signal with the help of MUSIC [99]. PARAFAC-MUSIC showed reduction in estimation error of DOA as compared to PARAFAC and MUSIC. A Reduced Dimensional PARAllel FACtor (RD-PARAFAC) was proposed for monostaic MIMO radar configuration and compared with Cramér–Rao Lower Bound (CRLB), PARAFAC, ESPRIT and PM [100]. According to the results in [100], RD-PARAFAC outperformed other methods and for low SNR, PM showed high estimation error. Tensor-ESPRIT showed less angle estimation error as compared to PARAFAC [101].

All the above mentioned methods are dedicated to the far field targets localization using bistatic MIMO radar. Very few methods can be found in the existing literature which can deal with the localization of near field targets using bistatic MIMO radar even though near field sources localization techniques using passive array radar are under constant development [1, 23, 25–28, 102]. In this thesis, we try to fill this gap related to the targets in the near field region of a bistatic MIMO radar. The near field region of an array can not be mathematically modeled the same as its far field region because the far field assumptions in near field region may lead to a significant estimation error. For a point like target, the signal wavefront is spherical which has a nonlinear mathematical expression. Taylor expansion is used on this expression to reduce its nonlinearity making the localization procedure relatively simple. Based on this approximated model, [26] presents a subspaces based technique to localize the targets in the near field region of a pseudo-monostatic MIMO radar. Inspired by their work, another method was proposed for the near field region of a bistatic MIMO radar [1]. Due to the combination of the near field situation and bistatic MIMO radar, we need to estimate four localization parameters viz. DOD, DOA, and two ranges belonging to the transmitting and receiving arrays. The basic strategy in most of the existing methods for the near field sources localization is to estimate DOAs before the estimation of their corresponding ranges. This strategy can work fine with the approximated model, however it won't work correctly for the accurate model. In this thesis, we present some novel methods to deal with the two models.

4 Organization of this Dissertation

This dissertation deals with some localization techniques to estimate the positions of the targets in the near field region of a bistatic MIMO system. To explain the methods, we need firstly to provide the signal model. Thus, in chapter 1, we formulate the signal model of a bistatic MIMO system. We start with a brief explanation of the modeling of targets in section 1.1, because the echoed signals have space-time varying random gains due to the interaction with the targets. There exists a huge amount of work on a bistatic MIMO system, thus, its signal model is easily available in the existing literature on it. In section 1.3, we explain the model of the near field region of a bistatic MIMO radar. Near field region, also referred to as Fresnel region, of an array of antennas is a finite 3D space. This finite region is bounded by the upper and lower limits of the radial distance from the center of the array. We also give the expressions to compute these limits in the same section. Approximation of the model is a common practice while dealing with the Fresnel region. The change in the signal model due to the Fresnel approximation of the spherical wavefront is elaborated in section 1.3.2. Another common practice in the near field sources localization methods is the use of symmetric Uniform Linear Array (ULA) whose mathematical meaning is provided in section 1.3.3. While locating a near field source using a linear array, its distance from the array's reference point and its angle at that reference point with respect to the axis of the array constitute its location parameters. In a bistatic MIMO system with linear arrays, we have four such location parameters belonging to the transmitting and receiving arrays. However, in 3D space we need only three coordinates. Additionally, it is more practical to visualize and analyze the location of target in terms of Cartesian coordinates. Thus, in section 1.4, we restate the signal model in terms of three Cartesian coordinates. To analyze the estimation accuracy of an estimator, the Root Mean Square Error (RMSE) of the estimated parameter is compared against its CRLB which serves as a benchmark. The expression to calculate the CRLBs of the location parameters of the targets in the near field region of a bistatic MIMO system can easily be found in the related work. Section 1.5 is dedicated to the expression used to calculate the CRLB of the location parameters in the bistatic MIMO case.

Chapter 2 contains two localization methods which use Fresnel approximation based signal model. Section 2.1 provides a summary of an existing near field target localization method using bistatic MIMO system which is used in this work to compare with our proposed methods. This method has very low computational complexity but the maximum number of localizable targets solely depends on the number of sensors in the receiving array. Contrary to it, the proposed method in section 2.2 is computationally costly however it can locate more number of targets by exploiting the MIMO technology. In section 2.3, we compare the RMSE of the four location parameters estimated by

the two methods in the presence of two targets.

As mentioned before, the Fresnel approximation introduces biases in the estimated location parameters. This bias can be considered as a systematic error which can easily be removed by calibrating the estimated localization parameters. In chapter 3, we propose two correction methods to reduce the bias introduced by the Fresnel approximation. The first method in section 3.2 is based on Look Up Table (LUT) of the biases in the discretized near field region; the second method in section 3.3 is based on the estimation of propagation path length vector from the estimated location parameters. The LUT based correction method is possible because the finite near field region leads to finite LUT. It is obvious that there can be infinite locations in the finite near field region. As a result, we discretize the near field region of each array and store the biases of the discretized spaces in the LUTs. There is no need to update a LUT unless the corresponding array parameters change. The arrays parameters, like number of sensors and interelement distance, are rarely modified in real life applications. The estimated location parameters of a target related to the transmitting and receiving arrays are corrected using a low complexity interpolation technique. Section 3.2 discusses the LUT creation and interpolation procedures in detail. An approach to deal with the accurate model is to estimate directional vectors and then extract the unbiased location parameters from them. The second proposed correction method described in section 3.3 uses this approach. The principle of this correction technique is explained in section 3.3.1 and the correction procedure is given in section 3.3.2. The correction performance of the proposed methods is analyzed in section 3.5 by correcting the location parameters estimated by the methods in chapter 2. The analysis is performed by comparing the standard deviations of the position errors before and after corrections. Cartesian coordinates based signal model allows us to study the estimation performance in terms of position error. A method to obtain the Cartesian coordinates from the four location parameters is provided in section 3.4.

In chapter 4, we describe two proposed methods which can directly handle the accurate model. Both methods use the same strategy in which the directional vectors are estimated firstly and then the unbiased location parameters are extracted from them. The method in section 4.1 is based on the subspace based technique whereas the method in section 4.2 uses tensor decomposition to estimate the directional vectors. Section 4.3 shows an example in which we compare the mean squares of position errors of the proposed methods against CRLB and a method which uses Fresnel approximation.

Finally, we conclude the work with perspectives and future works.

5 List of Related Publications

Letter

- Parth Raj Singh, Yide Wang, and Pascal Chargé, "Bistatic MIMO Radar for Near Field Source Localisation Using PARAFAC", Electronics Letters 52 (12), 1060-1061, April 2016. [103]

Articles

- Parth Raj Singh, Yide Wang, and Pascal Chargé, "An Exact Model-Based Method for Near-Field Sources Localization with Bistatic MIMO System", Sensors 17 (4), 723, 2017. [104]
- Parth Raj Singh, Yide Wang, and Pascal Chargé, "A Correction Method for the Near Field Approximated Model Based Localization Techniques", Elsevier Digital Signal Processing 67, pp. 76–80, 2017. [105]
- Parth Raj Singh, Yide Wang, and Pascal Chargé, "Performance Enhancement of Approximated Model Based Near Field Sources Localisation Techniques", IET Signal Processing 11(7), pp. 825–829, 2017. [106]

Conferences

- Parth Raj Singh, Yide Wang, and Pascal Chargé, "Near Field Targets Localization Using Bistatic MIMO System with Symmetric Arrays", EUSIPCO, pages 2467–2471, Kos island, Greece, August 2017. [107]
- Parth Raj Singh, Yide Wang, and Pascal Chargé, "Near Field Targets Localization Using Bistatic MIMO System with Spherical Wavefront Based Model", EUSIPCO, pages 2472–2476, Kos island, Greece, August 2017. [108]

1

Signal Model

In this chapter, we discuss the necessary mathematical models useful for understanding the context of the following chapters. At first, we introduce the distributions often used to model a complex target followed by the commonly used model of the received signal in a bistatic MIMO radar system. Next, we describe the signal model with Fresnel approximation in the near field region followed by the effect of this approximation. We also reformulate the signal model in Cartesian coordinates. At last, we provide the expressions to obtain the CRLBs of the location parameters for the signal models concerning spherical wavefront, quadric wavefront, and Cartesian coordinates.

1.1 Target Model

In an active radar, the targets are detected by analyzing the reflection of the transmitted signals from targets on the receiving antennas. The reflectivity of a target is measured in terms of its RCS which depends on the physical dimensions, geometry, orientation with respect to the incident wave, and constituent material of its surface. The reflectivity of the material of its exposed surface is a function of frequency [5]. Therefore, many practical radar systems use multiple frequencies to get sufficiently large RCS in order to increase the probability of detection as compared to the single frequency case. Regardless of that, in this study, we use a single carrier frequency with the assumption that RCS of each target is large enough at this particular frequency.

For some geometries of targets, a slight movement in their orientation may generate scintillation. Based on this, the targets can be categorized into fluctuating or nonfluc-

tuating. Nearly spherical objects generate negligible scintillation, thus, they fall under nonfluctuating targets [109]. The RCS of a fluctuating target is not easily tractable. As a result, the reflection coefficient of a fluctuating target is modeled as a random process [110]. Swerling cases are the most recognized models for the fluctuating targets [34, 109, 110]. Swerling cases I and II are applicable to non spherical targets with more than one large reflectors as compared to the wavelength of impinging signal like airplanes. Swerling cases III and IV are used to describe the targets with one large reflector and some small reflectors like ships. Swerling case zero is for nonfluctuating targets like meteors. In case of Swerling cases I and III, the power of the reflected signal from a target is nearly constant for all the pulses in a single scan but greatly changes from scan to scan. In the case of Swerling cases II and IV, the power fluctuates from pulse to pulse even in a single scan [109]. These cases are not enough to model the behavior of every fluctuating target [111]. There exist different distributions to model different complex targets, among which Rayleigh is mostly opted [4]. Hence, we use complex targets with Rayleigh distributed reflected signal gain.

1.2 Modeling of Bistatic MIMO System

Let P be the number of narrow-band stationary point sources in the near-field region of a bistatic MIMO system with ULAs. In the following, M and N represent, respectively, the number of omnidirectional antennas in the transmitting and receiving arrays of the bistatic MIMO system.

For such a bistatic MIMO system in the presence of P stationary point targets, the received matched filtered signal at time t can be written as [34, 41, 112]

$$\boldsymbol{y}(t) = \boldsymbol{A}\,\boldsymbol{s}(t) + \boldsymbol{w}(t) \tag{1.1}$$

with $\boldsymbol{A} = \boldsymbol{A_e} \boxdot \boldsymbol{A_r}$ where $\boldsymbol{A_e} \in \mathbb{C}^{M\times P}$ and $\boldsymbol{A_r} \in \mathbb{C}^{N\times P}$ contain the directional vectors of departure and arrival, respectively, $\boldsymbol{s}(t) \sim \mathcal{N}_c(0, \boldsymbol{R_s} = \text{diag}\{[\sigma_{s_1}^2, \sigma_{s_2}^2, \cdots, \sigma_{s_P}^2]\}) \in \mathbb{C}^P$ is the vector of the reflection coefficients at time t of the complex targets, and $\boldsymbol{w}(t) \sim \mathcal{N}_c(0, \sigma_w^2\, \boldsymbol{I}_{MN}) \in \mathbb{C}^{MN}$ is an additive noise vector. Here, $\sigma_{s_p}^2 = \text{E}\{[\boldsymbol{s}]_p(t)\,[\boldsymbol{s}^*]_p(t)\}$ and $\sigma_w^2 = \text{E}\{[\boldsymbol{w}]_{l'}(t)\,[\boldsymbol{w}^*]_{l'}(t)\}$ with $p \in \{1, 2, \cdots, P\}$ and $l' \in \{1, 2, \cdots, MN\}$.

Let $\boldsymbol{a_{e_p}}$ and $\boldsymbol{a_{r_p}}$ respectively be the pth columns of $\boldsymbol{A_e}$ and $\boldsymbol{A_r}$ given by

$$\boldsymbol{a_{e_p}} = \boldsymbol{a_e}(\rho_{e_p}, \theta_{e_p}) = \left[a_{e_{(1,\,p)}}, \cdots, a_{e_{(m_o-1,\,p)}}, 1, a_{e_{(m_o+1,\,p)}}, \cdots, a_{e_{(M,\,p)}}\right]^T \tag{1.2}$$

and

$$\boldsymbol{a_{r_p}} = \boldsymbol{a_r}(\rho_{r_p}, \theta_{r_p}) = \left[a_{r_{(p,\,1)}}, \cdots, a_{r_{(p,\,n_o-1)}}, 1, a_{r_{(p,\,n_o+1)}}, \cdots, a_{r_{(p,\,N)}}\right]^T \tag{1.3}$$

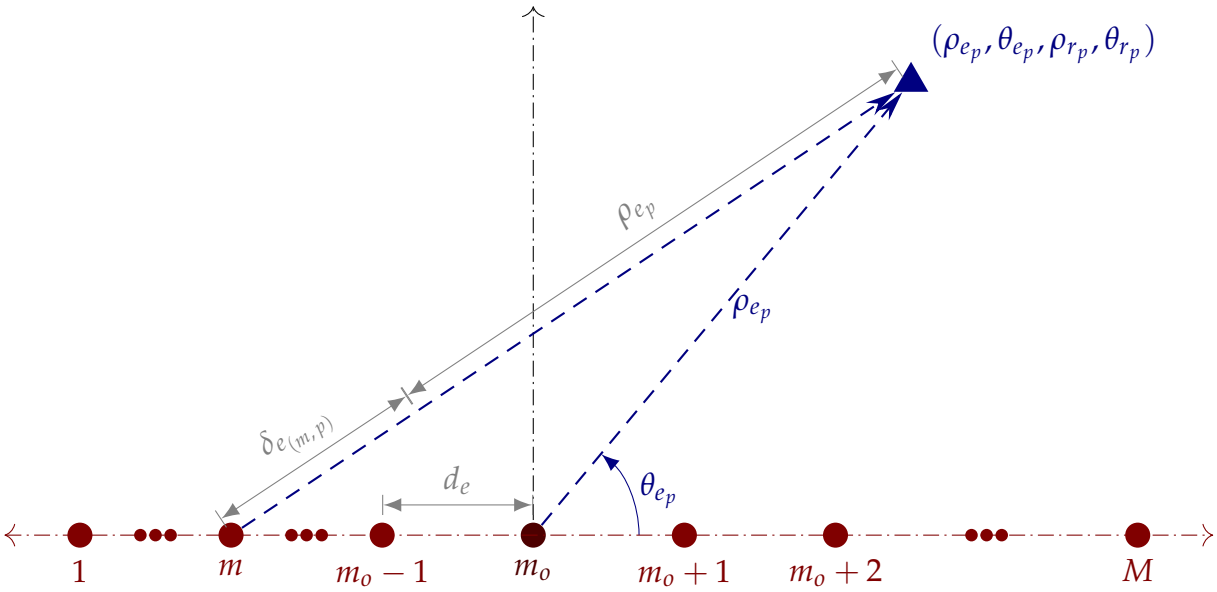

Figure 1.1 – Transmitting ULA parameters

where m_o and n_o are the indexes of the reference elements of the transmitting and receiving arrays, respectively, $a_{e_{(m,p)}} = a_{e_m}(\rho_{e_p}, \theta_{e_p}) = \exp(-j\,2\,\pi\,\delta_{e_{(m,p)}}/\lambda)$, and $a_{r_{(p,n)}} = a_{r_n}(\rho_{r_p}, \theta_{r_p}) = \exp(-j\,2\,\pi\,\delta_{r_{(p,n)}}/\lambda)$. $m \in \{1, 2, \cdots, m_o, \cdots, M\}$ and $n \in \{1, 2, \cdots, n_o, \cdots, N\}$ are the indexes of the antennas of the respective arrays. λ is the wavelength of the carrier. As shown in Figure 1.1, $\delta_{e_{(m,p)}}$ is the difference between the distance traveled by the transmitted signal from the mth transmitting antenna to the pth target and the distance traveled by the transmitted signal from the m_oth transmitting antenna to the pth target, which can be expressed for ULA as

$$\delta_{e_{(m,p)}} = \delta_{e_m}(\rho_{e_p}, \theta_{e_p}) = \sqrt{\rho_{e_p}^2 + (m - m_o)^2\, d_e^2 - 2\,(m - m_o)\, d_e\, \rho_{e_p} \cos\left(\theta_{e_p}\right)} - \rho_{e_p} \quad (1.4)$$

where ρ_{e_p} and θ_{e_p} are respectively the range and DOD of the pth target with respect to the reference transmitting antenna indexed by m_o, and d_e is the inter-element spacing in the transmitting ULA. Similarly, $\delta_{r_{(p,n)}}$ is the difference between the distance traveled by the reflected signal from the pth target to the nth receiving antenna and the distance traveled by the reflected signal from the pth target to the n_oth receiving antenna, which can be expressed for ULA as

$$\delta_{r_{(p,n)}} = \delta_{r_n}(\rho_{r_p}, \theta_{r_p}) = \sqrt{\rho_{r_p}^2 + (n - n_o)^2\, d_r^2 - 2\,(n - n_o)\, d_r\, \rho_{r_p} \cos\left(\theta_{r_p}\right)} - \rho_{r_p} \quad (1.5)$$

where ρ_{r_p} and θ_{r_p} are, respectively, the range and DOA of the pth target with respect to the reference receiving antenna indexed by n_o and d_r is the inter-element spacing in the receiving ULA [23].

Additionally, let

$$\boldsymbol{\delta}_{e_p} = \boldsymbol{\delta}_{\boldsymbol{e}}(\rho_{e_p}, \theta_{e_p}) = \left[\delta_{e_1}(\rho_{e_p}, \theta_{e_p}), \delta_{e_2}(\rho_{e_p}, \theta_{e_p}), \cdots, \delta_{e_M}(\rho_{e_p}, \theta_{e_p})\right]^T \in \mathbb{R}^M \tag{1.6}$$

and

$$\boldsymbol{\delta}_{r_p} = \boldsymbol{\delta}_{\boldsymbol{r}}(\rho_{r_p}, \theta_{r_p}) = \left[\delta_{r_1}(\rho_{r_p}, \theta_{r_p}), \delta_{r_2}(\rho_{r_p}, \theta_{r_p}), \cdots, \delta_{r_N}(\rho_{r_p}, \theta_{r_p})\right]^T \in \mathbb{R}^N. \tag{1.7}$$

$\delta_{e_m}(\rho_{e_p}, \theta_{e_p})$ and $\delta_{r_n}(\rho_{r_p}, \theta_{r_p})$ can be called as accurate relative propagation path lengths, which make $\boldsymbol{\delta}_{\boldsymbol{e}}(\rho_{e_p}, \theta_{e_p})$ and $\boldsymbol{\delta}_{\boldsymbol{r}}(\rho_{r_p}, \theta_{r_p})$, the accurate relative propagation path length vectors respectively.

1.3 Modeling of Near Field Targets

Based on the target-array distance with respect to the array's aperture, the target can be considered to lie in near or far field region of that array. The limit between near and far fields is defined by Fraunhofer distance in radar signal processing.

1.3.1 Fresnel Region

The lower and upper limit of the Fresnel region of an array can respectively be calculated as [2, 102]

$$\breve{F} = 0.62\sqrt{D^3/\lambda} \tag{1.8}$$

and

$$\overline{F} = 2\,D^2/\lambda \tag{1.9}$$

where D is the largest dimension of the array shown in Figure 1.2. Bistatic MIMO system has two arrays, therefore, we have three near field regions. Two near field regions correspond to the arrays and one to the whole system. This work mostly focuses on the shared near field regions of the arrays. For the transmitting and receiving ULAs, $D = (M-1)\,d_e$ and $D = (N-1)\,d_r$ respectively. Let $\breve{F}_e$ and $\overline{F}_e$ be the lower and upper limits of the Fresnel region of the transmitting array and $\breve{F}_r$ and $\overline{F}_r$ be the lower and upper limits of the Fresnel region of the receiving array respectively.

1.3.2 Wavefront Approximation in Near Field

Expressions in (1.4) and (1.5) are based on spherical wavefront which is often approximated to simplify the signal model. Since, (1.4) and (1.5) are similar expressions, the approximation processes of $\delta_{e_{(m,p)}}$ and $\delta_{r_{(p,n)}}$ are same. Hence, we only elaborate approximation in $\delta_{r_{(p,n)}}$ in the following.

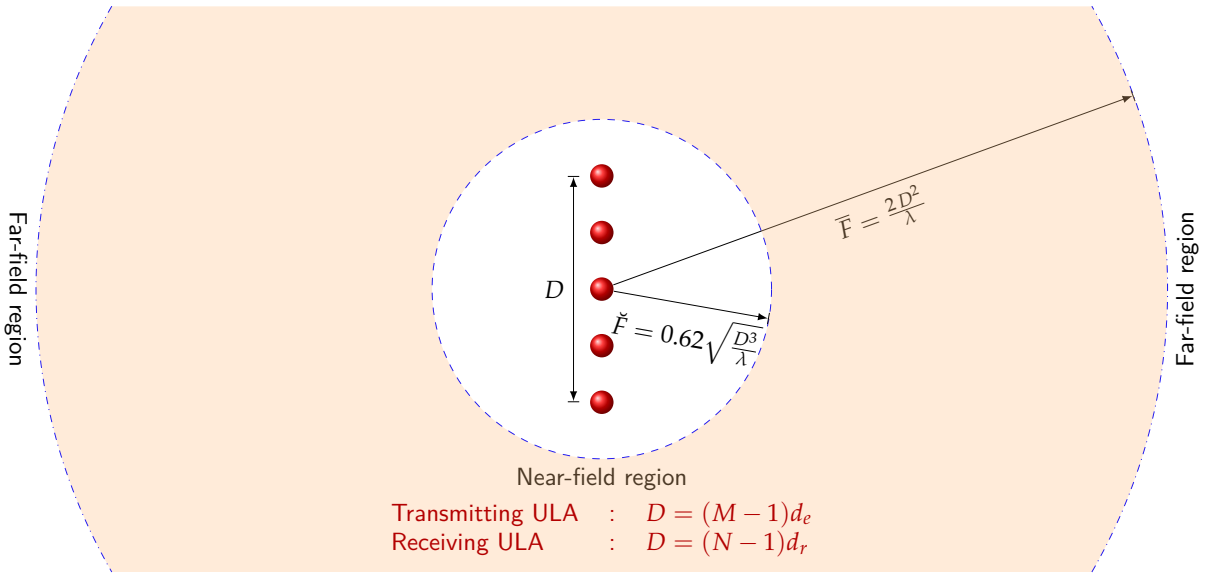

Figure 1.2 – Fresnel region.

Equation (1.5) can be rewritten as

$$\delta_{r_{(p,n)}} = \rho_{r_p}\left(\sqrt{1+\vartheta_{r_{(p,n)}}} - 1\right) \tag{1.10}$$

where

$$\vartheta_{r_{(p,n)}} = \frac{(n-n_o)^2\, d_r^2}{\rho_{r_p}^2} - 2\,\frac{(n-n_o)\, d_r}{\rho_{r_p}}\cos\left(\theta_{r_p}\right). \tag{1.11}$$

The square root term of (1.10) is usually approximated by using Maclaurin series (Taylor series centered at the origin), given by [2, 23, 24]

$$\sqrt{1+\vartheta_{r_{(p,n)}}} = 1 + \frac{1}{2}\vartheta_{r_{(p,n)}} - \frac{1}{8}\vartheta_{r_{(p,n)}}^2 + \frac{1}{16}\vartheta_{r_{(p,n)}}^3 + \cdots, \qquad \forall\, |\vartheta_{r_{(p,n)}}| < 1 \tag{1.12}$$

$$\begin{aligned} &= 1 + \frac{1}{2}\left[\frac{(n-n_o)^2\, d_r^2}{\rho_{r_p}^2} - 2\,\frac{(n-n_o)\, d_r}{\rho_{r_p}}\cos\left(\theta_{r_p}\right)\right] \\ &\quad - \frac{1}{8}\left[4\,\frac{(n-n_o)^2\, d_r^2}{\rho_{r_p}^2}\cos^2\left(\theta_{r_p}\right) - 4\frac{(n-n_o)^3\, d_r^3}{\rho_{r_p}^3}\cos\left(\theta_{r_p}\right)\right. \\ &\quad \left. + \frac{(n-n_o)^4\, d_r^4}{\rho_{r_p}^4}\right] + \cdots \end{aligned} \tag{1.13}$$

$$= 1 - \frac{(n-n_o)\, d_r}{\rho_{r_p}}\cos\left(\theta_{r_p}\right) + \frac{(n-n_o)^2\, d_r^2}{2\,\rho_{r_p}^2}\sin^2\left(\theta_{r_p}\right) + \gamma_{r_{(p,n)}} \tag{1.14}$$

where $\gamma_{r_{(p,n)}}$ represents the remainder with higher degree terms.

The maximum positive and minimum negative values of $n - n_o$ can be obtained when $n_o = 1$ and $n_o = N$ at $n = N$ and $n = 1$ respectively. We have $\max\{(n - n_o)\} = N - 1$ and $\min\{(n - n_o)\} = 1 - N$. Also, $\vartheta_{r_{(p,n)}}$ is inversely proportional to ρ_{r_p}.

Therefore, $\vartheta_{r_{(p,n)}}$ achieves maximum value when $\rho_{r_p} = \breve{F}_r$. Figure 1.3 and Figure 1.4 show the variation of $|\vartheta_{r_{(p,n)}}|$ for the two cases at $d_r = \lambda/2$. It can be observed that the curves in the two figures are mirror images of each other at $\theta_{r_p} = 90°$. Thus, exploring $n - n_o > 0$ situation is sufficient to understand $n - n_o < 0$ situation. For the completeness, Figure 1.5 shows the variation of $|\vartheta_{r_{(p,n)}}|$ with θ_{r_p} for some vital values of N when $d_r = \lambda/4$. Form the figures and (1.11), we can say that $|\vartheta_{r_{(p,n)}}|$ is maximum at $\rho_{r_p} = \breve{F}_r$ with $\theta_{r_p} = 180°$ and $\max\{(n - n_o)\}$ or $\theta_{r_p} = 0°$ and $\min\{(n - n_o)\}$.

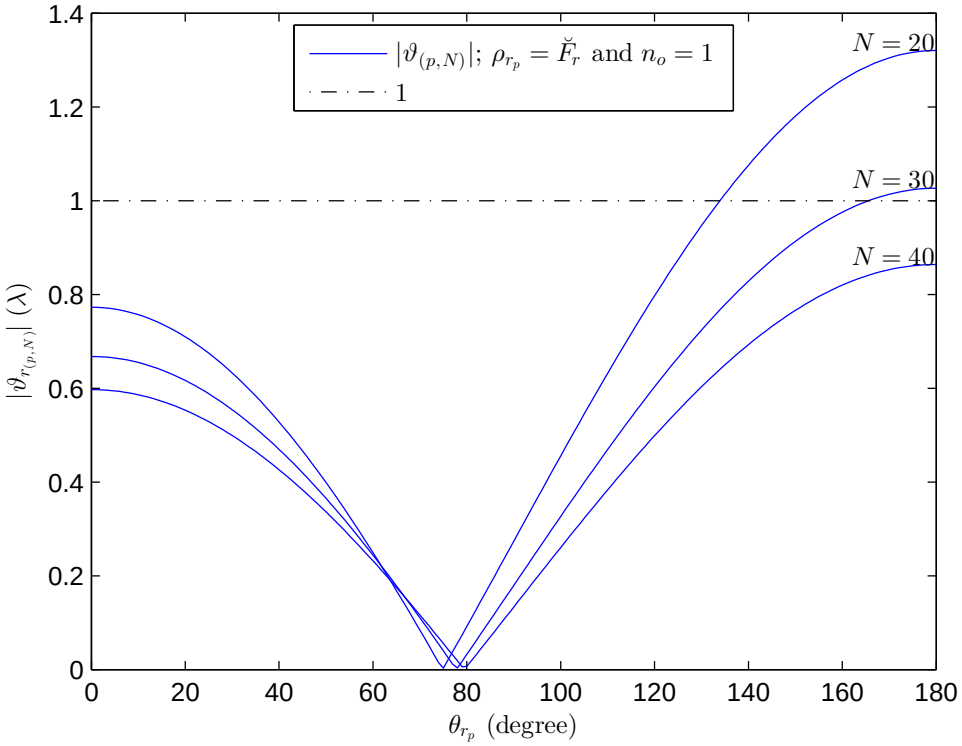

Figure 1.3 – Variation of $|\vartheta_{r_{(p,N)}}|$ with respect to θ_{r_p} when $\rho_{r_p} = \breve{F}_r$, $n_o = 1$, and $d_r = \lambda/2$.

The Maclaurin series in (1.12) converges only if $|\vartheta_{r_{(p,n)}}| < 1$ or

$$-1 < \frac{(n - n_o)^2 d_r^2}{\rho_{r_p}^2} - 2\frac{(n - n_o) d_r}{\rho_{r_p}} \cos\left(\theta_{r_p}\right) < 1 \tag{1.15}$$

If we consider $n - n_o > 0$ then with few operations of inequality, we can write

$$\frac{(n - n_o)^2 d_r^2 + \rho_{r_p}^2}{2(n - n_o) d_r \rho_{r_p}} > \cos\left(\theta_{r_p}\right) > \frac{(n - n_o)^2 d_r^2 - \rho_{r_p}^2}{2(n - n_o) d_r \rho_{r_p}} \tag{1.16}$$

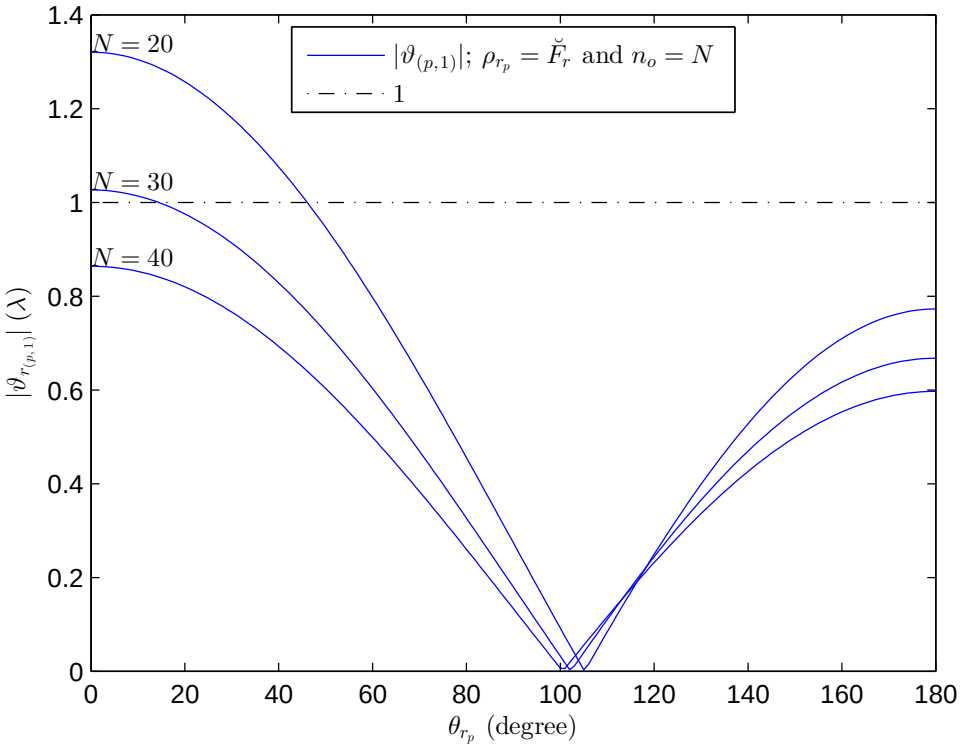

Figure 1.4 – Variation of $|\vartheta_{r_{(p,1)}}|$ with respect to θ_{r_p} when $\rho_{r_p} = \breve{F}_r$, $n_o = N$, and $d_r = \lambda/2$.

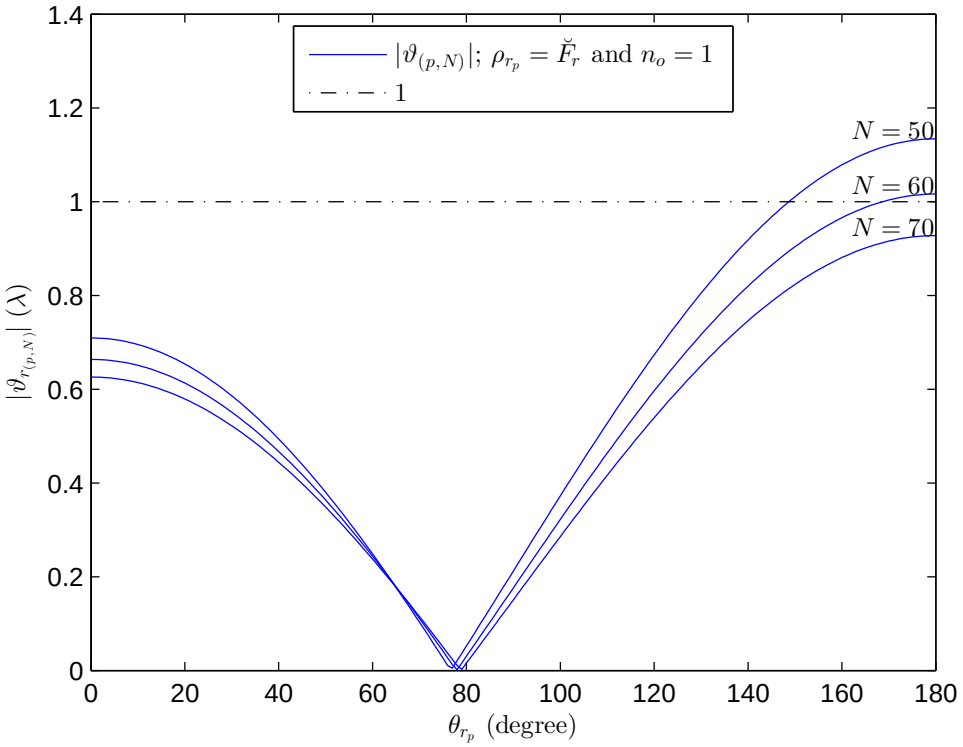

Figure 1.5 – Variation of $|\vartheta_{r_{(p,N)}}|$ with respect to θ_{r_p} when $\rho_{r_p} = \breve{F}_r$, $n_o = 1$, and $d_r = \lambda/4$.

which implies that to keep convergence of (1.12), it is necessary that

$$\frac{(n-n_o)^2 d_r^2 + \rho_{r_p}^2}{2(n-n_o) d_r \rho_{r_p}} > \max\left\{\cos\left(\theta_{r_p}\right)\right\} \tag{1.17}$$

and

$$\frac{(n-n_o)^2 d_r^2 - \rho_{r_p}^2}{2(n-n_o) d_r \rho_{r_p}} < \min\left\{\cos\left(\theta_{r_p}\right)\right\}. \tag{1.18}$$

As we know that $-1 \leq \cos\left(\theta_{r_p}\right) \leq 1$. Therefore, we can say

$$\rho_{r_p}^2 + (n-n_o)^2 d_r^2 > 2(n-n_o) d_r \rho_{r_p} \tag{1.19}$$

and

$$\rho_{r_p}^2 - (n-n_o)^2 d_r^2 > 2(n-n_o) d_r \rho_{r_p}. \tag{1.20}$$

Furthermore, $\rho_{r_p}^2 + (n-n_o)^2 d_r^2 > \rho_{r_p}^2 - (n-n_o)^2 d_r^2$, thus, inequality (1.20) is a sufficient condition for the convergence of (1.12). This inequality can further be used to calculate the minimum value of range for which the Fresnel approximation is valid. To obtain that, we need to rewrite (1.20) as

$$\left(\rho_{r_p} - (1+\sqrt{2})(n-n_o) d_r\right)\left(\rho_{r_p} - (1-\sqrt{2})(n-n_o) d_r\right) > 0. \tag{1.21}$$

In this inequality, $\rho_{r_p} - (1-\sqrt{2})(n-n_o) d_r > 0$ when $n - n_o > 0$, therefore $\rho_{r_p} > (1+\sqrt{2})(n-n_o) d_r$ is a necessary condition for the convergence of (1.12).

In the Fresnel region with Fresnel approximation, $\rho_{r_p} \geq \breve{F}_r > 0$ and $\rho_{r_p} > (1+\sqrt{2})(n-n_o) d_r$ for $n - n_o > 0$. Figure 1.6 and Figure 1.7 show these bounds as a function of N for d_r equal to $\lambda/2$ and $\lambda/4$ respectively. As compared to $\breve{F}_r$, $(1+\sqrt{2})(n-n_o) d_r$ is linear and grows slowly with the increase of the number of array elements. This linear bound can not be ignored in the arrays with small aperture. The similar conclusion can be made for the transmitting array.

For $n - n_o < 0$, the inequality (1.15) can be rearranged as

$$\frac{(n-n_o)^2 d_r^2 + \rho_{r_p}^2}{2(n-n_o) d_r \rho_{r_p}} < \cos\left(\theta_{r_p}\right) < \frac{(n-n_o)^2 d_r^2 - \rho_{r_p}^2}{2(n-n_o) d_r \rho_{r_p}}. \tag{1.22}$$

From the approach similar to $n - n_o > 0$ situation, we can say that $\rho_{r_p}^2 - (n-n_o)^2 d_r^2 > -2(n-n_o) d_r \rho_{r_p}$ is a necessary condition for the convergence of (1.12) when $n - n_o < 0$, which gives $\rho_{r_p} > -(1+\sqrt{2})(n-n_o) d_r$. Finally, we can simply say that for the convergence of (1.12),

$$\rho_{r_p} > (1+\sqrt{2})|n-n_o| d_r \tag{1.23}$$

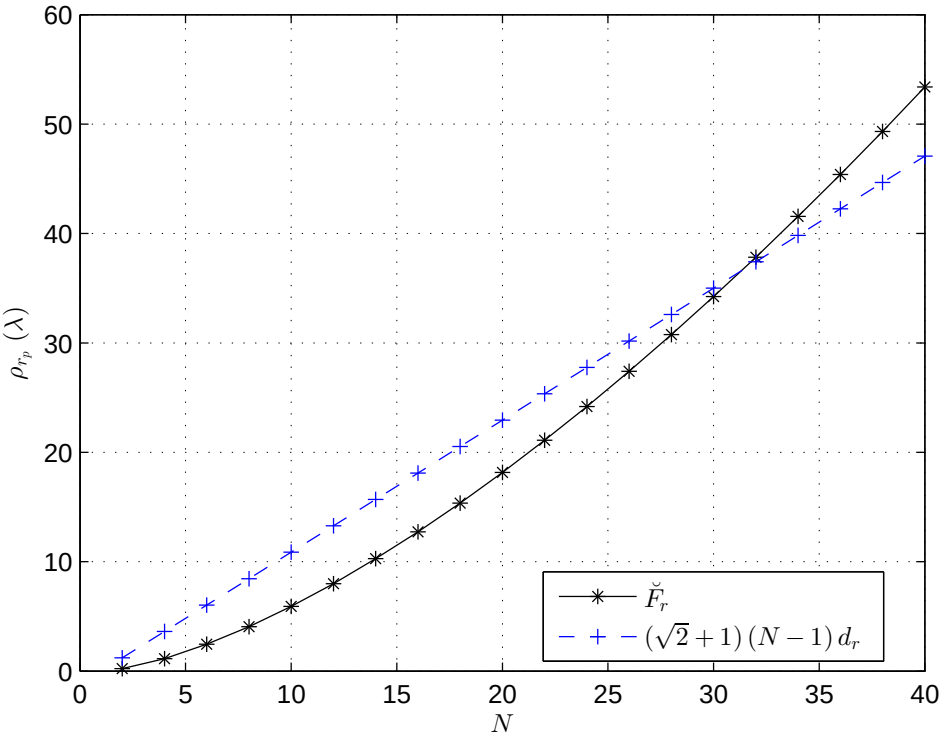

Figure 1.6 – Lower bounds of ρ_{r_p} as a function of N when $d_r = \lambda/2$.

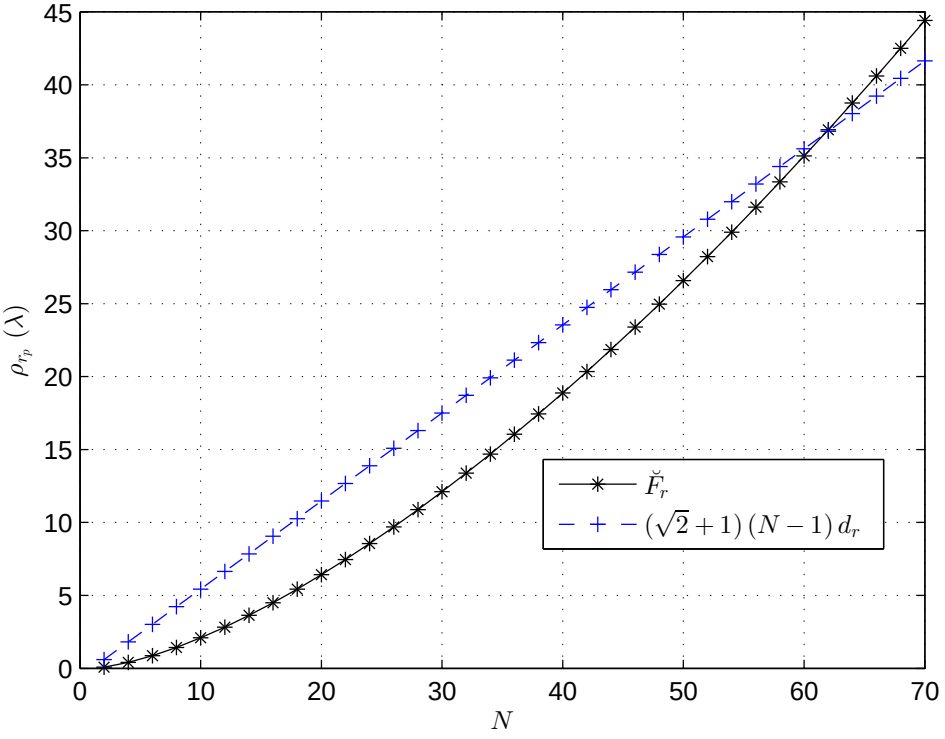

Figure 1.7 – Lower bounds of ρ_{r_p} as a function of N when $d_r = \lambda/4$.

is the necessary condition for any possible value of n. The maximum positive and minimum negative values of $n - n_o$ can be combined as $\max\{|n - n_o|\} = N - 1$. By using this in (1.23) at $\rho_{r_p} = \check{F}_r$, we can get

$$N > \lambda((1+\sqrt{2})/0.62)^2/d_r \tag{1.24}$$

which when substituted with $d_r = \lambda/2$ and $d_r = \lambda/4$ gives $N > 30.3248$ and $N > 60.6496$. The same results can be graphically validated from Figure 1.3, Figure 1.6, and Figure 1.7. Here, the value of N decreases with the increase of ρ_{r_p} and this constraint totally vanishes when $\rho_{r_p} > (1+\sqrt{2})(N-1)\,d_r$.

In far field situation, only the first degree term of (1.14) is used [41,97], which gives $\delta_{r_{(p,n)}} \approx -(n-n_o)\,d_r\,\cos\left(\theta_{r_p}\right)$. While in case of near field, where the second degree term is also used, the approximated relative path length is given by [2,3,23,24]

$$\widetilde{\delta}_{r_{(p,n)}} = \widetilde{\delta}_{r_n}(\rho_{r_p}, \theta_{r_p}) = -(n-n_o)\,\omega_{r_p} + (n-n_o)^2\,\phi_{r_p} \tag{1.25}$$

$$= \delta_{r_{(p,n)}} - \rho_{r_p}\,\gamma_{r_{(p,n)}} \tag{1.26}$$

where $\omega_{r_p} = d_r\,\cos(\theta_{r_p})$ and $\phi_{r_p} = d_r^2\,\sin^2(\theta_{r_p})/(2\,\rho_{r_p})$. Similarly, $\delta_{e_{(m,p)}}$ is approximated as

$$\widetilde{\delta}_{e_{(m,p)}} = \widetilde{\delta}_{e_m}(\rho_{e_p}, \theta_{e_p}) = -(m-m_o)\,\omega_{e_p} + (m-m_o)^2\,\phi_{e_p} \tag{1.27}$$

where $\omega_{e_p} = d_e\,\cos(\theta_{e_p})$ and $\phi_{e_p} = d_e^2\,\sin^2(\theta_{e_p})/(2\,\rho_{e_p})$.

Let $\widetilde{\boldsymbol{a}}_{\boldsymbol{e}_p}$ and $\widetilde{\boldsymbol{a}}_{\boldsymbol{r}_p}$ be the approximated (biased) directional vectors of the pth target associated with (1.27) and (1.25) respectively, which can be expressed as

$$\widetilde{\boldsymbol{a}}_{\boldsymbol{e}_p} = \widetilde{\boldsymbol{a}}_{\boldsymbol{e}}(\rho_{e_p}, \theta_{e_p}) = \left[\widetilde{a}_{e_{(1,p)}}, \cdots, \widetilde{a}_{e_{(m_o-1,p)}}, 1, \widetilde{a}_{e_{(m_o+1,p)}}, \cdots, \widetilde{a}_{e_{(M,p)}}\right]^T \tag{1.28}$$

and

$$\widetilde{\boldsymbol{a}}_{\boldsymbol{r}_p} = \widetilde{\boldsymbol{a}}_{\boldsymbol{r}}(\rho_{r_p}, \theta_{r_p}) = \left[\widetilde{a}_{r_{(p,1)}}, \cdots, \widetilde{a}_{r_{(p,n_o-1)}}, 1, \widetilde{a}_{r_{(p,n_o+1)}}, \cdots, \widetilde{a}_{r_{(p,N)}}\right]^T \tag{1.29}$$

where $\widetilde{a}_{e_{(m,p)}} = \exp\left(-j\,2\,\pi\,\widetilde{\delta}_{e_{(m,p)}}/\lambda\right)$ and $\widetilde{a}_{r_{(p,n)}} = \exp\left(-j\,2\,\pi\,\widetilde{\delta}_{r_{(p,n)}}/\lambda\right)$. Further, we can rewrite the received matched filtered signal vector, in (1.1), for the approximated model as

$$\widetilde{\boldsymbol{y}}(t) = \widetilde{\boldsymbol{A}}\,\boldsymbol{s}(t) + \boldsymbol{w}(t) \tag{1.30}$$

with $\widetilde{\boldsymbol{A}} = \widetilde{\boldsymbol{A}}_{\boldsymbol{e}} \boxdot \widetilde{\boldsymbol{A}}_{\boldsymbol{r}}$ where $\widetilde{\boldsymbol{A}}_{\boldsymbol{e}} = [\widetilde{\boldsymbol{a}}_{\boldsymbol{e}_1}, \widetilde{\boldsymbol{a}}_{\boldsymbol{e}_2}, \cdots, \widetilde{\boldsymbol{a}}_{\boldsymbol{e}_P}]$ and $\widetilde{\boldsymbol{A}}_{\boldsymbol{r}} = [\widetilde{\boldsymbol{a}}_{\boldsymbol{r}_1}, \widetilde{\boldsymbol{a}}_{\boldsymbol{r}_2}, \cdots, \widetilde{\boldsymbol{a}}_{\boldsymbol{r}_P}]$.

Similar to (1.6) and (1.7), let

$$\widetilde{\boldsymbol{\delta}}_{\boldsymbol{e}_p} = \widetilde{\boldsymbol{\delta}}_{\boldsymbol{e}}(\rho_{e_p}, \theta_{e_p}) = \left[\widetilde{\delta}_{e_1}(\rho_{e_p}, \theta_{e_p}), \widetilde{\delta}_{e_2}(\rho_{e_p}, \theta_{e_p}), \cdots, \widetilde{\delta}_{e_M}(\rho_{e_p}, \theta_{e_p})\right]^T \in \mathbb{R}^M \tag{1.31}$$

and

$$\widetilde{\boldsymbol{\delta}}_{\boldsymbol{r}_p} = \widetilde{\boldsymbol{\delta}}_{\boldsymbol{r}}(\rho_{r_p}, \theta_{r_p}) = \left[\widetilde{\delta}_{r_1}(\rho_{r_p}, \theta_{r_p}), \widetilde{\delta}_{r_2}(\rho_{r_p}, \theta_{r_p}), \cdots, \widetilde{\delta}_{r_N}(\rho_{r_p}, \theta_{r_p})\right]^T \in \mathbb{R}^N. \tag{1.32}$$

Further, we can also write

$$\widetilde{\boldsymbol{\delta}}_{\boldsymbol{e}_p} = \widetilde{\boldsymbol{\delta}}_{\boldsymbol{e}}(\rho_{e_p}, \theta_{e_p}) = \widetilde{\boldsymbol{\delta}}_{\boldsymbol{e}}(\omega_{e_p}, \phi_{e_p}) = \underline{\boldsymbol{M}} \begin{bmatrix} \omega_{e_p} \\ \phi_{e_p} \end{bmatrix} \tag{1.33}$$

and

$$\widetilde{\boldsymbol{\delta}}_{\boldsymbol{r}_p} = \widetilde{\boldsymbol{\delta}}_{\boldsymbol{r}}(\rho_{r_p}, \theta_{r_p}) = \widetilde{\boldsymbol{\delta}}_{\boldsymbol{r}}(\omega_{r_p}, \phi_{r_p}) = \underline{\boldsymbol{N}} \begin{bmatrix} \omega_{r_p} \\ \phi_{r_p} \end{bmatrix} \tag{1.34}$$

where

$$\underline{\boldsymbol{M}} = \begin{bmatrix} -(1-m_o) & -(2-m_o) & \cdots & 1 & 0 & -1 & \cdots & -(M-m_o) \\ (1-m_o)^2 & (2-m_o)^2 & \cdots & 1 & 0 & 1 & \cdots & (M-m_o)^2 \end{bmatrix}^T \in \mathbb{R}^{M\times 2} \tag{1.35}$$

and

$$\underline{\boldsymbol{N}} = \begin{bmatrix} -(1-n_o) & -(2-n_o) & \cdots & 1 & 0 & -1 & \cdots & -(N-n_o) \\ (1-n_o)^2 & (2-n_o)^2 & \cdots & 1 & 0 & 1 & \cdots & (N-n_o)^2 \end{bmatrix}^T \in \mathbb{R}^{N\times 2}. \tag{1.36}$$

1.3.3 Symmetric Arrays

It can be observed from the existing work on near field sources localization that most of the methods use symmetric arrays [2, 3, 23, 24]. Here, symmetry is in the relative indexes of the antennas with respect to the reference antenna in an array. Mathematically, we can use the following constraints to make the transmitting and receiving arrays of a bistatic MIMO system symmetric.

1. $M \in \{2\breve{M}+1 : \breve{M} \in \mathbb{N}_1\}$
2. $N \in \{2\breve{N}+1 : \breve{N} \in \mathbb{N}_1\}$
3. $m_o = (M+1)/2$
4. $n_o = (N+1)/2$

Like Figure 1.6 and Figure 1.7, Figure 1.8 and Figure 1.9 are drawn for the symmetric arrays. In a symmetric receiving array, n_o is always in the middle of the arrays, therefore the maximum positive and minimum negative values coexist in the same array which are $\breve{N}$ and $-\breve{N}$ respectively.

In the figures, it can be observed that the linear bound is not as dominating as in the case of the asymmetric arrays in Figure 1.6 and Figure 1.7. The reason is that $\max\{|n - n_o|\} = \breve{N} < N-1$. Like (1.24), we can also write $\breve{N} > \lambda((1+\sqrt{2})/0.62)^2/(8\,d_r)$ for the

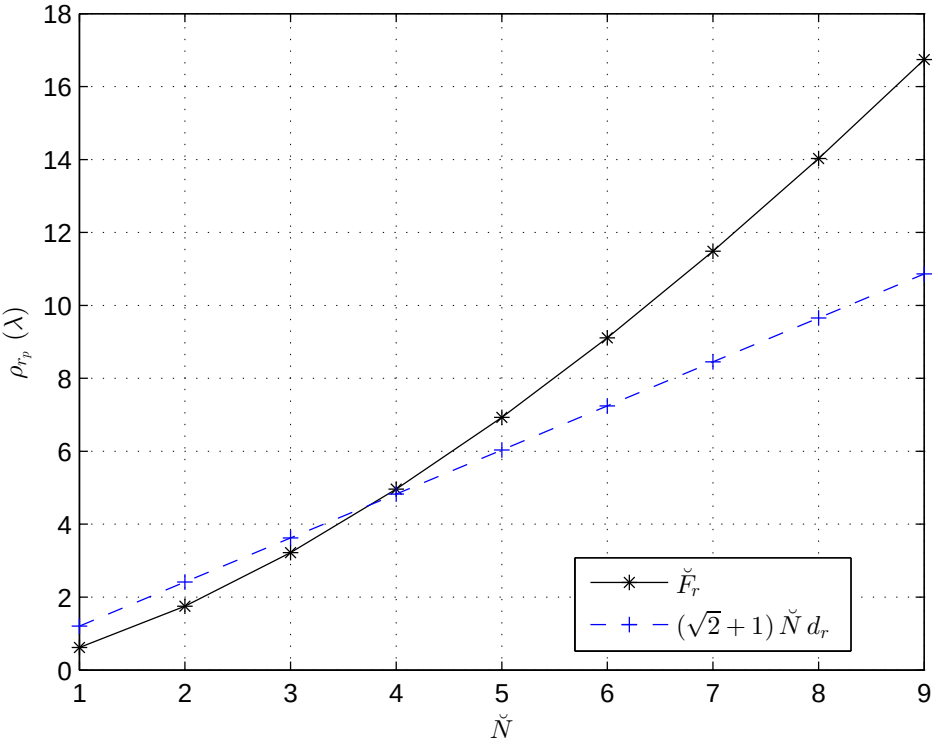

Figure 1.8 – Lower bounds of ρ_{r_p} as a function of $\breve{N}$ when $d_r = \lambda/2$ in a symmetric array.

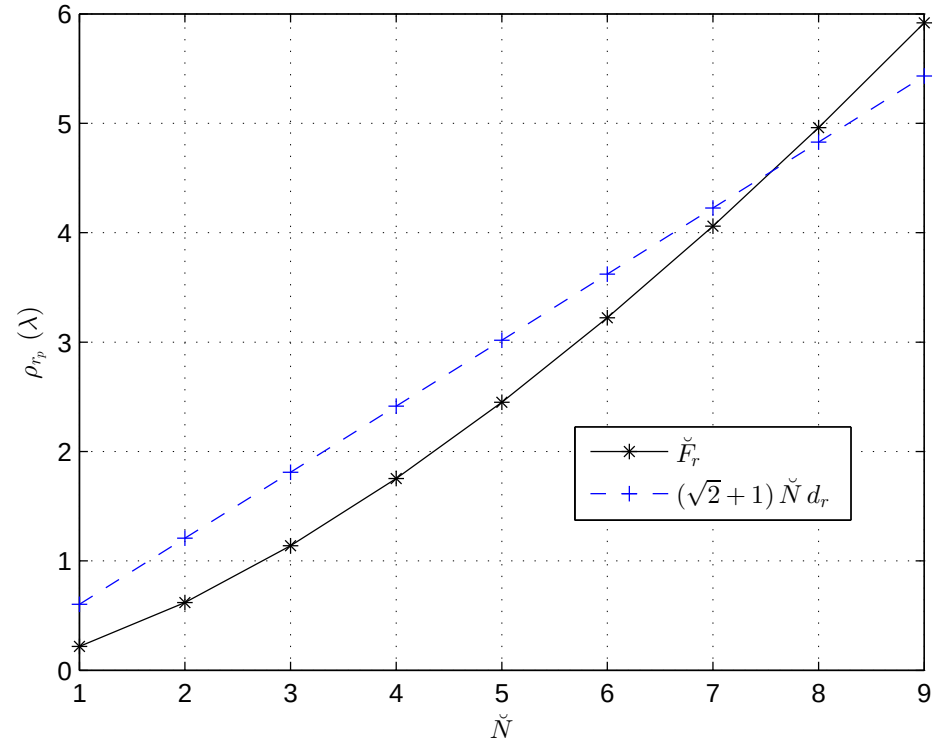

Figure 1.9 – Lower bounds of ρ_{r_p} as a function of $\breve{N}$ when $d_r = \lambda/4$ in a symmetric array.

symmetric array which give $\check{N} > 3.7906$ and $\check{N} > 7.5812$ for $d_r = \lambda/2$ and $d_r = \lambda/4$ respectively that can also be observed in Figure 1.8 and Figure 1.9. Throughout this thesis, we consider that the convergence condition of (1.12) is always satisfied.

1.4 Signal Model in Cartesian Coordinates System

Near field target localization using a bistatic MIMO system with ULAs requires the estimation of four location parameters, viz. DOD, DOA, and the distances from a target to the transmitting and receiving arrays [1]. However, in 3D space, three parameters are enough to define a location. In other words, the four location parameters have some redundancy. As a result, we remodel the directional vectors using three Cartesian coordinates. However, to do so, we need to assign a position vector to every antenna in transmitting and receiving arrays. Since, we are dealing with ULAs, the unit vector along the axis of the array and the position vector of its reference antenna are sufficient to obtain the position vectors of the remaining antennas of that array. Let $\boldsymbol{e_o}$ and $\boldsymbol{r_o}$ be the position vectors of the reference transmitting and receiving antennas respectively with respect to the origin of the Cartesian coordinates system and $\boldsymbol{d_{c_e}}$ and $\boldsymbol{d_{c_r}}$ are the unit vectors along the axes of the transmitting and receiving ULAs respectively.

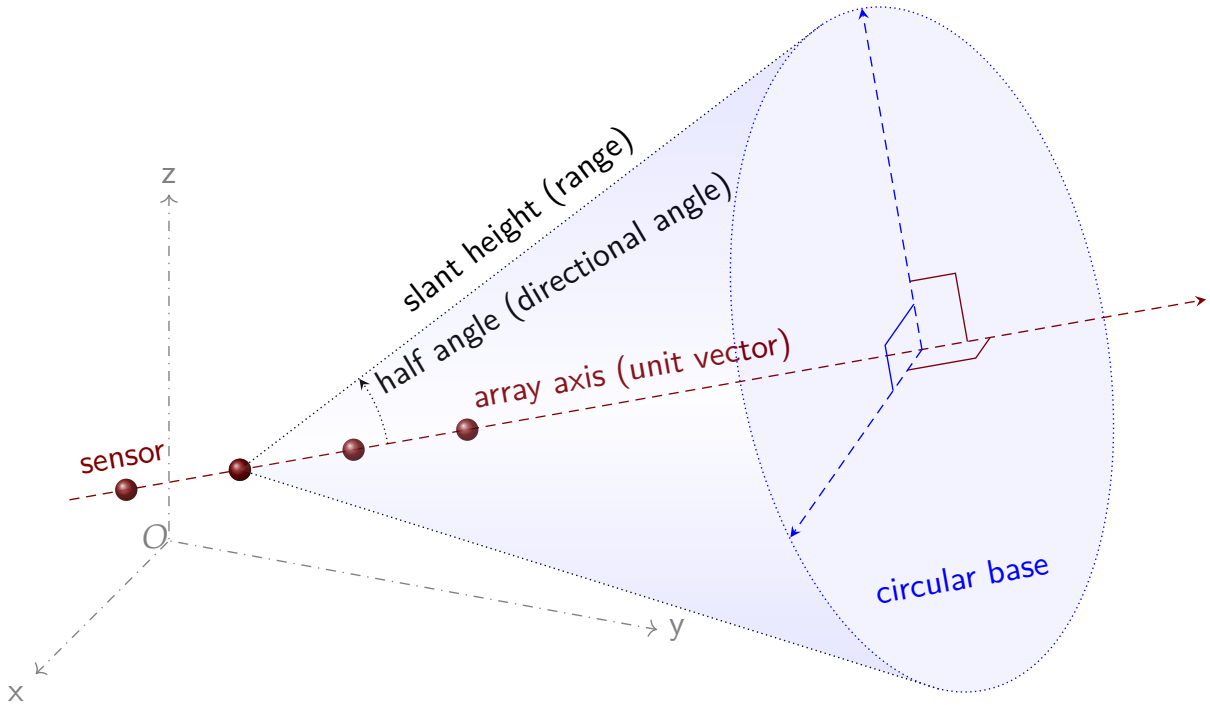

Figure 1.10 – Cone

In 3D space, the range and directional angle of a target with respect to a linear array make a circle related to the base of a cone, shown in Figure 1.10, with the range as its slant height and the directional angle as its half angle. In the bistatic case, we have two

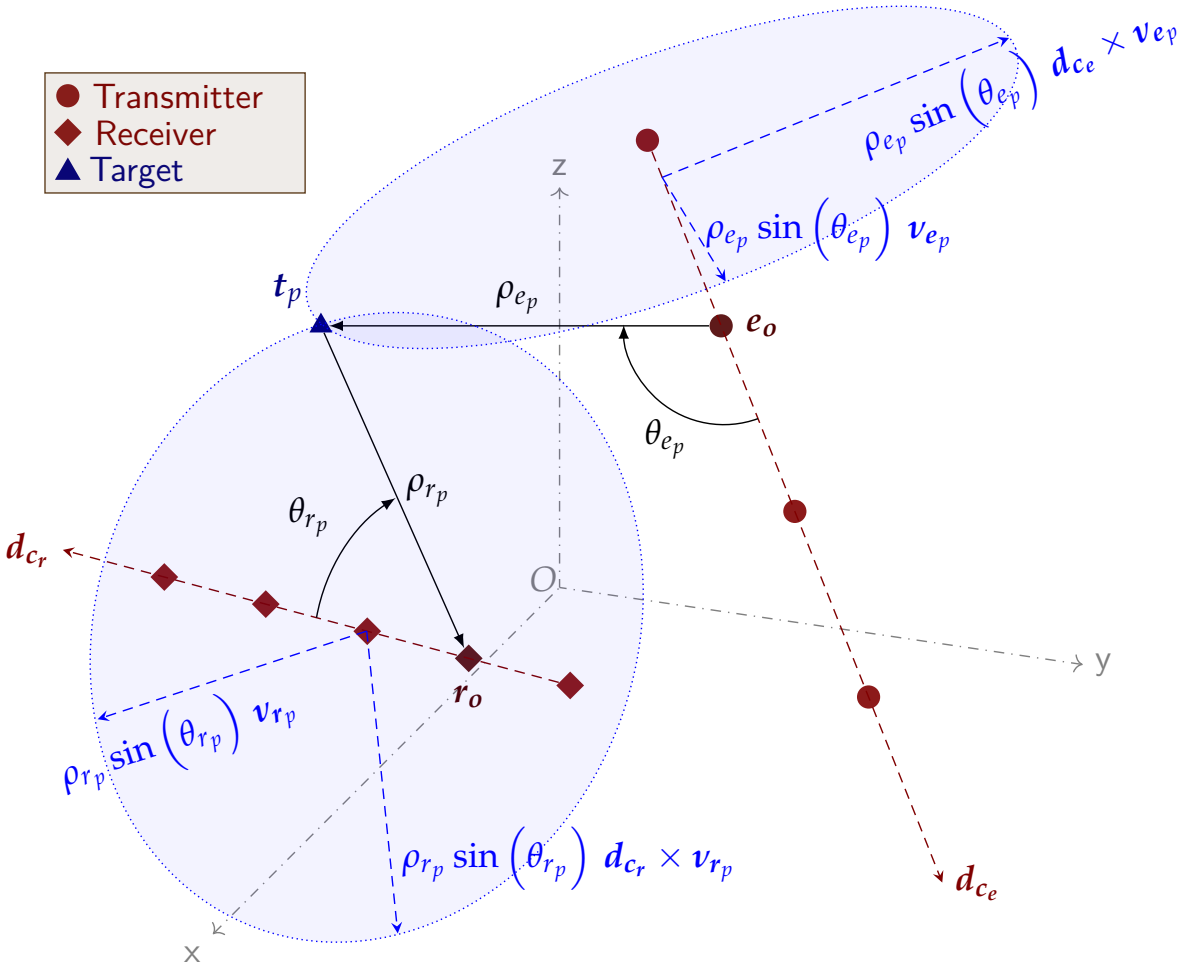

Figure 1.11 – A bistatic MIMO radar system with linear arrays.

such circles (shown in Figure 1.11). The target is located at the intersection of these two circles. In the figure, $\boldsymbol{v}_{e_p}$ and $\boldsymbol{v}_{r_p}$ are unit vectors on the planes of the respective circles. The parametric equations of the circles can be written as

$$\boldsymbol{\psi}_{e_p}(\varphi_e) = \rho_{e_p} \sin\left(\theta_{e_p}\right) \left[\cos(\varphi_e)\, \boldsymbol{v}_{e_p} + \sin(\varphi_e)\, \boldsymbol{d}_{c_e} \times \boldsymbol{v}_{e_p}\right] + \rho_{e_p} \cos\left(\theta_{e_p}\right) \boldsymbol{d}_{c_e} + \boldsymbol{e_o} \tag{1.37}$$

and

$$\boldsymbol{\psi}_{r_p}(\varphi_r) = \rho_{r_p} \sin\left(\theta_{r_p}\right) \left[\cos(\varphi_r)\, \boldsymbol{v}_{r_p} + \sin(\varphi_r)\, \boldsymbol{d}_{c_r} \times \boldsymbol{v}_{r_p}\right] + \rho_{r_p} \cos\left(\theta_{r_p}\right) \boldsymbol{d}_{c_r} + \boldsymbol{r_o} \tag{1.38}$$

where $\times$ denotes the cross-product operation between two vectors; $\boldsymbol{\psi}_{e_p}(\varphi_e)$ and $\boldsymbol{\psi}_{r_p}(\varphi_r)$ are the position vectors of a point on the respective circles at φ_e and φ_r, respectively. The equation parameters φ_e and φ_r independently vary from 0 to 2π rad to completely sweep the respective circles.

Let $\boldsymbol{t}_p = [x_{t_p}, y_{t_p}, z_{t_p}]^T$ be the position vector of the pth target. Then, the ranges and directional angles can be expressed in terms of the Cartesian coordinates as $\rho_{e_p} =$

$\|\boldsymbol{t}_p - \boldsymbol{e_o}\|_F$, $\rho_{r_p} = \|\boldsymbol{t}_p - \boldsymbol{r_o}\|_F$, $\theta_{e_p} = \arccos[(\boldsymbol{t}_p - \boldsymbol{e_o})^T \boldsymbol{d_{c_e}}/\rho_{e_p}]$, and $\theta_{r_p} = \arccos[(\boldsymbol{t}_p - \boldsymbol{r_o})^T \boldsymbol{d_{c_r}}/\rho_{r_p}]$. Thus, according to (1.2)–(1.5), $\boldsymbol{a_{e_p}}$ and $\boldsymbol{a_{r_p}}$ can respectively be determined by $\boldsymbol{t}_p$ as

$$a_{e_{(m,p)}} = a_{e_m}(\boldsymbol{t}_p) = \exp\left(-j\frac{2\pi}{\lambda}\left(\sqrt{\left\|\boldsymbol{t}_p - \boldsymbol{e_o}\right\|_F^2 + (m-m_o)^2 d_e^2 - 2(m-m_o) d_e \left(\boldsymbol{t}_p - \boldsymbol{e_o}\right)^T \boldsymbol{d_{c_e}}} - \left\|\boldsymbol{t}_p - \boldsymbol{e_o}\right\|_F\right)\right) \quad (1.39)$$

and

$$a_{r_{(p,n)}} = a_{r_n}(\boldsymbol{t}_p) = \exp\left(-j\frac{2\pi}{\lambda}\left(\sqrt{\left\|\boldsymbol{t}_p - \boldsymbol{r_o}\right\|_F^2 + (n-n_o)^2 d_r^2 - 2(n-n_o) d_r \left(\boldsymbol{t}_p - \boldsymbol{r_o}\right)^T \boldsymbol{d_{c_r}}} - \left\|\boldsymbol{t}_p - \boldsymbol{r_o}\right\|_F\right)\right). \quad (1.40)$$

1.5 Cramér-Rao Lower Bound (CRLB)

CRLB is a lower bound of the variance of an unknown parameter computed by a minimum variance unbiased estimator which serves as the benchmark to compare the performance of other estimation techniques used to estimate that unknown parameter from the signal containing it along with a random variable [113]. The variance corresponding to the CRLB is given by the inverse of the Fischer information. In our case, we have three or four unknown parameters corresponding to each target. Therefore, the CRLBs of these parameters are given by the diagonal elements of the inverse of the Fischer information matrix.

CRLB for the ranges and DOA of multiple near field sources has already been derived in [24] from [114]. We can directly use their closed form expression by making some minor modifications to adapt the four location parameters of each target due to the use of a bistatic MIMO system. The submatrix of the inverse of the Fischer information matrix corresponding to the desired parameters (i.e. the four location parameters of P targets) can be expressed as [24]

$$\text{CRLB}(\boldsymbol{\eta}) = \frac{\sigma_w^2}{2L}\left[\Re\left\{\left(\mathring{\boldsymbol{A}}^H \boldsymbol{\Pi}_{\boldsymbol{A}}^{\perp} \mathring{\boldsymbol{A}}\right) \odot \left[\underline{\mathbf{1}}_4 \otimes \left(\boldsymbol{R_s} \boldsymbol{A}^H \boldsymbol{R}^{-1} \boldsymbol{A} \boldsymbol{R_s}\right)^T\right]\right\}\right]^{-1} \quad (1.41)$$

where $\text{CRLB}(\boldsymbol{\eta}) \in \mathbb{R}^{4P\times 4P}$, $\boldsymbol{\eta} = [\rho_{e_1}, \cdots, \rho_{e_P}, \theta_{e_1}, \cdots, \theta_{e_P}, \rho_{r_1}, \cdots, \rho_{r_P}, \theta_{r_1}, \cdots, \theta_{r_P}]^T$ is the vector of the desired location parameters of P targets, L is the number of data samples, $\boldsymbol{R} = \boldsymbol{A}\boldsymbol{R_s}\boldsymbol{A}^H + \sigma_w^2 \boldsymbol{I}_{MN}$, $\boldsymbol{\Pi}_{\boldsymbol{A}}^{\perp} = \boldsymbol{I}_{MN} - \boldsymbol{A}\boldsymbol{A}^{\dagger}$, $\underline{\mathbf{1}}_4$ is the 4×4 matrix whose all

components are equal to 1, and

$$\mathring{\boldsymbol{A}} = [\partial(\boldsymbol{a}_{e_1} \otimes \boldsymbol{a}_{r_1})/\partial\rho_{e_1}, \cdots, \partial(\boldsymbol{a}_{e_P} \otimes \boldsymbol{a}_{r_P})/\partial\rho_{e_P}, \partial(\boldsymbol{a}_{e_1} \otimes \boldsymbol{a}_{r_1})/\partial\theta_{e_1}, \cdots, \partial(\boldsymbol{a}_{e_P} \otimes \boldsymbol{a}_{r_P})/\partial\theta_{e_P}, \partial(\boldsymbol{a}_{e_1} \otimes \boldsymbol{a}_{r_1})/\partial\rho_{r_1}, \cdots, \partial(\boldsymbol{a}_{e_P} \otimes \boldsymbol{a}_{r_P})/\partial\rho_{r_P}, \partial(\boldsymbol{a}_{e_1} \otimes \boldsymbol{a}_{r_1})/\partial\theta_{r_1}, \cdots, \partial(\boldsymbol{a}_{e_P} \otimes \boldsymbol{a}_{r_P})/\partial\theta_{r_P}]. \quad (1.42)$$

The main diagonal of (1.41) contains the lower bounds of all the location parameters in terms of variance for all the targets based on the accurate model. Let $\varepsilon(\eta_p)$ be the standard deviation of $\eta_p \in \{\rho_{e_p}, \theta_{e_p}, \rho_{r_p}, \theta_{r_p}\}$. The CRLB for the approximated model can simply be obtained by replacing the accurate directional vectors with the approximated directional vectors in (1.41) and (1.42). However, for the signal model with Cartesian coordinates, (1.41) changes to

$$\mathrm{CRLB}_c(\boldsymbol{\eta_c}) = \frac{\sigma_w^2}{2L}\left[\Re\left\{\left(\mathring{\boldsymbol{A}}_c^H \boldsymbol{\Pi}_A^{\perp} \mathring{\boldsymbol{A}}_c\right) \odot \left[\underline{\mathbf{1}}_3 \otimes \left(\boldsymbol{R_s}\, \boldsymbol{A}^H\, \boldsymbol{R}^{-1}\, \boldsymbol{A}\, \boldsymbol{R_s}\right)^T\right]\right\}\right]^{-1} \quad (1.43)$$

where $\mathrm{CRLB}_c(\boldsymbol{\eta_c}) \in \mathbb{R}^{3P\times 3P}$, $\boldsymbol{\eta_c} = [x_{t_1}, \cdots, x_{t_P}, y_{t_1}, \cdots, y_{t_P}, z_{t_1}, \cdots, z_{t_P}]^T$ is the vector of the desired Cartesian coordinates of P targets, $\underline{\mathbf{1}}_3$ is the 3×3 matrix of ones, and

$$\mathring{\boldsymbol{A}}_{\boldsymbol{c}} = [\partial(\boldsymbol{a}_{e_1} \otimes \boldsymbol{a}_{r_1})/\partial x_{t_1}, \cdots, \partial(\boldsymbol{a}_{e_P} \otimes \boldsymbol{a}_{r_P})/\partial x_{t_P}, \partial(\boldsymbol{a}_{e_1} \otimes \boldsymbol{a}_{r_1})/\partial y_{t_1}, \cdots, \partial(\boldsymbol{a}_{e_P} \otimes \boldsymbol{a}_{r_P})/\partial y_{t_P}, \partial(\boldsymbol{a}_{e_1} \otimes \boldsymbol{a}_{r_1})/\partial z_{t_1}, \cdots, \partial(\boldsymbol{a}_{e_P} \otimes \boldsymbol{a}_{r_P})/\partial z_{t_P}]. \quad (1.44)$$

The CRLBs of the Cartesian coordinates of the pth target can be combined as

$$\varepsilon(\boldsymbol{t}_p) = \sqrt{[\mathrm{diag}\{\mathrm{CRLB}_c(\boldsymbol{\eta_c})\}]_p + [\mathrm{diag}\{\mathrm{CRLB}_c(\boldsymbol{\eta_c})\}]_{P+p} + [\mathrm{diag}\{\mathrm{CRLB}_c(\boldsymbol{\eta_c})\}]_{2P+p}} \quad (1.45)$$

1.6 Conclusion

The signal models formulated in this chapter are going to serve as the starting point of the discussion of the methods in the coming chapters. In the next chapter, both the methods use Fresnel approximation based model. Consequently, the approximated model is used throughout the next chapter to discuss and analyze the methods.

2

Approximated Model Based Methods

In this chapter, we present an existing approximated model based method and we propose a new approximated model based method to locate the targets in the near field region of a bistatic MIMO system with symmetric ULAs. Since the both methods use the approximated model, we use the approximated signal model given in the previous chapter to describe the methods and CRLB expression with the approximated model parameters for the performance analysis of these methods.

2.1 Summary of [1]

In this section, we provide a summary of the method recently proposed in [1]. The received signal vector, $\widetilde{\boldsymbol{y}}(t)$ in (1.30), can also be expressed as $\widetilde{\boldsymbol{y}}(\boldsymbol{t}) = [\acute{\boldsymbol{y}}_1^T(t),\, \acute{\boldsymbol{y}}_2^T(t),\, \cdots,\, \acute{\boldsymbol{y}}_{m_o}^T(t),\, \cdots,\, \acute{\boldsymbol{y}}_M^T(t)]^T$ with

$$\acute{\boldsymbol{y}}_m(t) = \widetilde{\boldsymbol{A}}_{\boldsymbol{r}}\, \widetilde{\boldsymbol{D}}_m\, \boldsymbol{s}(t) + \acute{\boldsymbol{w}}_m(t) \tag{2.1}$$

where $\widetilde{\boldsymbol{D}}_m = \text{diag}\left\{\left[\widetilde{a}_{e_{(m,1)}},\, \widetilde{a}_{e_{(m,2)}},\, \cdots,\, \widetilde{a}_{e_{(m,P)}}\right]\right\}$ and $\acute{\boldsymbol{w}}_m(t)$ is the corresponding noise sub-vector. The method in [1] is a subspace based method which needs symmetric transmitting and receiving arrays with $d_e \leq \lambda/4$ and $d_r \leq \lambda/4$.

Along with the above constraints, the method in [1] uses $M = 5$ transmitting antennas to explain their method. Consequently, we also use the same number of transmitting antennas in its summary. The method begins with the construction of four cross covariance matrices, $\acute{\boldsymbol{R}}_m = \text{E}\{\acute{\boldsymbol{y}}_m(t)\, \acute{\boldsymbol{y}}_{m_o}^H(t)\}$ such that $m \neq m_o$. The four cross

covariance matrices are as follows:

$$\acute{\boldsymbol{R}}_1 = \mathrm{E}\{\acute{\boldsymbol{y}}_1(t)\,\acute{\boldsymbol{y}}_3^H(t)\} = \widetilde{\boldsymbol{A}}_r\,\widetilde{\boldsymbol{D}}_1\,\boldsymbol{R}_s\,\widetilde{\boldsymbol{A}}_r^H, \tag{2.2}$$

$$\acute{\boldsymbol{R}}_2 = \mathrm{E}\{\acute{\boldsymbol{y}}_2(t)\,\acute{\boldsymbol{y}}_3^H(t)\} = \widetilde{\boldsymbol{A}}_r\,\widetilde{\boldsymbol{D}}_2\,\boldsymbol{R}_s\,\widetilde{\boldsymbol{A}}_r^H, \tag{2.3}$$

$$\acute{\boldsymbol{R}}_4 = \mathrm{E}\{\acute{\boldsymbol{y}}_4(t)\,\acute{\boldsymbol{y}}_3^H(t)\} = \widetilde{\boldsymbol{A}}_r\,\widetilde{\boldsymbol{D}}_4\,\boldsymbol{R}_s\,\widetilde{\boldsymbol{A}}_r^H, \tag{2.4}$$

$$\acute{\boldsymbol{R}}_5 = \mathrm{E}\{\acute{\boldsymbol{y}}_5(t)\,\acute{\boldsymbol{y}}_3^H(t)\} = \widetilde{\boldsymbol{A}}_r\,\widetilde{\boldsymbol{D}}_5\,\boldsymbol{R}_s\,\widetilde{\boldsymbol{A}}_r^H \tag{2.5}$$

where $\mathrm{E}\{\acute{\boldsymbol{w}}_m(t)\,\acute{\boldsymbol{w}}_3^H(t)\} = \underline{\boldsymbol{0}}_N$ for $m \neq 3$ with $\underline{\boldsymbol{0}}_N$ beign a $N \times N$ square matrix containing only zeros. From the first two and last two pairs of the cross covariance matrices, we can write

$$\acute{\boldsymbol{R}}_1 = \widetilde{\boldsymbol{A}}_r\,\widetilde{\boldsymbol{D}}_1\,\widetilde{\boldsymbol{D}}_2^*\left(\widetilde{\boldsymbol{A}}_r^H\,\widetilde{\boldsymbol{A}}_r\right)^{-1}\widetilde{\boldsymbol{A}}_r^H\,\acute{\boldsymbol{R}}_2 \tag{2.6}$$

$$\acute{\boldsymbol{R}}_5 = \widetilde{\boldsymbol{A}}_r\,\widetilde{\boldsymbol{D}}_5\,\widetilde{\boldsymbol{D}}_4^*\left(\widetilde{\boldsymbol{A}}_r^H\,\widetilde{\boldsymbol{A}}_r\right)^{-1}\widetilde{\boldsymbol{A}}_r^H\,\acute{\boldsymbol{R}}_4 \tag{2.7}$$

which can further be written as

$$\acute{\boldsymbol{R}}_1\,\acute{\boldsymbol{R}}_2^+ = \widetilde{\boldsymbol{A}}_r\,\widetilde{\boldsymbol{D}}_1\,\widetilde{\boldsymbol{D}}_2^*\left(\widetilde{\boldsymbol{A}}_r^H\,\widetilde{\boldsymbol{A}}_r\right)^{-1}\widetilde{\boldsymbol{A}}_r^H\,\acute{\boldsymbol{R}}_2\,\acute{\boldsymbol{R}}_2^+ \tag{2.8}$$

$$\acute{\boldsymbol{R}}_5\,\acute{\boldsymbol{R}}_4^+ = \widetilde{\boldsymbol{A}}_r\,\widetilde{\boldsymbol{D}}_5\,\widetilde{\boldsymbol{D}}_4^*\left(\widetilde{\boldsymbol{A}}_r^H\,\widetilde{\boldsymbol{A}}_r\right)^{-1}\widetilde{\boldsymbol{A}}_r^H\,\acute{\boldsymbol{R}}_4\,\acute{\boldsymbol{R}}_4^+ \tag{2.9}$$

where $\acute{\boldsymbol{R}}_2\,\acute{\boldsymbol{R}}_2^+ = \acute{\boldsymbol{R}}_4\,\acute{\boldsymbol{R}}_4^+ = \widetilde{\boldsymbol{A}}_r\left(\widetilde{\boldsymbol{A}}_r^H\,\widetilde{\boldsymbol{A}}_r\right)^{-1}\widetilde{\boldsymbol{A}}_r^H$ and $[\cdot]^+$ denotes the pseudo inverse operation using singular value decomposition which is explained below.

As mentioned in [1], the inverse of $\acute{\boldsymbol{R}}_m$ should be calculated by using the singular values and vectors corresponding to the P largest singular values to improve the robustness in a noisy environment. Because for $P < N$, $\acute{\boldsymbol{R}}_m$ is rank deficient therefore $\acute{\boldsymbol{R}}_m^{-1}$ does not exist. Hence, $\acute{\boldsymbol{R}}_m^+$ is used to represent its inverse. Let $\acute{\boldsymbol{R}}_m = \boldsymbol{U}_m\,\boldsymbol{\Sigma}_m\,\boldsymbol{V}_m^H$ where $\boldsymbol{U}_m \in \mathbb{C}^{N\times N}$, $\boldsymbol{\Sigma}_m \in \mathbb{R}^{N\times N}$, and $\boldsymbol{V}_m \in \mathbb{C}^{N\times N}$ are the matrices containing the left singular vectors, singular values, and right singular vectors respectively. Then, $\acute{\boldsymbol{R}}_m^+ = \acute{\boldsymbol{V}}_m\,\acute{\boldsymbol{\Sigma}}_m^{-1}\,\acute{\boldsymbol{U}}_m^H$ where $\acute{\boldsymbol{U}}_m \in \mathbb{C}^{N\times P}$, $\acute{\boldsymbol{\Sigma}}_m \in \mathbb{R}^{P\times P}$, and $\acute{\boldsymbol{V}}_m \in \mathbb{C}^{N\times P}$ are the matrices that contain the left singular vectors associated with the P largest singular values, the corresponding P singular values and right singular vectors respectively. In theory, the remaining $(N-P)$ singular values will be zero.

By right multiplying both sides of the above equations with $\widetilde{\boldsymbol{A}}_r$, the following expressions can be obtained

$$\acute{\boldsymbol{R}}_1\,\acute{\boldsymbol{R}}_2^+\,\widetilde{\boldsymbol{A}}_r = \widetilde{\boldsymbol{A}}_r\,\widetilde{\boldsymbol{D}}_1\,\widetilde{\boldsymbol{D}}_2^* \tag{2.10}$$

and

$$\acute{\boldsymbol{R}}_5\,\acute{\boldsymbol{R}}_4^+\,\widetilde{\boldsymbol{A}}_r = \widetilde{\boldsymbol{A}}_r\,\widetilde{\boldsymbol{D}}_5\,\widetilde{\boldsymbol{D}}_4^*. \tag{2.11}$$

From (2.10) and (2.11), it is clear that $\widetilde{\boldsymbol{D}}_1\,\widetilde{\boldsymbol{D}}_2^*$ and $\widetilde{\boldsymbol{D}}_5\,\widetilde{\boldsymbol{D}}_4^*$ correspond to the P largest

eigenvalues of $\acute{\boldsymbol{R}}_1\,\acute{\boldsymbol{R}}_2^{+}$ and $\acute{\boldsymbol{R}}_5\,\acute{\boldsymbol{R}}_4^{+}$ respectively. Let $\overline{\boldsymbol{u}}_p$ and $\boldsymbol{u}_p$ be the eigenvectors of $\acute{\boldsymbol{R}}_1\,\acute{\boldsymbol{R}}_2^{+}$ and $\acute{\boldsymbol{R}}_5\,\acute{\boldsymbol{R}}_4^{+}$ associated to their P largest eigenvalues respectively. The subspace spanned by $[\overline{\boldsymbol{u}}_1,\,\overline{\boldsymbol{u}}_2,\,\cdots,\,\overline{\boldsymbol{u}}_P]$ and $[\boldsymbol{u}_1,\,\boldsymbol{u}_2,\,\cdots,\,\boldsymbol{u}_P]$ is also spanned by the columns of $\boldsymbol{A}_{\boldsymbol{r}}$, thus, we have $\overline{\boldsymbol{u}}_p = \overline{q}_p\,\widetilde{\boldsymbol{a}}_{\boldsymbol{r}_p}$ and $\boldsymbol{u}_p = q_p\,\widetilde{\boldsymbol{a}}_{\boldsymbol{r}_p}$, where $\overline{q}_p$ and q_p are the constants which appear during the eigenvalue decomposition.

From the P largest eigenvalues of $\acute{\boldsymbol{R}}_1\,\acute{\boldsymbol{R}}_2^{+}$ and $\acute{\boldsymbol{R}}_5\,\acute{\boldsymbol{R}}_4^{+}$, we can have

$$\widetilde{\boldsymbol{D}}_1\,\widetilde{\boldsymbol{D}}_2^{*} = \mathrm{diag}\left\{\left[\exp(-j\,2\,\pi\,(\omega_{e_1} + 3\,\phi_{e_1})/\lambda), \exp(-j\,2\,\pi\,(\omega_{e_2} + 3\,\phi_{e_2})/\lambda),\right.\right. \\ \left.\left. \cdots, \exp(-j\,2\,\pi\,(\omega_{e_P} + 3\,\phi_{e_P})/\lambda)\right]\right\}. \quad (2.12)$$

and

$$\widetilde{\boldsymbol{D}}_5\,\widetilde{\boldsymbol{D}}_4^{*} = \mathrm{diag}\left\{\left[\exp(-j\,2\,\pi\,(-\omega_{e_1} + 3\,\phi_{e_1})/\lambda), \exp(-j\,2\,\pi\,(-\omega_{e_2} + 3\,\phi_{e_2})/\lambda),\right.\right. \\ \left.\left. \cdots, \exp(-j\,2\,\pi\,(-\omega_{e_P} + 3\,\phi_{e_P})/\lambda)\right]\right\}. \quad (2.13)$$

Further from (2.12) and (2.13), the following can be obtained

$$\left(\widetilde{\boldsymbol{D}}_1\,\widetilde{\boldsymbol{D}}_2^{*}\right)^{*}\,\widetilde{\boldsymbol{D}}_5\,\widetilde{\boldsymbol{D}}_4^{*} = \mathrm{diag}\left\{\left[\exp(j\,4\,\pi\,\omega_{e_1}/\lambda), \exp(j\,4\,\pi\,\omega_{e_2}/\lambda), \cdots, \exp(j\,4\,\pi\,\omega_{e_P}/\lambda)\right]\right\}. \quad (2.14)$$

However, before using (2.14), the eigenvalues of $\acute{\boldsymbol{R}}_1\,\acute{\boldsymbol{R}}_2^{+}$ and $\acute{\boldsymbol{R}}_5\,\acute{\boldsymbol{R}}_4^{+}$ should be paired by comparing the inner product of the corresponding eigenvectors from the fact that the inner product of two aligned vectors is greater than that of two nonaligned vectors [1]. The DOD of the pth target can be calculated from the estimated value of ω_{e_p} obtained from the arguments of the diagonal elements in (2.14) as

$$\hat{\theta}_{e_p} = \arccos\left(\hat{\omega}_{e_p}/d_e\right). \quad (2.15)$$

Similar to (2.14), the following can also be written

$$\left(\widetilde{\boldsymbol{D}}_1\,\widetilde{\boldsymbol{D}}_2^{*}\,\widetilde{\boldsymbol{D}}_5\,\widetilde{\boldsymbol{D}}_4^{*}\right)^{*} = \mathrm{diag}\left\{\left[\exp(j\,12\,\pi\,\phi_{e_1}/\lambda), \exp(j\,12\,\pi\,\phi_{e_2}/\lambda), \cdots, \exp(j\,12\,\pi\,\phi_{e_P}/\lambda)\right]\right\} \quad (2.16)$$

From the arguments of the diagonal elements in (2.16), ϕ_{e_p} can be estimated and then the range to the transmitter can be calculated by using the following relation

$$\hat{\rho}_{e_p} = d_e^2\,\sin^2\left(\hat{\theta}_{e_p}\right)/(2\,\hat{\phi}_{e_p}). \quad (2.17)$$

To estimate the angle of arrival, let $\breve{\boldsymbol{u}}_p = \overline{\boldsymbol{u}}_p \odot \boldsymbol{J}_N\,\boldsymbol{u}_p^{*} = \overline{q}_p\,q_p^{*}(\widetilde{\boldsymbol{a}}_{\boldsymbol{r}_p} \odot \boldsymbol{J}_N\,\widetilde{\boldsymbol{a}}_{\boldsymbol{r}_p}^{*})$, which

gives

$$\breve{\boldsymbol{u}}_p = \overline{q}_p\, q_p^* \left[\exp(-4\,\pi\, j\, \breve{N}\, \omega_{r_p}/\lambda), \cdots, 1, \exp(4\,\pi\, j\, \omega_{r_p}/\lambda), \cdots, \exp(4\,\pi\, j\, \breve{N}\, \omega_{r_p}/\lambda)\right]^T \tag{2.18}$$

where

$$\boldsymbol{J}_N = \begin{bmatrix} 0 & 0 & \cdots & 0 & 1 \\ 0 & 0 & \cdots & 1 & 0 \\ \vdots & \vdots & \iddots & \vdots & \vdots \\ 0 & 1 & \cdots & 0 & 0 \\ 1 & 0 & \cdots & 0 & 0 \end{bmatrix} \in \mathbb{R}^{N\times N} \tag{2.19}$$

is the exchange matrix.

From (2.18), ω_{r_p} can be estimated as

$$\hat{\omega}_{r_p} = \frac{\lambda}{4\,\pi\,(N-1)} \sum_{i=1}^{N-1} \angle\left\{[\breve{\boldsymbol{u}}_p]_i / [\breve{\boldsymbol{u}}_p]_{i+1}\right\}. \tag{2.20}$$

Then, the angle of arrival is given by

$$\hat{\theta}_{r_p} = \arccos\left(\hat{\omega}_{r_p}/d_r\right) \tag{2.21}$$

Let $\widetilde{\boldsymbol{u}}_p = \overline{\boldsymbol{u}}_p^* \odot \boldsymbol{J_N}\, \boldsymbol{u}_p^* = \overline{q}_p^*\, q_p^* (\widetilde{\boldsymbol{a}}_{\boldsymbol{r}_p}^* \odot \boldsymbol{J}_N\, \widetilde{\boldsymbol{a}}_{\boldsymbol{r}_p}^*)$, which gives

$$\widetilde{\boldsymbol{u}}_p = \overline{q}_p^*\, q_p^* \left[\exp(4\,\pi\, j\, \breve{N}^2\, \phi_{r_p}/\lambda), \cdots, 1, \exp(4\,\pi\, j\, \phi_{r_p}/\lambda), \cdots, \exp(4\,\pi\, j\, \breve{N}^2\, \phi_{r_p}/\lambda)\right]^T \tag{2.22}$$

From (2.22), ϕ_{r_p} can be estimated as

$$\hat{\phi}_{r_p} = \frac{\lambda}{8\,\pi\,\breve{N}} \sum_{i=1}^{\breve{N}} \left[\arg\left\{[\widetilde{\boldsymbol{u}}_p]_{\breve{N}-i+1} / [\widetilde{\boldsymbol{u}}_p]_{\breve{N}+1}\right\} + \arg\left\{[\widetilde{\boldsymbol{u}}_p]_{\breve{N}+i+1} / [\widetilde{\boldsymbol{u}}_p]_{\breve{N}+1}\right\}\right] / i^2. \tag{2.23}$$

The angles should be unwrapped before using (2.20) and (2.23) to remove the phase ambiguities which appear because the argument of a complex number can only be retrieved in its principal value. The process of unwrapping angles is given in [115]. In the unwrapping process, the discontinued principal values of the components of $\widetilde{\boldsymbol{u}}_p$ are added or subtracted by a multiple of 2π to obtain a smooth transition along the phases. As we know that the argument of the reference component should be zero. The remaining unwrapped phases can be shifted according to it to get the arguments of the components of $\widetilde{\boldsymbol{u}}_p$ which can be used in (2.23) to compute $\hat{\phi}_{r_p}$. Finally, the range to the receiving array can be computed as

$$\hat{\rho}_{r_p} = d_r^2\, \sin^2\left(\hat{\theta}_{r_p}\right) / (2\,\hat{\phi}_{r_p}). \tag{2.24}$$

In this method, $\acute{\boldsymbol{R}}_1\,\acute{\boldsymbol{R}}_2^{+}$ and $\acute{\boldsymbol{R}}_5\,\acute{\boldsymbol{R}}_4^{+}$ are $N \times N$ complex valued matrices, therefore, the maximum number of localizable targets is N. Beside, there are some other constraints in this method like quarter wavelength inter element spacing. These extra constraints appear due to the fact that the argument of a complex number can only be retrieved in its principal form belonging to $(-\pi, \pi]$. This impacts the parameter retrieval from (2.14), (2.16), (2.18), and (2.22). For (2.14) and (2.16), the constraints are $-\pi < 4\,\pi\,\omega_{e_p}/\lambda \leq \pi$ and $-\pi < 12\,\pi\,\phi_{e_p}/\lambda \leq \pi$ which are directly visible in the expression. On manipulating these constraints further, we can get

$$\arccos\left(\frac{\lambda}{4\,d_e}\right) < \theta_{e_p} \leq \arccos\left(-\frac{\lambda}{4\,d_e}\right) \tag{2.25}$$

and

$$\rho_{e_p} \geq 6\,d_e^2\,\sin^2\left(\theta_{e_p}\right)/\lambda. \tag{2.26}$$

All the elements of $\breve{\boldsymbol{u}}_p$ contain the information about a single target. To retrieve the necessary information from $\breve{\boldsymbol{u}}_p$, [1] proposed to use difference between the phases of its consecutive elements which should be unambiguous. Thus, we can say $-\pi < 4\,\pi\,\omega_{r_p}/\lambda \leq \pi$ is a constraint that can be rewritten as

$$\arccos\left(\frac{\lambda}{4\,d_r}\right) < \theta_{r_p} \leq \arccos\left(-\frac{\lambda}{4\,d_r}\right). \tag{2.27}$$

Like the elements of $\breve{\boldsymbol{u}}_p$, the elements of $\widetilde{\boldsymbol{u}}_p$ also belong to a single target. To avoid ambiguity in this case, the arguments of the elements adjacent to the reference element should be between $-\pi$ and π, i.e. $-\pi < 4\,\pi\,\phi_{r_p}/\lambda \leq \pi$. Accordingly, we can write

$$\rho_{r_p} \geq 2\,d_r^2\,\sin^2\left(\theta_{r_p}\right)/\lambda. \tag{2.28}$$

The constraints on the DOD and DOA, given in (2.25) and (2.27) respectively, are similar. It can be found out from the expressions that the unambiguous sweeps of θ_{e_p} and θ_{r_p} will decrease if the inter element spacings increase beyond $\lambda/4$ to reduce the mutual coupling between array antennas. Figure 2.1 shows the variation of the unambiguous region of θ_{e_p} with respect to d_e varying from $\lambda/4$ to $\lambda/2$. Below $\lambda/4$, $0 \leq \theta_{e_p} \leq \pi$ and $0 \leq \theta_{r_p} \leq \pi$ because the lower and upper limits of DOD and DOA are physically controlled by the array geometry. Consequently, the method in [1] can only work for the inter element spacings less than or equal to $\lambda/4$.

At $d_e = d_r = \lambda/4$, (2.26) and (2.28) are the functions of only θ_{e_p} and θ_{r_p} respectively. Figure 2.2 and Figure 2.3 respectively show the unambiguous region of ρ_{e_p} and ρ_{r_p} with respect to θ_{e_p} and θ_{r_p} at quarter wavelength. From the figures, we can say that the ambiguities in the ranges are maximum at $\theta_{e_p} = \theta_{r_p} = 90^\circ$ because of their squared sine function. However, their magnitudes differ. By making comparison with

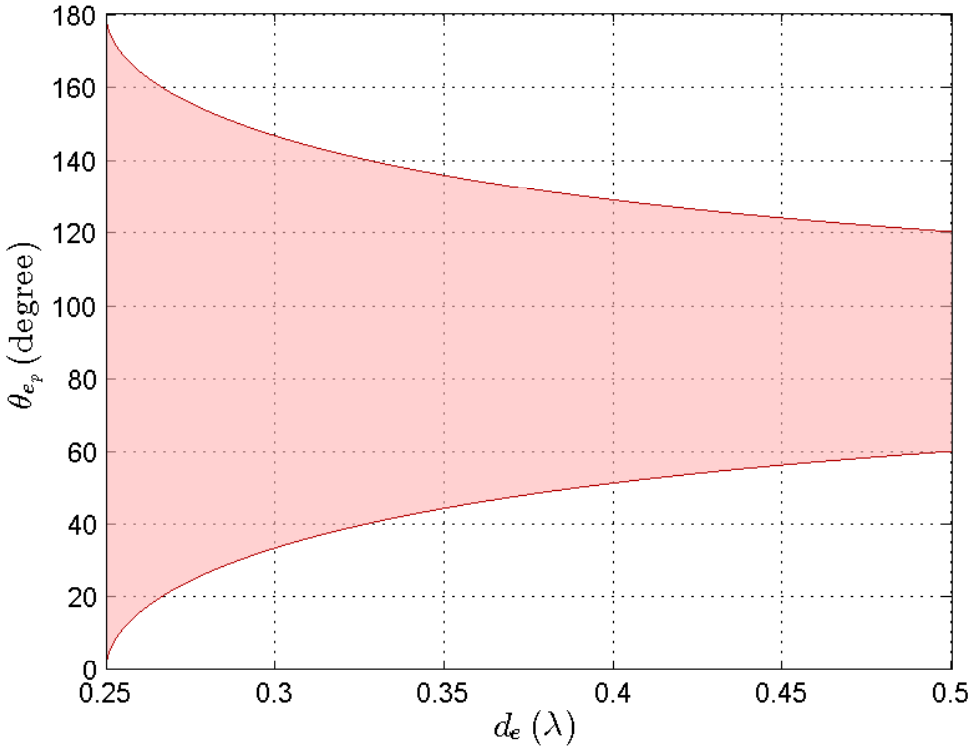

Figure 2.1 – Variation of unambiguous region of θ_{e_p} with d_e. It is same for θ_{r_p} with respect to d_r.

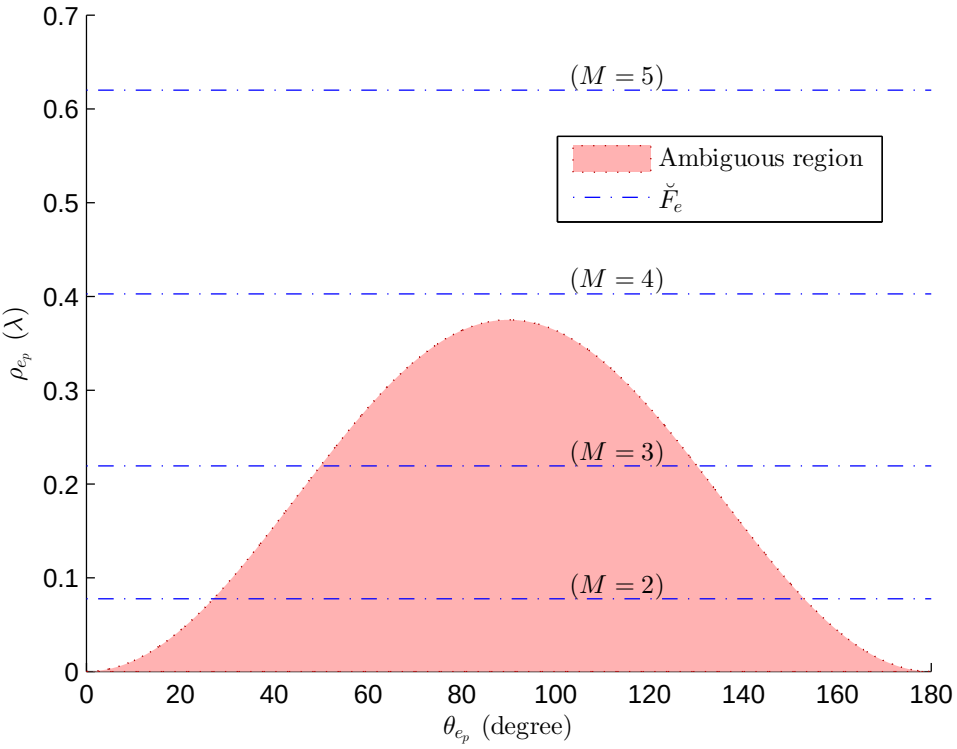

Figure 2.2 – Ambiguous region of ρ_{e_p} with respect to θ_{e_p} at $d_e = \lambda/4$.

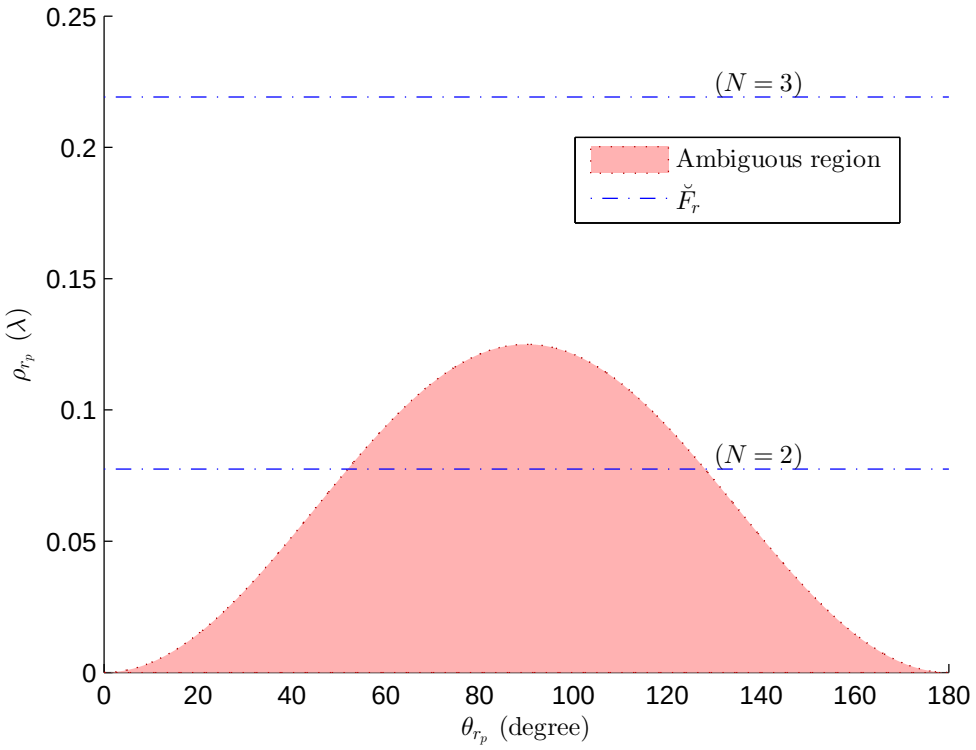

Figure 2.3 – Ambiguous region of ρ_{r_p} with respect to θ_{r_p} at $d_r = \lambda/4$.

the lower limit of the Fresnel region, we can conclude that the ambiguity in the range corresponding to transmitting array doesn't exist for $M \geq 4$ and the ambiguity in the range corresponding to receiving array doesn't exist for $N \geq 3$. As mentioned in the beginning of this section, the method in [1] uses symmetric arrays, therefore N will always be greater than or equal to 3. And also $M = 5$. Hence, the ambiguity due to the range will never occur while using this method.

2.2 Extended [2] for MIMO Systems

In this section, we propose a new method which can be considered as an extension of the method in [2] to deal with MIMO systems. As the previously presented method [1], the proposed one also uses symmetric arrays. [2] uses two subarrays, however, the division of the array into two subarrays is unnecessary. Thus, in the proposed method, we use the whole array and its permuted version.

The symmetry in the transmitting ULA allows us to write the following relation

$$\boldsymbol{J}_M\,\widetilde{\boldsymbol{a}}_{\boldsymbol{e}_p} = \begin{bmatrix} \exp(-j\,2\,\pi(-\breve{M}\,\omega_{e_p} + \breve{M}^2\,\phi_{e_p})/\lambda) \\ \vdots \\ 1 \\ \vdots \\ \exp(-j\,2\,\pi(\breve{M}\,\omega_{e_p} + \breve{M}^2\,\phi_{e_p})/\lambda) \end{bmatrix} = \boldsymbol{d}_{\boldsymbol{e}}(\theta_{e_p}) \odot \widetilde{\boldsymbol{a}}_{\boldsymbol{e}_p} \tag{2.29}$$

where $\boldsymbol{J}_M$ is the $M \times M$ exchange matrix, $\odot$ is the Hadamard product, and

$$\boldsymbol{d}_{\boldsymbol{e}}(\theta_{e_p}) = \begin{bmatrix} \exp(j\,4\,\pi\,\breve{M}\,\omega_{e_p}/\lambda) \\ \vdots \\ 1 \\ \vdots \\ \exp(-j\,4\,\pi\,\breve{M}\,\omega_{e_p}/\lambda) \end{bmatrix}. \tag{2.30}$$

As mentioned in [2], $d_e \leq \lambda/4$ is a necessary condition to avoid the phase ambiguity in the elements of $\boldsymbol{d}_{\boldsymbol{e}}(\theta_{e_p})$.

By using the above relation, we can write

$$\breve{\boldsymbol{J}}\,\widetilde{\boldsymbol{A}} = (\boldsymbol{D}_{\boldsymbol{e}} \boxdot \underline{\boldsymbol{1}}_{N\times P}) \odot \widetilde{\boldsymbol{A}} \tag{2.31}$$

where $\breve{\boldsymbol{J}} = \boldsymbol{J}_M \otimes \boldsymbol{I}_N$, $\boldsymbol{I}_N$ is the $N \times N$ identity matrix, $\underline{\boldsymbol{1}}_{N\times P}$ is the $N \times P$ dimensional matrix with all its components equal to one, and $\boldsymbol{D}_{\boldsymbol{e}} = [\boldsymbol{d}_{\boldsymbol{e}}(\theta_{e_1}),\, \boldsymbol{d}_{\boldsymbol{e}}(\theta_{e_2}),\, \cdots,\, \boldsymbol{d}_{\boldsymbol{e}}(\theta_{e_P})]$.

The covariance matrix of $\widetilde{\boldsymbol{y}}(t)$ is given by

$$\begin{aligned} \widetilde{\boldsymbol{R}} &= \mathrm{E}\{\widetilde{\boldsymbol{y}}(t)\,\widetilde{\boldsymbol{y}}^H(t)\} \in \mathbb{C}^{MN\times MN} \\ &= \widetilde{\boldsymbol{A}}\,\boldsymbol{R}_{\boldsymbol{s}}\,\widetilde{\boldsymbol{A}}^H + \sigma_w^2 \boldsymbol{I}_{MN}. \end{aligned} \tag{2.32}$$

The eigendecomposition of $\widetilde{\boldsymbol{R}}$ can be written as

$$\widetilde{\boldsymbol{R}} = \boldsymbol{U}_{\boldsymbol{s}}\,\boldsymbol{\Lambda}_{\boldsymbol{s}}\,\boldsymbol{U}_{\boldsymbol{s}}^H + \sigma_w^2 \boldsymbol{U}_{\boldsymbol{n}}\boldsymbol{U}_{\boldsymbol{n}}^H \tag{2.33}$$

where the diagonal elements of $\boldsymbol{\Lambda}_{\boldsymbol{s}} \in \mathbb{R}^{P\times P}$ are the P largest eigenvalues and the columns of $\boldsymbol{U}_{\boldsymbol{s}} \in \mathbb{C}^{MN\times P}$ are their corresponding eigenvectors spanning the signal subspace. The columns of $\boldsymbol{U}_{\boldsymbol{n}} \in \mathbb{C}^{MN\times(MN-P)}$ span the noise subspace. From (2.32) and (2.33), we can write

$$\widetilde{\boldsymbol{A}}\,\boldsymbol{T} = \boldsymbol{U}_{\boldsymbol{s}} \tag{2.34}$$

with $\boldsymbol{T} \in \mathbb{C}^{P\times P}$ being an invertible square matrix.

For an arbitrary angle θ, we can write

$$\begin{aligned} \boldsymbol{F_e}(\theta) &= \check{\boldsymbol{J}}\,\boldsymbol{U_s} - [\boldsymbol{d_e}(\theta) \otimes \underline{\mathbf{1}}_{N\times P}] \odot \boldsymbol{U_s} \qquad (2.35)\\ &= \check{\boldsymbol{J}}\,\widetilde{\boldsymbol{A}}\,\boldsymbol{T} - [\boldsymbol{d_e}(\theta) \otimes \underline{\mathbf{1}}_{N\times P}] \odot \widetilde{\boldsymbol{A}}\,\boldsymbol{T}\\ &= (\boldsymbol{D_e} \boxdot \underline{\mathbf{1}}_{N\times P}) \odot \widetilde{\boldsymbol{A}}\,\boldsymbol{T} - [\boldsymbol{d_e}(\theta) \otimes \underline{\mathbf{1}}_{N\times P}] \odot \widetilde{\boldsymbol{A}}\,\boldsymbol{T}\\ &= ([\boldsymbol{d_e}(\theta_{e_1}) - \boldsymbol{d_e}(\theta),\, \boldsymbol{d_e}(\theta_{e_2}) - \boldsymbol{d_e}(\theta),\, \cdots,\, \boldsymbol{d_e}(\theta_{e_P}) - \boldsymbol{d_e}(\theta)] \boxdot \underline{\mathbf{1}}_{N\times P}) \odot \boldsymbol{U_s} \qquad (2.36) \end{aligned}$$

from (2.31) and (2.34) (see [2] and [116]). At $\theta = \theta_{e_p}$, all the components of the pth column of $\boldsymbol{F_e}(\theta)$ become zero and $\boldsymbol{F_e}(\theta)$ becomes rank deficient. Thus, we can use the following spectrum function to estimate DODs [2, 116]

$$S_e(\theta) = \frac{1}{\det\{\boldsymbol{F_e}^H(\theta)\,\boldsymbol{F_e}(\theta)\}}. \qquad (2.37)$$

The estimated DODs (say $\hat{\theta}_{e_p}$) of the P targets correspond to the P highest peaks of $S_e(\theta)$ when θ is varied from 0° to 180°.

Using the orthogonality between the signal and noise subspaces, we can write [59]

$$\left[\widetilde{\boldsymbol{a}}_{\boldsymbol{e}}(\rho_{e_p},\, \theta_{e_p}) \otimes \widetilde{\boldsymbol{a}}_{\boldsymbol{r}}(\rho_{r_p},\, \theta_{r_p})\right]^H \boldsymbol{U_n}\,\boldsymbol{U_n}^H \left[\widetilde{\boldsymbol{a}}_{\boldsymbol{e}}(\rho_{e_p},\, \theta_{e_p}) \otimes \widetilde{\boldsymbol{a}}_{\boldsymbol{r}}(\rho_{r_p},\, \theta_{r_p})\right] = 0. \qquad (2.38)$$

Since,

$$\widetilde{\boldsymbol{a}}_{\boldsymbol{e}}(\rho_{e_p},\, \theta_{e_p}) \otimes \widetilde{\boldsymbol{a}}_{\boldsymbol{r}}(\rho_{r_p},\, \theta_{r_p}) = \left[\widetilde{\boldsymbol{a}}_{\boldsymbol{e}}(\rho_{e_p},\, \theta_{e_p}) \otimes \boldsymbol{I}_N\right] \widetilde{\boldsymbol{a}}_{\boldsymbol{r}}(\rho_{r_p},\, \theta_{r_p}). \qquad (2.39)$$

Hence, we can also say [59]

$$\det\left\{\left[\widetilde{\boldsymbol{a}}_{\boldsymbol{e}}(\rho_{e_p},\, \theta_{e_p}) \otimes \boldsymbol{I}_N\right]^H \boldsymbol{U_n}\,\boldsymbol{U_n}^H \left[\widetilde{\boldsymbol{a}}_{\boldsymbol{e}}(\rho_{e_p},\, \theta_{e_p}) \otimes \boldsymbol{I}_N\right]\right\} = 0 \qquad (2.40)$$

i.e. the subspace spanned by the directional vector of departure is orthogonal to the noise subspace, therefore, the estimated range corresponding to $\hat{\theta}_{e_p}$ can be given by

$$\hat{\rho}_{e_p} = \underset{\check{F}_e \le \rho \le \overline{F}_e}{\arg\max} \frac{1}{\det\{\boldsymbol{G}^H(\rho)\,\boldsymbol{G}(\rho)\}} \qquad (2.41)$$

where $\boldsymbol{G}(\rho) = \boldsymbol{U_n}^H[\widetilde{\boldsymbol{a}}_{\boldsymbol{e}}(\rho,\, \hat{\theta}_{e_p}) \otimes \boldsymbol{I}_N] \in \mathbb{C}^{(MN-P)\times N}$. In (2.41), when $MN - P \ge N$ and $\rho \neq \rho_{e_p}$, $\boldsymbol{G}(\rho)$ has full rank and $\det\{\boldsymbol{G}^H(\rho)\,\boldsymbol{G}(\rho)\}$ is not zero. At $\rho = \rho_{e_p}$, $\det\{\boldsymbol{G}^H(\rho)\,\boldsymbol{G}(\rho)\}$ tends towards zero due to the orthogonality between the noise subspace and the subspace spanned by the directional vector of departure corresponding to the pth target.

Like the transmitting array, the receiving array is also a symmetric ULA. Therefore, we can write

$$\check{\boldsymbol{I}}\,\widetilde{\boldsymbol{A}} = (\underline{\mathbf{1}}_{M\times P} \boxdot \boldsymbol{D_r}) \odot \widetilde{\boldsymbol{A}} \qquad (2.42)$$

where $\breve{\boldsymbol{I}} = \boldsymbol{I}_M \otimes \boldsymbol{J}_N$ and $\boldsymbol{D_r} = [\boldsymbol{d_r}(\theta_{r_1}),\ \boldsymbol{d_r}(\theta_{r_2}),\ \cdots,\ \boldsymbol{d_r}(\theta_{r_P})]$ with

$$\boldsymbol{d_r}(\theta_{r_p}) = \begin{bmatrix} \exp(j\,4\,\pi\,\breve{N}\,d_r\,\cos(\theta_{r_p})/\lambda) \\ \vdots \\ 1 \\ \vdots \\ \exp(-j\,4\,\pi\,\breve{N}\,d_r\,\cos(\theta_{r_p})/\lambda) \end{bmatrix}. \tag{2.43}$$

$d_r \leq \lambda/4$ is a necessary condition to avoid the phase ambiguity in the elements of $\boldsymbol{D_r}$ [2].

Like before, the DOAs can be estimated by using the following spectrum function

$$S_r(\theta) = \frac{1}{\det\{\boldsymbol{F_r}^H(\theta)\,\boldsymbol{F_r}(\theta)\}}. \tag{2.44}$$

where

$$\boldsymbol{F_r}(\theta) = \breve{\boldsymbol{I}}\,\boldsymbol{U_s} - [\underline{\boldsymbol{1}}_{M\times P} \otimes \boldsymbol{d_r}(\theta)] \odot \boldsymbol{U_s} \tag{2.45}$$

$$= (\underline{\boldsymbol{1}}_{M\times P} \boxdot [\boldsymbol{d_r}(\theta_{r_1}) - \boldsymbol{d_r}(\theta),\ \cdots,\ \boldsymbol{d_r}(\theta_{r_P}) - \boldsymbol{d_r}(\theta)]) \odot \boldsymbol{U_s} \tag{2.46}$$

can be obtained from (2.34) and (2.42). The estimated DOAs (say $\hat{\theta}_{r_p}$) of the P targets correspond to the P highest peaks of $S_r(\theta)$ when θ is varied from 0° to 180°. However, the DOAs are not paired.

Finally, to get the estimation of the receiver side range of the pth target, we use 2D MUSIC as

$$(\hat{\rho}_{r_p},\ \hat{\theta}_{r_p}) = \underset{\substack{\check{F}_r \leq \rho \leq \bar{F}_r \\ \theta \in \{\hat{\theta}_{r_1}, \cdots, \hat{\theta}_{r_P}\}}}{\arg\max} \frac{1}{\widetilde{\boldsymbol{a}}_{\boldsymbol{r}}^H(\rho,\,\theta)\,\boldsymbol{Q}\,\widetilde{\boldsymbol{a}}_{\boldsymbol{r}}(\rho,\,\theta)} \tag{2.47}$$

where $\boldsymbol{Q} = [\widetilde{\boldsymbol{a}}_{\boldsymbol{e}}(\hat{\rho}_{e_p},\,\hat{\theta}_{e_p}) \otimes \boldsymbol{I}_N]^H\,\boldsymbol{U_n}\,\boldsymbol{U_n}^H\,[\widetilde{\boldsymbol{a}}_{\boldsymbol{e}}(\hat{\rho}_{e_p},\,\hat{\theta}_{e_p}) \otimes \boldsymbol{I}_N]$. Here, θ is chosen from the set of unpaired DOAs which reduces the computational cost. 2D MUSIC automatically pairs the transmitting and receiving sides location parameters for each target. Because when $\boldsymbol{Q}$ belongs to the pth target, the pair of range and DOA which minimizes the 2D MUSIC cost function will correspond to that pth target.

Initially, all the P DODs and DOAs are estimated in one 1D search each. And then, the ranges belonging to transmitting and receiving arrays of each target are estimated separately by handling one target at a time. Therefore, all the location parameters are automatically paired. Algorithm 2.1 provides the complete procedure of this proposed method.

Algorithm 2.1 Proposed Approximated Model Based Method.

1: Estimate the covariance matrix $\widetilde{\boldsymbol{R}}$ of the matched filtered received signals $\widetilde{\boldsymbol{y}}(t)$ using L samples.
2: Separate the eigenvectors corresponding to the signal and noise subspaces using the P largest eigenvalues of $\widetilde{\boldsymbol{R}}$.
3: Estimate θ_{e_p} and θ_{r_p} by finding P largest peaks of $S_e(\theta)$ and $S_r(\theta)$ respectively.
4: For each estimated θ_{e_p}, estimate ρ_{e_p} by using (2.41).
5: For each estimated ρ_{e_p} and θ_{e_p}, calculate $\boldsymbol{Q}$ and use it in (2.47) to estimate ρ_{r_p} and pair estimated θ_{r_p}.

The maximum number localizable targets in this method is $N(M-1)$, which is bounded due to the denominator of the cost function in (2.41).

2.3 Numerical Example

Consider a bistatic MIMO system with $M = 9$ ($\check{M} = 4$) transmitting and $N = 11$ ($\check{N} = 5$) receiving antennas. The reference antennas indexes are $m_o = 5$ and $n_o = 6$ to get symmetric ULAs. The arrays elements are uniformly spaced by $d_e = d_r = \lambda/4$. λ is used as the unit of length throughout the simulation. To analyze the performance of the methods described in section 2.1 and section 2.2, we show the variations in RMSEs of the location parameters with respect to SNR when the methods process $L = 10^3$ signal data temporal samples. The RMSE of each location parameter is calculated by using $K = 10^3$ Monte Carlo trials in the following formula

$$\epsilon\left(\eta_p\right) = \sqrt{\frac{1}{K}\sum_{k=1}^{K}\left(\hat{\eta}_p(k) - \eta_p\right)^2} \tag{2.48}$$

where $\eta_p \in \{\rho_{e_p}, \theta_{e_p}, \rho_{r_p}, \theta_{r_p}\}$ is the true value of the location parameter of the pth target and $\hat{\eta}_p(k) \in \{\hat{\rho}_{e_p}(k), \hat{\theta}_{e_p}(k), \hat{\rho}_{r_p}(k), \hat{\theta}_{r_p}(k)\}$ is the estimated value of the corresponding location parameter in the kth trial.

Almost all of the existing approximated model based methods [1–3, 23, 24] simulate the received signals by using Fresnel approximation to analyze the performance of their methods. The methods in section 2.1 and section 2.2 are based on the approximated model, thus, we also use the model corresponding to (1.30) as the input signal to show the performance of our method.

In Figure 2.4, Figure 2.5, Figure 2.6, and Figure 2.7, we compare the RMSE in the location parameters (range associated with the transmitting array, DOD, range associated with the receiving array, and DOA respectively) of two targets estimated by the

proposed method and the method in [1] in terms of SNR. The SNR is varied from 0 dB to 30 dB with an interval of 5 dB. The location parameters $(\rho_{e_p}, \theta_{e_p}, \rho_{r_p}, \theta_{r_p})$ of the two targets are $(1.5\lambda, 50^\circ, 2.5\lambda, 140^\circ)$ and $(3.5\lambda, 110.5^\circ, 5\lambda, 60^\circ)$. The CRLBs of the location parameters are calculated from (1.41) by replacing the accurate model parameters with the approximated model parameters. In the figures, $\varepsilon(\eta_p)$ denotes the CRLB of the η_p parameter belonging to the pth target in terms of standard deviation.

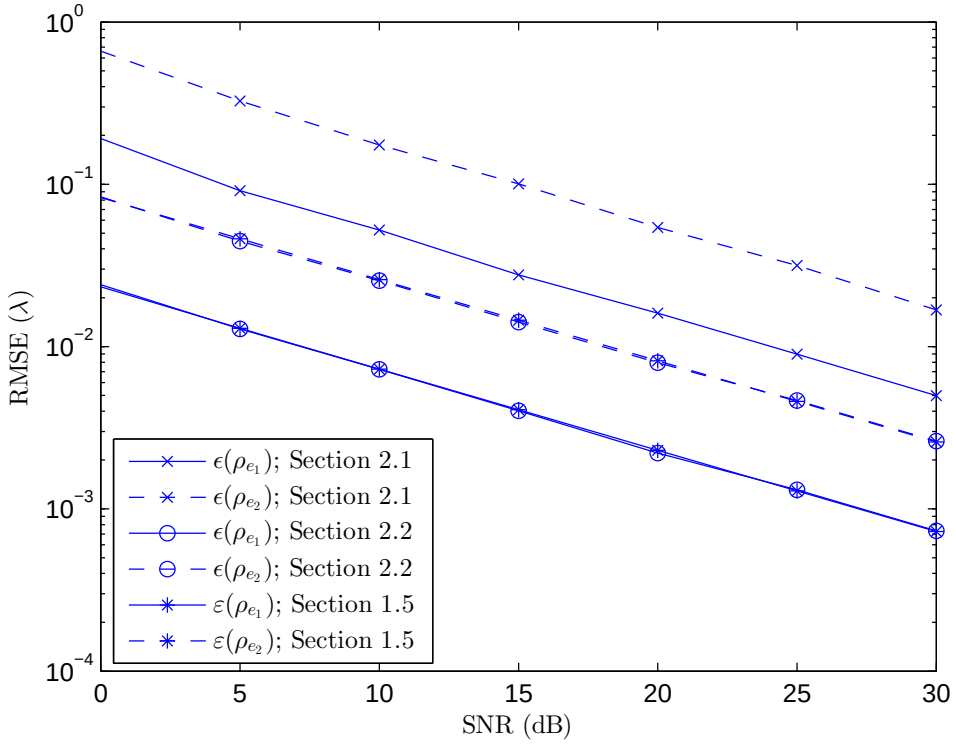

Figure 2.4 – RMSE in range associated with the transmitting array estimated by the method in [1] and the proposed method versus SNR. The CRLBs are calculated using (1.41).

From the above figures, we can observe that the proposed method has better performance in terms of RMSE than that of the method in [1]. The primary reason of the poor performance of the method in [1] is that it does not exploit all the available information. Additionally, the RMSEs of the ranges estimated by the proposed method are very close to their respective CRLBs.

2.4 Conclusion

In this chapter, we have proposed an extension of the method [2] to localize near field targets using a bistatic MIMO system consisting of symmetric transmitting and receiving ULAs. Compared to the existing method in [1], the proposed method has better performance in terms of RMSE because we exploit all the available information.

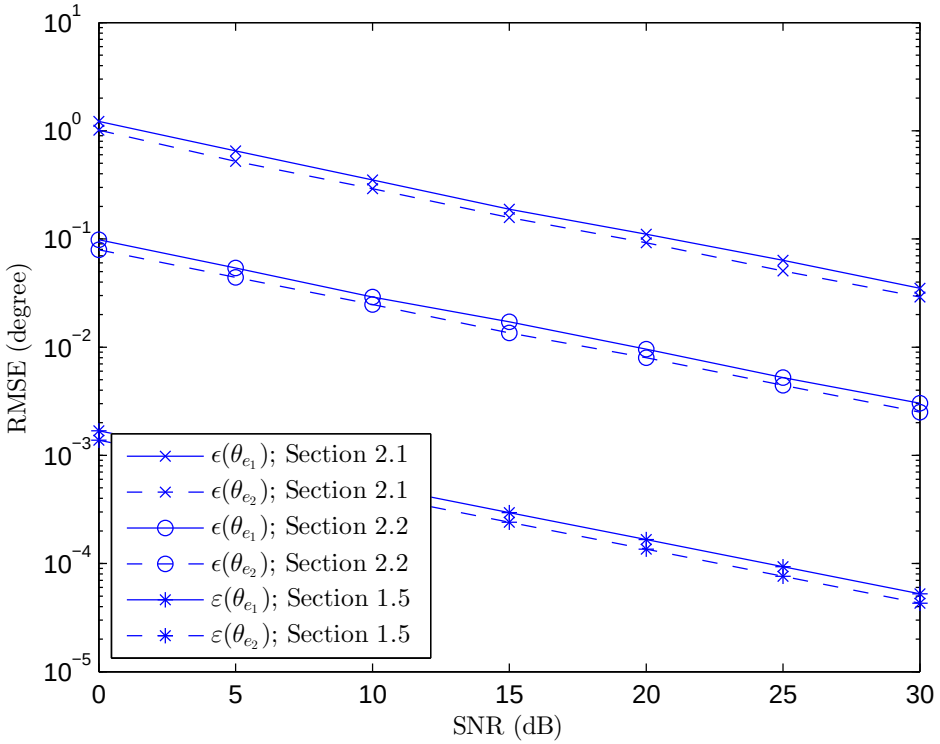

Figure 2.5 – RMSE in DOD estimated by the method in [1] and the proposed method versus SNR. The CRLBs are calculated using (1.41).

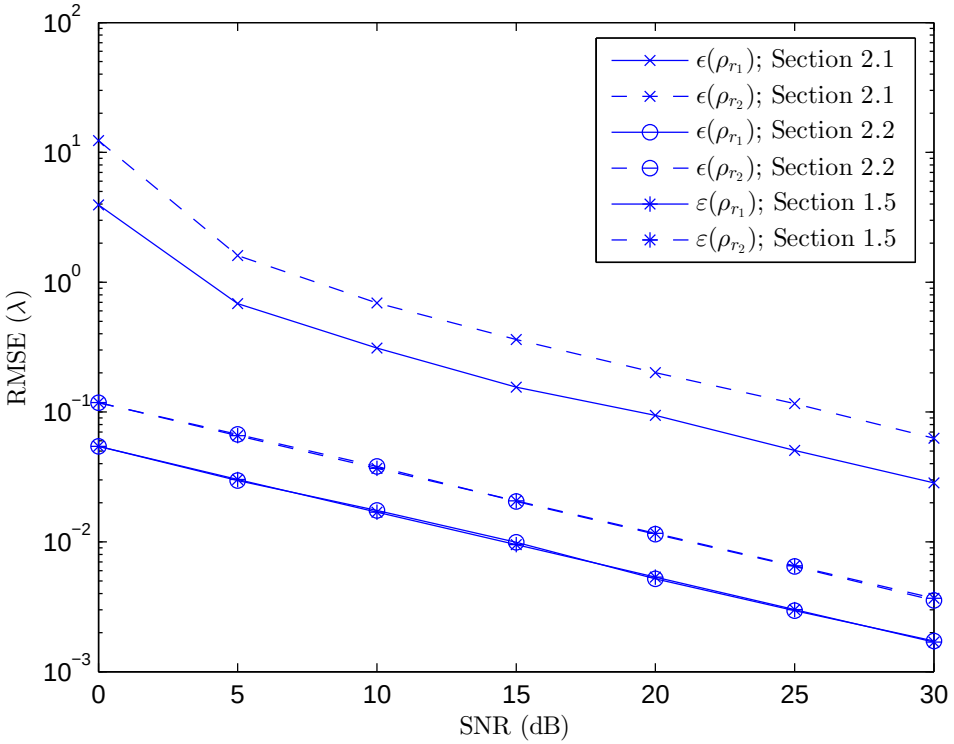

Figure 2.6 – RMSE in range associated with the receiving array estimated by the method in [1] and the proposed method versus SNR. The CRLBs are calculated using (1.41).

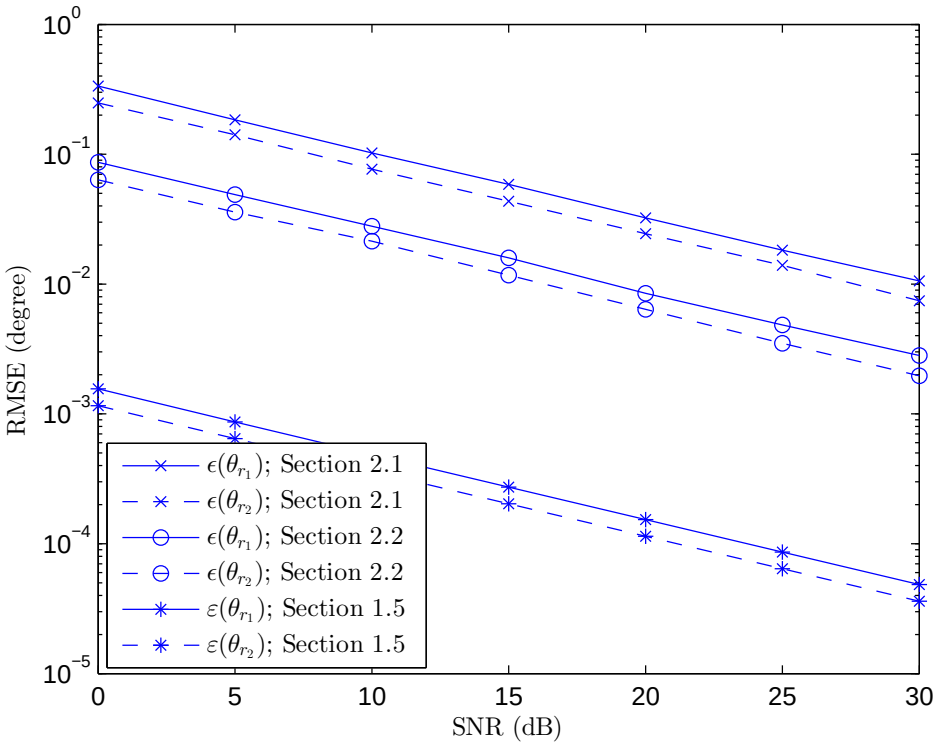

Figure 2.7 – RMSE in DOA estimated by the method in [1] and the proposed method versus SNR. The CRLBs are calculated using (1.41).

Along with it, the proposed method automatically pairs all the four location parameters. [1] uses submatrices of the covariance matrix, therefore, the maximum number of localizable targets is limited by the number of receiving antennas, i.e. N. However, the maximum number of localizable targets in the proposed method is given by $N(M-1)$. Both the methods discussed here use Fresnel approximation which introduces biases in the estimated location parameters. This bias is a function of location which remains constant for an array if its parameters are not modified. Consequently, this bias can be considered as an offset and can be removed by calibration. Hence, in the next chapter, we propose two methods to reduce this bias from the location parameters.

3

Correction Methods

In the previous chapter, we have elaborated two methods which are based on the approximated signal model which signifies quadric wavefront. However, in practice the wavefront is spherical. Thus, the location parameters estimated by every approximated model based method is biased. This bias is of systematic type and therefore its effect can be reduced. In this chapter, we propose two approaches to reduce the effects of Fresnel approximation on the location parameters. The first method is based on LUTs whereas the second method uses Least Squares (LS) estimation.

3.1 Approximation Error

From (1.26), we can observe that the approximated model is biased. This bias is like a location parameters dependent systematic error added to the accurate model. Thus, when a biased approximated model based method has to deal with the unbiased accurate model, this bias shows up in the estimated location parameters and decreases their precisions. Testing an approximated model based method with the accurate model based input signals is perfectly fair because the wavefront of a point source is spherical in reality. In the considered bistatic MIMO system, there are two ULAs which go through Fresnel approximation independently. However, the effect of this approximation is the same for both the arrays. As a result, explaining one explains the other.

3.2 LUT Based Correction

In the near field region, LUT based correction is possible in the first place because it is finite. A LUT based correction method is one of the most primitive but an effective way to minimize the approximation bias from the estimated location parameters. A key point to note is that this bias in an estimated location parameter is the result of the propagation of the systematic error, introduced by the Fresnel approximation, through the localization process of an approximated model based method. The final result of an error propagation depends on the path which the error takes. Since, two different localization techniques use two different algorithms, therefore, the path taken by the systematic error to reach location parameters will be different. Consequently, different approximation biases will be observed in the same location parameters for different localization techniques which can be seen in Appendix A where six different approaches to obtain biased location parameters are compared. However, if we are looking for one method to reduce the effect of the Fresnel approximation, LS based LUT inspired by section A.1.3 can be a right choice which is described in the following.

The whole LUT based correction method can be divided into two major steps. First step is the creation of LUT, which only depends on the system's physical parameters. The second step is the correction of the location parameters using the LUT created in the first step.

3.2.1 LUT Creation

For a bistatic MIMO system, we need to construct two 2D LUTs to map the true location parameters with the corresponding biased location parameters obtained due to the use of the approximated model. A LUT should be finite even if a bounded space has infinite locations. Thus, to construct a LUT, we need to calculate the biased location parameters at some discrete locations in the near field region of an array by varying the range from lower to upper Fresnel limit and the direction angle from 0 to π by some small intervals. Figure 3.1 shows a discretized near field region of a linear array when the range and directional angle are sampled by constant intervals. The intersection points, which can be seen in Figure 3.1, of the curves corresponding to the range and directional angle inside the Fresnel region are the locations whose biased parameters are recorded in the LUT.

For the transmitting array, let $\overline{\rho}_{e_q}$ and $\overline{\theta}_{e_q}$ be the range and DOD at the qth intersection point (or discrete location) respectively such that $\check{F}_e \leq \overline{\rho}_{e_q} \leq \overline{F}_e$ and $0 \leq \overline{\theta}_{e_q} \leq \pi$. The next sensitive step is to calculate the biased location parameters from $\boldsymbol{\delta_e}(\overline{\rho}_{e_q}, \overline{\theta}_{e_q})$ by minimizing its distance with $\widetilde{\boldsymbol{\delta}}_{\boldsymbol{e}}(\overline{\rho}_{e_q}, \overline{\theta}_{e_q})$, like an approximated model based technique.

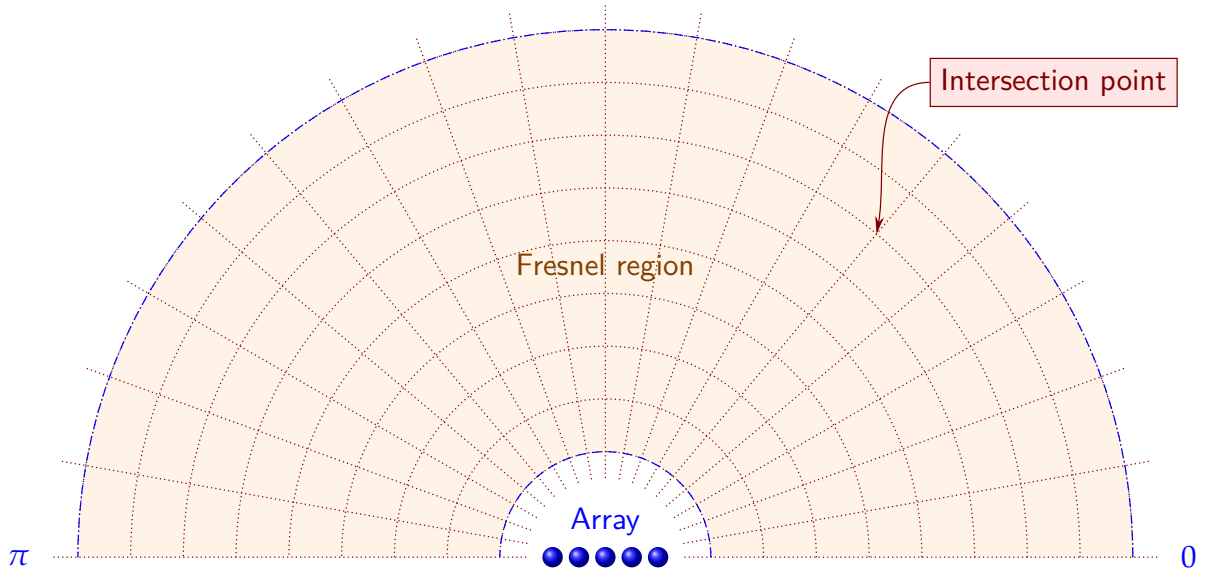

Figure 3.1 – Discretized Fresnel region of an array.

In other words,

$$\left(\widetilde{\overline{\rho}}_{e_q},\, \widetilde{\overline{\theta}}_{e_q}\right) = \underset{(\rho_e,\,\theta_e)}{\arg\min} \left\| \widetilde{\boldsymbol{\delta}}_{\boldsymbol{e}}(\rho_e,\,\theta_e) - \boldsymbol{\delta}_{\boldsymbol{e}}(\overline{\rho}_{e_q},\,\overline{\theta}_{e_q}) \right\|_F^2 \tag{3.1}$$

where $\widetilde{\overline{\rho}}_{e_q}$ and $\widetilde{\overline{\theta}}_{e_q}$ are respectively the biased range and DOD at the qth discrete location. The cost function in (3.2) can easily be solved using an iterative method like Newton's minimization. However, an iterative approach is often time consuming. Thus, to obtain a closed form expression based solution, we modify the cost function in (3.2) by using (1.33) that gives

$$(\widetilde{\overline{\omega}}_{e_q},\, \widetilde{\overline{\phi}}_{e_q}) = \underset{(\omega_e,\,\phi_e)}{\arg\min} \left\| \underline{\boldsymbol{M}} \begin{bmatrix} \omega_e \\ \phi_e \end{bmatrix} - \boldsymbol{\delta}_{\boldsymbol{e}}(\overline{\rho}_{e_q},\,\overline{\theta}_{e_q}) \right\|_F^2 . \tag{3.2}$$

The closed form solution of (3.2) in the LS sense can be given by

$$\begin{bmatrix} \widetilde{\overline{\omega}}_{e_q} \\ \widetilde{\overline{\phi}}_{e_q} \end{bmatrix} = \underline{\boldsymbol{M}}^{\dagger}\, \boldsymbol{\delta}_{\boldsymbol{e}}(\overline{\rho}_{e_q},\,\overline{\theta}_{e_q}). \tag{3.3}$$

Finally,

$$\widetilde{\overline{\theta}}_{e_q} = \arccos\left(\widetilde{\overline{\omega}}_{e_q}/d_e\right) \tag{3.4}$$

and

$$\widetilde{\overline{\rho}}_{e_q} = d_e^2\, \sin^2\left(\widetilde{\overline{\theta}}_{e_q}\right) / \left(2\,\widetilde{\overline{\phi}}_{e_q}\right). \tag{3.5}$$

Similar to the transmitting array, a separated LUT can be created for the receiving array by replacing the transmitting array side parameters with the receiving array side

parameters in (3.3), (3.4), and (3.5). Algorithm 3.1 summarizes the LUTs creation steps.

Algorithm 3.1 Look Up Tables Creation Method.

1: Discretize the near field region of the transmitting and receiving arrays.
2: Construct the accurate relative propagation path length vector for every discretized location using (1.6) and (1.7).
3: Calculate the biased location parameters for every discretized location using (3.3), (3.4), and (3.5) for the transmitting array and similar expressions for the receiving array.

3.2.2 Correction using LUT

The aim of the correction method is to get back the true location parameters from the biased location parameters estimated by an approximated model based localization technique. Therefore, when using the LUT in the correction method, $\widetilde{\overline{\rho}}_{e_q}$ and $\widetilde{\overline{\theta}}_{e_q}$ will be the inputs, and $\overline{\rho}_{e_q}$ and $\overline{\theta}_{e_q}$ will be the outputs of the LUT.

Figure 3.2 shows one block of the grid shown in Figure 3.1 inside which we have the biased location parameters, corresponding to the transmitting array, of the pth target, when estimated by an approximated model based localization method. In Figure 3.2, $(\rho_{e_p}, \theta_{e_p})$ is the pair of true transmitting array side location parameters of the pth target and $(\widetilde{\rho}_{e_p}, \widetilde{\theta}_{e_p})$ is its corresponding biased location parameters. $(\widetilde{\overline{\rho}}_{e_1}, \widetilde{\overline{\theta}}_{e_1})$, $(\widetilde{\overline{\rho}}_{e_2}, \widetilde{\overline{\theta}}_{e_2})$, $(\widetilde{\overline{\rho}}_{e_3}, \widetilde{\overline{\theta}}_{e_3})$, and $(\widetilde{\overline{\rho}}_{e_4}, \widetilde{\overline{\theta}}_{e_4})$ are four biased location parameters from the LUT, obtained using the method described in section 3.2.1, that are adjacent to $(\widetilde{\rho}_{e_p}, \widetilde{\theta}_{e_p})$. $(\overline{\rho}_{e_1}, \overline{\theta}_{e_1})$, $(\overline{\rho}_{e_2}, \overline{\theta}_{e_2})$, $(\overline{\rho}_{e_3}, \overline{\theta}_{e_3})$, and $(\overline{\rho}_{e_4}, \overline{\theta}_{e_4})$ are the corresponding true location parameters registered in the LUT. $\widetilde{d}_q$ represents the distance between $(\widetilde{\rho}_{e_p}, \widetilde{\theta}_{e_p})$ and $(\widetilde{\overline{\rho}}_{e_q}, \widetilde{\overline{\theta}}_{e_q})$ where $q \in \{1, 2, 3, 4\}$. It is calculated as

$$\widetilde{d}_q = \sqrt{\left(\widetilde{\overline{\rho}}_{e_q} - \widetilde{\rho}_{e_p}\right)^2 + \left(\widetilde{\overline{\theta}}_{e_q} - \widetilde{\theta}_{e_p}\right)^2}. \tag{3.6}$$

From Figure 3.2, $\widetilde{d}_1$, $\widetilde{d}_2$, $\widetilde{d}_3$, and $\widetilde{d}_4$ can be viewed as four minimum distances between the biased location parameters in LUT and $(\widetilde{\rho}_{e_p}, \widetilde{\theta}_{e_p})$. For these four nearest points, $[\widetilde{\overline{\rho}}_{e_q} - \overline{\rho}_{e_q}, \widetilde{\overline{\theta}}_{e_q} - \overline{\theta}_{e_q}]^T$, $\forall\, q \in \{1, 2, 3, 4\}$, can be considered as an approximation error vector. The main idea is to interpolate the approximation error vector corresponding to the pth target by using the known approximation error vectors at the four nearest neighbors. One of the low complexity interpolation methods suitable for such a situation is the natural neighbor interpolation with inverse distance weighting [117]. In our case, the mathematical expression of the natural neighbor interpolation can be

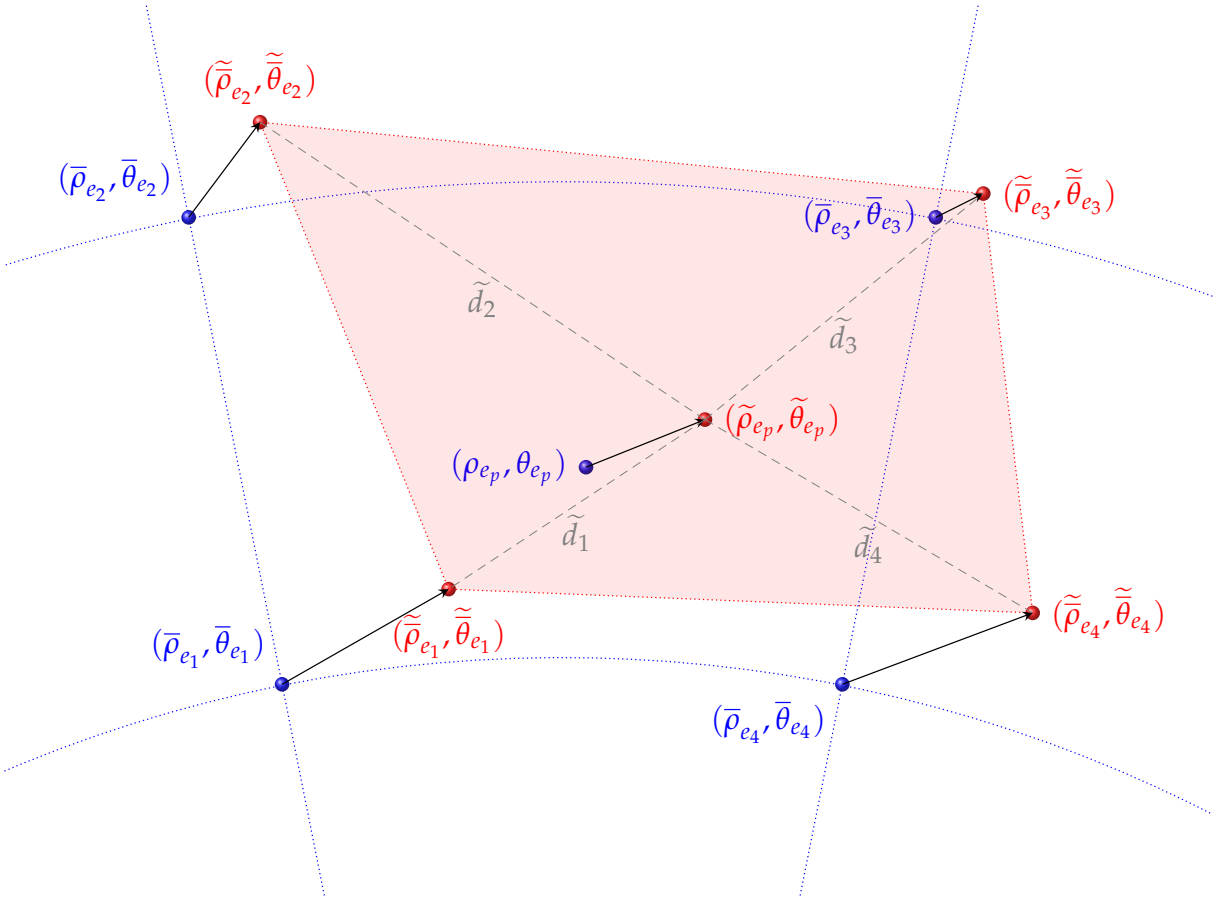

Figure 3.2 – A block of discretized 2D near field region.

written as

$$\begin{bmatrix} \hat{\rho}_{e_p} - \widetilde{\rho}_{e_p} \\ \hat{\theta}_{e_p} - \widetilde{\theta}_{e_p} \end{bmatrix} = \sum_{q=1}^{4} \overline{d}_q \begin{bmatrix} \overline{\rho}_{e_q} - \widetilde{\overline{\rho}}_{e_q} \\ \overline{\theta}_{e_q} - \widetilde{\overline{\theta}}_{e_q} \end{bmatrix} \tag{3.7}$$

where $\hat{\rho}_{e_p}$ and $\hat{\theta}_{e_p}$ are respectively the corrected range from the transmitting array and DOD and

$$\overline{d}_q = \left(\widetilde{d}_q \sum_{q'=1}^{4} 1/\widetilde{d}_{q'} \right)^{-1} \tag{3.8}$$

represents the inverse distance weighting. When $\widetilde{d}_q = 0$, for one value of q ($q \in \{1,2,3,4\}$); $\hat{\rho}_{e_p} = \overline{\rho}_{e_q}$ and $\hat{\theta}_{e_p} = \overline{\theta}_{e_q}$. It is impossible that two or more distances are simultaneously zero.

From (3.7), the corrected location parameters can be calculated as

$$\begin{bmatrix} \hat{\rho}_{e_p} \\ \hat{\theta}_{e_p} \end{bmatrix} = \begin{bmatrix} \widetilde{\rho}_{e_p} \\ \widetilde{\theta}_{e_p} \end{bmatrix} + \begin{bmatrix} \overline{\rho}_{e_1} - \widetilde{\overline{\rho}}_{e_1} & \overline{\rho}_{e_2} - \widetilde{\overline{\rho}}_{e_2} & \overline{\rho}_{e_3} - \widetilde{\overline{\rho}}_{e_3} & \overline{\rho}_{e_4} - \widetilde{\overline{\rho}}_{e_4} \\ \overline{\theta}_{e_1} - \widetilde{\overline{\theta}}_{e_1} & \overline{\theta}_{e_2} - \widetilde{\overline{\theta}}_{e_2} & \overline{\theta}_{e_3} - \widetilde{\overline{\theta}}_{e_3} & \overline{\theta}_{e_4} - \widetilde{\overline{\theta}}_{e_4} \end{bmatrix} \begin{bmatrix} \overline{d}_1 \\ \overline{d}_2 \\ \overline{d}_3 \\ \overline{d}_4 \end{bmatrix}. \tag{3.9}$$

Similar to the transmitting array side location parameters correction using LUT, the receiving array side location parameters can be corrected by using the same approach. Algorithm 3.2 provides the steps to make corrections using LUTs.

Algorithm 3.2 Look Up Tables Based Correction Method.

1: Estimate the DOD, DOA, and ranges of targets by an approximated model based method.
2: Search in the LUT belonging to the transmitting array for the four nearest neighbors of $(\widetilde{\rho}_{e_p}, \widetilde{\theta}_{e_p})$ on the basis of the distances calculated using (3.6).
3: Calculate the corresponding weights from the four distances using (3.8).
4: Use (3.9) to obtain the corrected location parameters $(\hat{\rho}_{e_p}, \hat{\theta}_{e_p})$.
5: Repeat the above steps from 2 to 4 for the receiving array side range and DOA with similar mathematical expressions.

3.3 Correction using Estimated Accurate Relative Propagation Path Length Vector

3.3.1 Principle

Consider a single near field target with location parameters $(\rho_{e_o}, \theta_{e_o}, \rho_{r_o}, \theta_{r_o})$ and reflection coefficient $s(t)$. Corresponding to it, the received signal can be written as

$$\boldsymbol{y}(t) = [\boldsymbol{a_e}(\rho_{e_o}, \theta_{e_o}) \otimes \boldsymbol{a_r}(\rho_{r_o}, \theta_{r_o})]\, s(t) + \boldsymbol{w}(t). \tag{3.10}$$

The noise subspace associated to $\boldsymbol{y}(t)$, in (3.10), can be given by

$$\boldsymbol{\Pi_n} = \boldsymbol{I}_{MN} - \frac{1}{MN} [\boldsymbol{a_e}(\rho_{e_o}, \theta_{e_o}) \otimes \boldsymbol{a_r}(\rho_{r_o}, \theta_{r_o})]\, [\boldsymbol{a_e}(\rho_{e_o}, \theta_{e_o}) \otimes \boldsymbol{a_r}(\rho_{r_o}, \theta_{r_o})]^H. \tag{3.11}$$

An accurate model based subspace technique finds the DOA (θ_r), DOD (θ_e), and ranges (ρ_e and ρ_r) of the target such that

$$[\boldsymbol{a_e}(\rho_{e_o}, \theta_{e_o}) \otimes \boldsymbol{a_r}(\rho_{r_o}, \theta_{r_o})]^H\, \boldsymbol{\Pi_n}\, [\boldsymbol{a_e}(\rho_{e_o}, \theta_{e_o}) \otimes \boldsymbol{a_r}(\rho_{r_o}, \theta_{r_o})] = 0. \tag{3.12}$$

The solution of (3.12) is given by $\rho_e = \rho_{e_o}$, $\theta_e = \theta_{e_o}$, $\rho_r = \rho_{r_o}$, and $\theta_r = \theta_{r_o}$, which

means

$$[\boldsymbol{a_e}(\rho_{e_o}, \theta_{e_o}) \otimes \boldsymbol{a_r}(\rho_{r_o}, \theta_{r_o})]^H \left(\boldsymbol{I}_{MN} - \frac{1}{MN} [\boldsymbol{a_e}(\rho_{e_o}, \theta_{e_o}) \otimes \boldsymbol{a_r}(\rho_{r_o}, \theta_{r_o})] \right. \tag{3.13}$$
$$\left. [\boldsymbol{a_e}(\rho_{e_o}, \theta_{e_o}) \otimes \boldsymbol{a_r}(\rho_{r_o}, \theta_{r_o})]^H \right) [\boldsymbol{a_e}(\rho_{e_o}, \theta_{e_o}) \otimes \boldsymbol{a_r}(\rho_{r_o}, \theta_{r_o})]$$
$$= [\boldsymbol{a_e}(\rho_{e_o}, \theta_{e_o}) \otimes \boldsymbol{a_r}(\rho_{r_o}, \theta_{r_o})]^H [\boldsymbol{a_e}(\rho_{e_o}, \theta_{e_o}) \otimes \boldsymbol{a_r}(\rho_{r_o}, \theta_{r_o})]$$
$$- \frac{1}{MN} [\boldsymbol{a_e}(\rho_{e_o}, \theta_{e_o}) \otimes \boldsymbol{a_r}(\rho_{r_o}, \theta_{r_o})]^H [\boldsymbol{a_e}(\rho_{e_o}, \theta_{e_o}) \otimes \boldsymbol{a_r}(\rho_{r_o}, \theta_{r_o})]$$
$$[\boldsymbol{a_e}(\rho_{e_o}, \theta_{e_o}) \otimes \boldsymbol{a_r}(\rho_{r_o}, \theta_{r_o})]^H [\boldsymbol{a_e}(\rho_{e_o}, \theta_{e_o}) \otimes \boldsymbol{a_r}(\rho_{r_o}, \theta_{r_o})]$$
$$= MN - \frac{1}{MN} M^2 N^2 = 0. \tag{3.14}$$

An approximated model based subspace technique finds the DOA, DOD, and ranges by minimizing the following cost function:

$$(\widetilde{\rho}_e, \widetilde{\theta}_e, \widetilde{\rho}_r, \widetilde{\theta}_r) = \underset{(\rho_e, \theta_e, \rho_r, \theta_r)}{\arg\min} [\widetilde{\boldsymbol{a}}_{\boldsymbol{e}}(\rho_e, \theta_e) \otimes \widetilde{\boldsymbol{a}}_{\boldsymbol{r}}(\rho_r, \theta_r)]^H \boldsymbol{\Pi_n} [\widetilde{\boldsymbol{a}}_{\boldsymbol{e}}(\rho_e, \theta_e) \otimes \widetilde{\boldsymbol{a}}_{\boldsymbol{r}}(\rho_r, \theta_r)] \tag{3.15}$$
$$= \underset{(\rho_e, \theta_e, \rho_r, \theta_r)}{\arg\min} \left\{ [\widetilde{\boldsymbol{a}}_{\boldsymbol{e}}(\rho_e, \theta_e) \otimes \widetilde{\boldsymbol{a}}_{\boldsymbol{r}}(\rho_r, \theta_r)]^H [\widetilde{\boldsymbol{a}}_{\boldsymbol{e}}(\rho_e, \theta_e) \otimes \widetilde{\boldsymbol{a}}_{\boldsymbol{r}}(\rho_r, \theta_r)] \right.$$
$$- \frac{1}{MN} [\widetilde{\boldsymbol{a}}_{\boldsymbol{e}}(\rho_e, \theta_e) \otimes \widetilde{\boldsymbol{a}}_{\boldsymbol{r}}(\rho_r, \theta_r)]^H [\boldsymbol{a_e}(\rho_{e_o}, \theta_{e_o}) \otimes \boldsymbol{a_r}(\rho_{r_o}, \theta_{r_o})]$$
$$\left. [\boldsymbol{a_e}(\rho_{e_o}, \theta_{e_o}) \otimes \boldsymbol{a_r}(\rho_{r_o}, \theta_{r_o})]^H [\widetilde{\boldsymbol{a}}_{\boldsymbol{e}}(\rho_e, \theta_e) \otimes \widetilde{\boldsymbol{a}}_{\boldsymbol{r}}(\rho_r, \theta_r)] \right\}$$
$$= \underset{(\rho_e, \theta_e, \rho_r, \theta_r)}{\arg\min} \left[MN - \frac{1}{MN} \left| [\widetilde{\boldsymbol{a}}_{\boldsymbol{e}}(\rho_e, \theta_e) \otimes \widetilde{\boldsymbol{a}}_{\boldsymbol{r}}(\rho_r, \theta_r)]^H \right. \right.$$
$$\left. \left. [\boldsymbol{a_e}(\rho_{e_o}, \theta_{e_o}) \otimes \boldsymbol{a_r}(\rho_{r_o}, \theta_{r_o})] \right|^2 \right]$$
$$= \underset{(\rho_e, \theta_e, \rho_r, \theta_r)}{\arg\max} \left| [\widetilde{\boldsymbol{a}}_{\boldsymbol{e}}(\rho_e, \theta_e) \otimes \widetilde{\boldsymbol{a}}_{\boldsymbol{r}}(\rho_r, \theta_r)]^H [\boldsymbol{a_e}(\rho_{e_o}, \theta_{e_o}) \otimes \boldsymbol{a_r}(\rho_{r_o}, \theta_{r_o})] \right|^2 \tag{3.16}$$
$$= \underset{(\rho_e, \theta_e, \rho_r, \theta_r)}{\arg\min} \| [\widetilde{\boldsymbol{a}}_{\boldsymbol{e}}(\rho_e, \theta_e) \otimes \widetilde{\boldsymbol{a}}_{\boldsymbol{r}}(\rho_r, \theta_r)] - [\boldsymbol{a_e}(\rho_{e_o}, \theta_{e_o}) \otimes \boldsymbol{a_r}(\rho_{r_o}, \theta_{r_o})] \|_F^2 . \tag{3.17}$$

Ideally, the minimum of the cost function in (3.17) should be equal to zero. However, from (1.2), (1.3), (1.28), and (1.29), we can say that $\boldsymbol{a_e}(\rho_{e_o}, \theta_{e_o}) \neq \widetilde{\boldsymbol{a}}_{\boldsymbol{e}}(\rho_{e_o}, \theta_{e_o})$ and $\boldsymbol{a_r}(\rho_{r_o}, \theta_{r_o}) \neq \widetilde{\boldsymbol{a}}_{\boldsymbol{r}}(\rho_{r_o}, \theta_{r_o})$, or, $\boldsymbol{a_e}(\rho_{e_o}, \theta_{e_o}) \otimes \boldsymbol{a_r}(\rho_{r_o}, \theta_{r_o})$ and $\widetilde{\boldsymbol{a}}_{\boldsymbol{e}}(\rho_{e_o}, \theta_{e_o}) \otimes \widetilde{\boldsymbol{a}}_{\boldsymbol{r}}(\rho_{r_o}, \theta_{r_o})$ are not collinear. As a result, the problem becomes to find $(\widetilde{\rho}_e, \widetilde{\theta}_e, \widetilde{\rho}_r, \widetilde{\theta}_r)$ such that the

correlation between $\boldsymbol{a_e}(\rho_{e_o},\, \theta_{e_o}) \otimes \boldsymbol{a_r}(\rho_{r_o},\, \theta_{r_o})$ and $\widetilde{\boldsymbol{a}}_{\boldsymbol{e}}(\rho_e,\, \theta_e) \otimes \widetilde{\boldsymbol{a}}_{\boldsymbol{r}}(\rho_r,\, \theta_r)$ maximizes:

$$(\widetilde{\rho}_e,\, \widetilde{\theta}_e,\, \widetilde{\rho}_r,\, \widetilde{\theta}_r) = \underset{(\rho_e, \theta_e, \rho_r, \theta_r)}{\arg\max} \left| [\widetilde{\boldsymbol{a}}_{\boldsymbol{e}}(\rho_e,\, \theta_e) \otimes \widetilde{\boldsymbol{a}}_{\boldsymbol{r}}(\rho_r,\, \theta_r)]^H \; [\boldsymbol{a_e}(\rho_{e_o},\, \theta_{e_o}) \otimes \boldsymbol{a_r}(\rho_{r_o},\, \theta_{r_o})] \right| \tag{3.18}$$

$$= \underset{(\rho_e, \theta_e, \rho_r, \theta_r)}{\arg\max} \left| \sum_{m=1}^{M} \sum_{n=1}^{N} \exp\Big(j\, 2\, \pi \Big(\widetilde{\delta}_{e_m}(\rho_e,\, \theta_e) + \widetilde{\delta}_{r_n}(\rho_r,\, \theta_r) - \delta_{e_m}(\rho_{e_o},\, \theta_{e_o}) - \delta_{r_n}(\rho_{r_o},\, \theta_{r_o}) \Big) / \lambda \Big) \right|. \tag{3.19}$$

The cost function in (3.19) is a nonlinear maximization problem, therefore, its solution in a closed form expression is difficult to achieve. However, two suboptimal solutions can be found as

$$(\widetilde{\rho}_e,\, \widetilde{\theta}_e) = \underset{(\rho_e, \theta_e)}{\arg\min} \sum_{m=0}^{M-1} \left| \widetilde{\delta}_{e_m}(\rho_e,\, \theta_e) - \delta_{e_m}(\rho_{e_o},\, \theta_{e_o}) \right|^2 = \underset{(\rho_e, \theta_e)}{\arg\min} \left\| \widetilde{\boldsymbol{\delta}}_{\boldsymbol{e}}(\rho_e,\, \theta_e) - \boldsymbol{\delta_e}(\rho_{e_o},\, \theta_{e_o}) \right\|_F^2 \tag{3.20}$$

and

$$(\widetilde{\rho}_r,\, \widetilde{\theta}_r) = \underset{(\rho_r, \theta_r)}{\arg\min} \sum_{n=0}^{N-1} \left| \widetilde{\delta}_{r_n}(\rho_r,\, \theta_r) - \delta_{r_n}(\rho_{r_o},\, \theta_{r_o}) \right|^2 = \underset{(\rho_r, \theta_r)}{\arg\min} \left\| \widetilde{\boldsymbol{\delta}}_{\boldsymbol{r}}(\rho_r,\, \theta_r) - \boldsymbol{\delta_r}(\rho_{r_o},\, \theta_{r_o}) \right\|_F^2. \tag{3.21}$$

It is obvious from (3.20) that

$$\begin{aligned} \min_{(\rho_e, \theta_e)} \left\| \widetilde{\boldsymbol{\delta}}_{\boldsymbol{e}}(\rho_e,\, \theta_e) - \boldsymbol{\delta_e}(\rho_{e_o},\, \theta_{e_o}) \right\|_F^2 &= \left\| \widetilde{\boldsymbol{\delta}}_{\boldsymbol{e}}(\widetilde{\rho}_e,\, \widetilde{\theta}_e) - \boldsymbol{\delta_e}(\rho_{e_o},\, \theta_{e_o}) \right\|_F^2 \\ &\leq \left\| \widetilde{\boldsymbol{\delta}}_{\boldsymbol{e}}(\rho_{e_o},\, \theta_{e_o}) - \boldsymbol{\delta_e}(\rho_{e_o},\, \theta_{e_o}) \right\|_F^2 \end{aligned} \tag{3.22}$$

which means that $\widetilde{\boldsymbol{\delta}}_{\boldsymbol{e}}(\widetilde{\rho}_e, \widetilde{\theta}_e)$ is a better estimate of the true $\boldsymbol{\delta_e}(\rho_{e_o}, \theta_{e_o})$ than $\widetilde{\boldsymbol{\delta}}_{\boldsymbol{e}}(\rho_{e_o}, \theta_{e_o})$ and that $(\widetilde{\rho}_e, \widetilde{\theta}_e)$ is a biased estimation of $(\rho_{e_o}, \theta_{e_o})$. $\widetilde{\boldsymbol{\delta}}_{\boldsymbol{e}}(\widetilde{\rho}_e, \widetilde{\theta}_e)$ being an optimal estimate of $\boldsymbol{\delta_e}(\rho_{e_o}, \theta_{e_o})$ in LS sense, a better estimate of $(\rho_{e_o}, \theta_{e_o})$ can be expected from it. The same can be said for the receiving array side range and DOA from (3.21).

3.3.2 Procedure

Let $(\widetilde{\rho}_{e_p},\, \widetilde{\theta}_{e_p}, \widetilde{\rho}_{r_p},\, \widetilde{\theta}_{r_p})$ be the location parameters of the pth target estimated by an approximated model based method. $\delta_{e_m}(\rho_{e_p}, \theta_{e_p})$ and $\delta_{r_n}(\rho_{r_p}, \theta_{r_p})$ can respectively be estimated by substituting these values in (1.27) and (1.25) as

$$\hat{\delta}_{e_{(m,\,p)}} = \widetilde{\delta}_{e_m}(\widetilde{\rho}_{e_p}, \widetilde{\theta}_{e_p}) \tag{3.23}$$

and

$$\hat{\delta}_{r_{(p,n)}} = \widetilde{\delta}_{r_n}(\widetilde{\rho}_{r_p}, \widetilde{\theta}_{r_p}). \tag{3.24}$$

On replacing $\delta_{e_m}(\rho_{e_p}, \theta_{e_p})$ by $\hat{\delta}_{e_{(m,p)}}$ in the rearranged form of (1.4), we can get

$$2\,(m - m_o)\,d_e\,\rho_{e_p}\,\cos\left(\theta_{e_p}\right) + 2\,\hat{\delta}_{e_{(m,p)}}\,\rho_{e_p} = (m - m_o)^2\,d_e^2 - \hat{\delta}^2_{e_{(m,p)}} \tag{3.25}$$

For all values of m, we can construct an overdetermined system of M linear equations with $\rho_{e_p}\,\cos(\theta_{e_p})$ and ρ_{e_p} as the unknowns. Since, $\hat{\delta}_{e_{(m,p)}}$ appears on the either sides of (3.25), Total Least Squares (TLS) is a better approach to solve this system of linear equations than the conventional LS according to [118]. In order to obtain TLS solutions, let $\boldsymbol{v}_{e_p} \in \mathbb{R}^3$ be the right-singular-vector associated to the smallest singular value of the following matrix constructed from the coefficients of (3.25):

$$\begin{bmatrix} 2\,(1 - m_o)\,d_e & 2\,\hat{\delta}_{e_{(1,p)}} & (1 - m_o)^2\,d_e^2 - \hat{\delta}^2_{e_{(1,p)}} \\ 2\,(2 - m_o)\,d_e & 2\,\hat{\delta}_{e_{(2,p)}} & (2 - m_o)^2\,d_e^2 - \hat{\delta}^2_{e_{(2,p)}} \\ \vdots & \vdots & \vdots \\ 2\,(m - m_o)\,d_e & 2\,\hat{\delta}_{e_{(m,p)}} & (m - m_o)^2\,d_e^2 - \hat{\delta}^2_{e_{(m,p)}} \\ \vdots & \vdots & \vdots \\ 2\,(M - m_o)\,d_e & 2\,\hat{\delta}_{e_{(M,p)}} & (M - m_o)^2\,d_e^2 - \hat{\delta}^2_{e_{(M,p)}} \end{bmatrix}. \tag{3.26}$$

From $\boldsymbol{v}_{e_p}$, the estimates of the transmitting array side range and DOD of the pth target can be calculated as $\hat{\rho}_{e_p} = -[\boldsymbol{v}_{e_p}]_2/[\boldsymbol{v}_{e_p}]_3$ and $\hat{\theta}_{e_p} = \arccos([\boldsymbol{v}_{e_p}]_1/[\boldsymbol{v}_{e_p}]_2)$ respectively.

Similar to (3.25), replacing $\delta_{r_n}(\rho_{r_p}, \theta_{r_p})$ by $\hat{\delta}_{r_{(p,n)}}$ in the rearranged form of (1.5) leads to

$$2\,(n - n_o)\,d_r\,\rho_{r_p}\,\cos\left(\theta_{r_p}\right) + 2\,\hat{\delta}_{r_{(p,n)}}\,\rho_{r_p} = (n - n_o)^2\,d_r^2 - \hat{\delta}^2_{r_{(p,n)}} \tag{3.27}$$

which can be used to construct an overdetermined system of N linear equations in $\rho_{r_p}\,\cos(\theta_{r_p})$ and ρ_{r_p} for all the values of n. Like above, let $\boldsymbol{v}_{r_p} \in \mathbb{R}^3$ be the right-singular-vector associated with the smallest singular value of the following matrix constructed from the coefficients of (3.27):

$$\begin{bmatrix} 2\,(1 - n_o)\,d_r & 2\,\hat{\delta}_{r_{(p,1)}} & (1 - n_o)^2\,d_r^2 - \hat{\delta}^2_{r_{(p,1)}} \\ 2\,(2 - n_o)\,d_r & 2\,\hat{\delta}_{r_{(p,2)}} & (2 - n_o)^2\,d_r^2 - \hat{\delta}^2_{r_{(p,2)}} \\ \vdots & \vdots & \vdots \\ 2\,(n - n_o)\,d_r & 2\,\hat{\delta}_{r_{(p,n)}} & (n - n_o)^2\,d_r^2 - \hat{\delta}^2_{r_{(p,n)}} \\ \vdots & \vdots & \vdots \\ 2\,(N - n_o)\,d_r & 2\,\hat{\delta}_{r_{(p,N)}} & (N - n_o)^2\,d_r^2 - \hat{\delta}^2_{r_{(p,N)}} \end{bmatrix}. \tag{3.28}$$

The receiving array side range and DOA of the pth target can respectively be calculated by $\hat{\rho}_{r_p} = -[\boldsymbol{v}_{r_p}]_2/[\boldsymbol{v}_{r_p}]_3$ and $\hat{\theta}_{r_p} = \arccos([\boldsymbol{v}_{r_p}]_1/[\boldsymbol{v}_{r_p}]_2)$.

The complete correction procedure is summarized in Algorithm 3.3.

Algorithm 3.3 Estimated Relative Path Length Vector Based Correction Method.

1: Estimate the DOA, DOD, and ranges of targets by an approximated model based technique.
2: Calculate $\hat{\delta}_{e_{(m,p)}}$ and $\hat{\delta}_{r_{(p,n)}}$ for the pth target using (3.23) and (3.24).
3: Construct the matrices (3.26) and (3.28) from $\hat{\delta}_{e_{(m,p)}}$ and $\hat{\delta}_{r_{(p,n)}}$ respectively.
4: Using TLS method, get $\hat{\rho}_{e_p}$, $\hat{\theta}_{e_p}$, $\hat{\rho}_{r_p}$, and $\hat{\theta}_{r_p}$ of the pth target.
5: Repeat the above steps from 2 to 4 for each target.

3.4 Four Location Parameters to Cartesian Coordinates

As mention in section 1.4 that three independent coordinates are sufficient to define a position in a 3D space and analyzing the four location parameters individually is also not very practical. Hence, we convert the four redundant location parameters to three independent Cartesian coordinates so that we can easily calculate the localization error in terms of the Euclidean distance between the true and estimated positions of a target.

The estimated DOA, DOD, and ranges of a target can be used in (1.37) and (1.38) to construct the parametric equations of the circles corresponding to that target as

$$\boldsymbol{\psi}_{\boldsymbol{e}_p}(\varphi_e) = \hat{\rho}_{e_p} \sin\left(\hat{\theta}_{e_p}\right) \left[\cos(\varphi_e)\ \boldsymbol{\nu}_{\boldsymbol{e}_p} + \sin(\varphi_e)\ \boldsymbol{d}_{\boldsymbol{c}_e} \times \boldsymbol{\nu}_{\boldsymbol{e}_p}\right] + \hat{\rho}_{e_p} \cos\left(\hat{\theta}_{e_p}\right) \boldsymbol{d}_{\boldsymbol{c}_e} + \boldsymbol{e}_{\boldsymbol{o}} \tag{3.29}$$

and

$$\boldsymbol{\psi}_{\boldsymbol{r}_p}(\varphi_r) = \hat{\rho}_{r_p} \sin\left(\hat{\theta}_{r_p}\right) \left[\cos(\varphi_r)\ \boldsymbol{\nu}_{\boldsymbol{r}_p} + \sin(\varphi_r)\ \boldsymbol{d}_{\boldsymbol{c}_r} \times \boldsymbol{\nu}_{\boldsymbol{r}_p}\right] + \hat{\rho}_{r_p} \cos\left(\hat{\theta}_{r_p}\right) \boldsymbol{d}_{\boldsymbol{c}_r} + \boldsymbol{r}_{\boldsymbol{o}}. \tag{3.30}$$

As shown in Figure 1.11, the required coordinates are at the intersection of these circles. However, due to the estimation error and noise, the circles may not intersect; thus, we propose to minimize the following cost function:

$$(\hat{\varphi}_e,\ \hat{\varphi}_r) = \underset{(\varphi_e,\,\varphi_e)}{\arg\min} \left\{ \left\| \boldsymbol{\psi}_{\boldsymbol{e}_p}(\varphi_e) - \boldsymbol{\psi}_{\boldsymbol{r}_p}(\varphi_r) \right\|_F^2 \right\} \tag{3.31}$$

where $\left\| \boldsymbol{\psi}_{\boldsymbol{e}_p}(\varphi_e) - \boldsymbol{\psi}_{\boldsymbol{r}_p}(\varphi_r) \right\|_F^2$ can be interpreted as the square of the Euclidean distance between the two points on the two circles in 3D space.

A coarse solution of (3.31) can be calculated by exhaustive grid search, and then it can be finely tuned by Newton's minimization method. Finally, the position vector of

the pth target can be computed as $\hat{\boldsymbol{t}}_p = \boldsymbol{\psi}_{\boldsymbol{e}_p}(\hat{\varphi}_e)$, $\hat{\boldsymbol{t}}_p = \boldsymbol{\psi}_{\boldsymbol{r}_p}(\hat{\varphi}_r)$, or the average of these two position vectors.

3.5 Numerical Example

For the simulations in this section, we generate the signal data from the accurate signal model explained in section 1.4. Then, we use the methods described in chapter 2 to obtain the four location parameters from this accurate signal model data. Because of the Fresnel approximation, the location parameters estimated from the methods have some biases. We try to reduce this bias from each location parameter by using the proposed correction methods in this chapter. Consequently, we have four corrected location parameters with redundant information for each target. Thus, we compute the corresponding Cartesian coordinates from the method provided in section 3.4. Finally, we express the localization error as the Euclidean distances between the true and estimated positions of a target to analyze the correction performance of the proposed methods.

Assume a bistatic MIMO system, as shown in Figure 1.11, with $M = 7$ ($\check{M} = 3$) transmitting and $N = 9$ ($\check{N} = 4$) receiving antennas. The methods discussed in chapter 2 require symmetric ULAs with inter element spacings $d_e = d_r = \lambda/4$. Therefore, $m_o = 4$ and $n_o = 5$. Like before, here too, λ is considered as the unit of length. To use the signal model in section 1.4, we need the following additional parameters of the bistatic MIMO system:

1. $\boldsymbol{e_o} = [0.6\lambda, \lambda, 1.4\lambda]^T$,
2. $\boldsymbol{r_o} = [0.5\lambda, -0.4\lambda, -0.9\lambda]^T$,
3. $\boldsymbol{d}_{\boldsymbol{c}_e} = [\cos(80^\circ), \cos(70^\circ), \sqrt{1 - \cos^2(80^\circ) - \cos^2(70^\circ)}]^T$, and
4. $\boldsymbol{d}_{\boldsymbol{c}_r} = [\cos(40^\circ), \cos(110^\circ), \sqrt{1 - \cos^2(40^\circ) - \cos^2(110^\circ)}]^T$.

The values of these parameters are arbitrarily chosen such that there exists a near field region of significant size which is shared by both ULAs.

Unlike in section 2.3, the performance of the proposed correction methods elaborated in this chapter is analyzed as the root of mean squares of the Euclidean distances between the true and K estimated positions of a target, with respect to SNR, calculated as

$$\epsilon\left(\boldsymbol{t}_p\right) = \sqrt{\frac{1}{K}\sum_{k=1}^{K}\left\|\hat{\boldsymbol{t}}_p(k) - \boldsymbol{t}_p\right\|_F^2} \tag{3.32}$$

where K is the total number of Monte Carlo trials at each SNR and $\hat{\boldsymbol{t}}_p(k)$ is the estimated position of the pth target at the kth trial.

In Figure 3.3, we compare $\epsilon(\boldsymbol{t}_p)$ of two near field targets whose location parameters are estimated by the methods described in chapter 2 and corrected using the LUT based correction method given in section 3.2. The position vectors of the two targets are $[4\lambda, 3\lambda, 2\lambda]^T$ and $[-2.9\lambda, 1.7\lambda, 1.5\lambda]^T$. Figure 3.4 shows the similar plots when the correction is performed using the proposed method elaborated in section 3.3.

From Figure 2.4 to Figure 2.7, we can conclude that the proposed method in section 2.2 provides better precision than the existing method summarized in section 2.1. The same can be observed in Figure 3.3 and Figure 3.4 when the input signals are modeled without Fresnel approximation. The presence of systematic bias in the estimated position due to the Fresnel approximation can be seen in both the figures as the floor effect at high SNR in the curves corresponding to the method in section 2.2 before correction. At low SNR, this systematic bias is not distinguishable in the estimated position because the noise contributes more to the localization error than the systematic bias. The proposed correction methods only reduce the effect of the systematic bias added during the Fresnel approximation. The estimation errors in the positions estimated by the method in section 2.1 for the two chosen targets are so large that the floor effect is not visible in the figures.

It can be observed in both the figures that both of the proposed correction methods have high performance when the estimates are good, because the performance of each correction method also depends upon the performance of the used approximated model based method. Also, both the proposed correction methods have almost similar correction performance. However, the computation complexity of the method in section 3.3 is much lower than the LUT based correction method in section 3.2.

Additionally, the two proposed correction methods are applicable to a single receiving array. Therefore, they can also be used for the near field sources localization techniques based on the approximated model such as [2] and [3]. Appendix B shows the further analysis of the correction methods on such approximated model based methods.

3.6 Conclusion

The proposed correction methods can significantly reduce the systemic biases appeared in the estimated location parameters due to the Fresnel approximation at high SNR when the effect of the bias dominates the additive noise. The correction performance of both methods improves with the decrease in the estimation error. In the simulation, a numerical example with symmetric ULAs having quarter wavelength inter element spacings is considered. However, the proposed correction methods have no such requirements. In other words, the proposed correction methods can be applied to an approximated model based method which uses non-symmetric arrays with inter

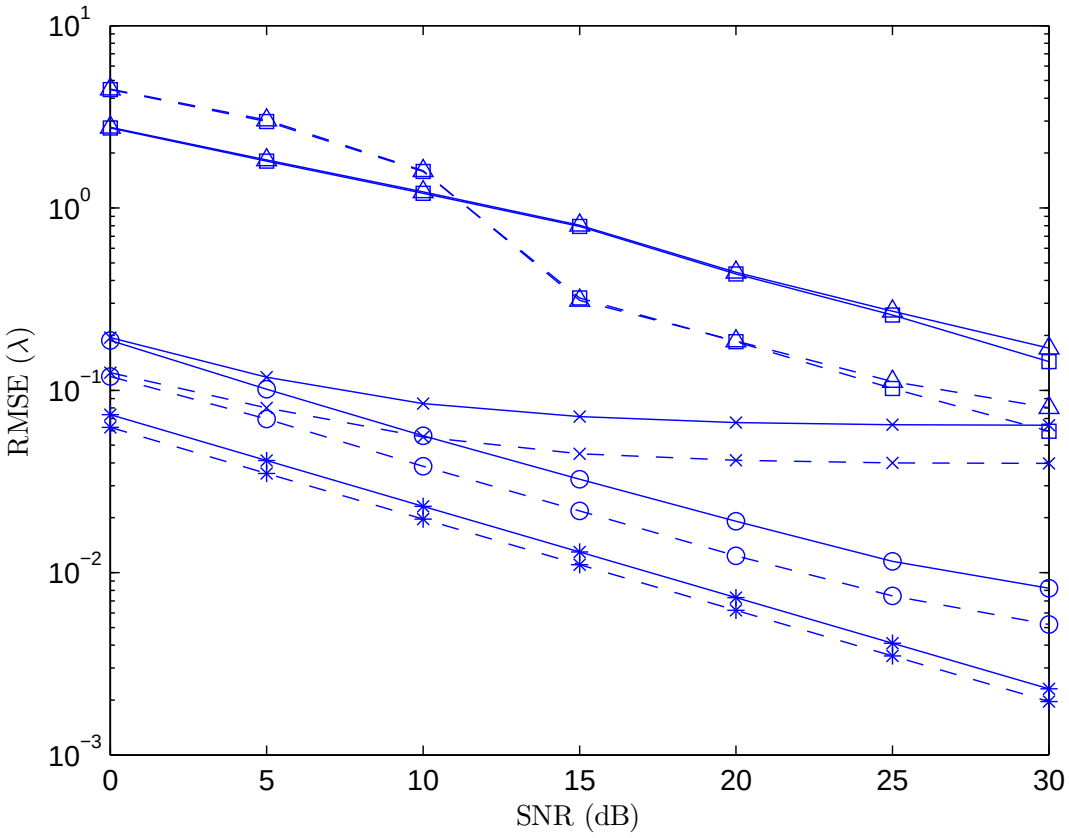

Figure 3.3 – RMSE in the position estimated by the methods described in Chapter 2 and corrected by the proposed method explained in section 3.2 versus SNR. The CRLBs are calculated using (1.43) and (1.45).

The legends of the figure are as follows:

- $\epsilon(\boldsymbol{t}_1)$; Section 2.1
- $\epsilon(\boldsymbol{t}_2)$; Section 2.1
- $\epsilon(\boldsymbol{t}_1)$; Section 2.1 & Section 3.2
- $\epsilon(\boldsymbol{t}_2)$; Section 2.1 & Section 3.2
- $\epsilon(\boldsymbol{t}_1)$; Section 2.2
- $\epsilon(\boldsymbol{t}_2)$; Section 2.2
- $\epsilon(\boldsymbol{t}_1)$; Section 2.2 & Section 3.2
- $\epsilon(\boldsymbol{t}_2)$; Section 2.2 & Section 3.2
- $\varepsilon(\boldsymbol{t}_1)$; Section 1.5
- $\varepsilon(\boldsymbol{t}_2)$; Section 1.5

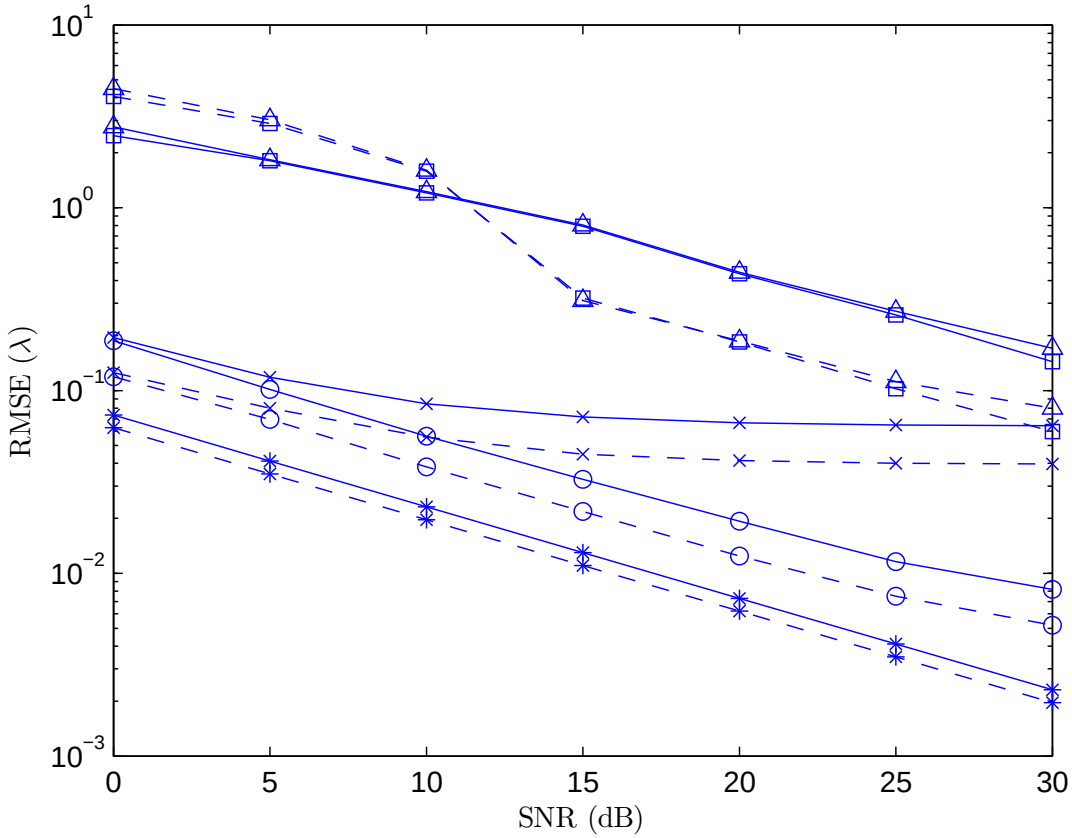

Figure 3.4 – RMSE in the position estimated by the methods described in Chapter 2 and corrected by the proposed method explained in section 3.3 versus SNR. The CRLBs are calculated using (1.43) and (1.45).

The legends of the figure are as follows:

- $\epsilon(\boldsymbol{t}_1)$; Section 2.1
- $\epsilon(\boldsymbol{t}_2)$; Section 2.1
- $\epsilon(\boldsymbol{t}_1)$; Section 2.1 & Section 3.3
- $\epsilon(\boldsymbol{t}_2)$; Section 2.1 & Section 3.3
- $\epsilon(\boldsymbol{t}_1)$; Section 2.2
- $\epsilon(\boldsymbol{t}_2)$; Section 2.2
- $\epsilon(\boldsymbol{t}_1)$; Section 2.2 & Section 3.3
- $\epsilon(\boldsymbol{t}_2)$; Section 2.2 & Section 3.3
- $\varepsilon(\boldsymbol{t}_1)$; Section 1.5
- $\varepsilon(\boldsymbol{t}_2)$; Section 1.5

element spacings less than or equal to $\lambda/2$. Fresnel approximation is the cause of the biases in the location parameter, therefore, by avoiding it, we can directly obtain unbiased location parameters. In the next chapter, we propose two methods which do not use Fresnel approximation.

4

Accurate Model Based Methods

Beside reducing the bias due to the Fresnel approximation, we can directly exploit the accurate model. In this chapter, we discuss two proposed methods which can directly deal with the accurate signal model. The key strategy used by both the proposed methods is to estimate δ_{e_p} and δ_{r_p} first, then use the accurate model on them to obtain the estimates of ρ_{e_p}, θ_{e_p}, ρ_{r_p}, and θ_{r_p}. The first proposed method in this chapter is an improvement of [1] to deal with the accurate signal model. The second proposed method in this chapter uses a tensor decomposition technique known as PARAFAC to estimate the directional vectors.

4.1 Improved [1] for Accurate Model

As in [1], the received signal vector is subdivided into M subvectors belonging to each transmitting antenna as $\boldsymbol{y}(t) = [\overline{\boldsymbol{y}}_1^T(t), \overline{\boldsymbol{y}}_2^T(t), \cdots, \overline{\boldsymbol{y}}_M^T(t)]^T$. The subvector corresponding to the mth transmitter can be written as

$$\overline{\boldsymbol{y}}_m(t) = \breve{\boldsymbol{y}}_m(t) + \overline{\boldsymbol{w}}_m(t) \tag{4.1}$$

where $\overline{\boldsymbol{w}}_m(t)$ is the corresponding noise subvector and $\breve{\boldsymbol{y}}_m(t) = \boldsymbol{A_r}\,\boldsymbol{D}_m\,\boldsymbol{s}(t)$ where

$$\boldsymbol{D}_m = \text{diag}\left\{\left[a_{e_{(m,1)}}, a_{e_{(m,2)}}, \cdots, a_{e_{(m,P)}}\right]\right\} \tag{4.2}$$

is the diagonal matrix with the elements of the mth row of $\boldsymbol{A_e}$ as its diagonal components.

The eigendecomposition of the covariance matrix $\boldsymbol{R} = \mathrm{E}\{\boldsymbol{y}(t)\,\boldsymbol{y}^H(t)\} \in \mathbb{C}^{MN\times MN}$ can be written as

$$\boldsymbol{R} = \boldsymbol{U}\,\boldsymbol{\Lambda}\,\boldsymbol{U}^H \tag{4.3}$$

where the columns of $\boldsymbol{U}$ are the eigenvectors and the diagonal elements of $\boldsymbol{\Lambda}$ are the corresponding eigenvalues. If the eigenvalues are sorted in descending order, then the qth eigenvalue can be expressed as

$$\mu_q = \begin{cases} \breve{\mu}_q + \sigma_w^2 & \text{if } q \in \{1, 2, \cdots, P\} \\ \sigma_w^2 & \text{if } q \in \{P+1, P+2, \cdots, MN\} \end{cases} \tag{4.4}$$

where $\breve{\mu}_q$ is the qth eigenvalue among the P nonzero eigenvalues of $\boldsymbol{A}\,\boldsymbol{R_s}\,\boldsymbol{A}^H$ arranged in descending order with $\boldsymbol{R_s} = \mathrm{E}\{\boldsymbol{s}(t)\,\boldsymbol{s}^H(t)\}$. The following subspace based approach can be used to remove the additive noise, in which the noiseless covariance matrix is reconstructed from $\boldsymbol{U}$ and $\boldsymbol{\Lambda}$ of $\boldsymbol{R}$ as [119]

$$\breve{\boldsymbol{R}} = \boldsymbol{U_s}\,\mathrm{diag}\{[\mu_1 - \sigma_w^2, \mu_2 - \sigma_w^2, \cdots, \mu_P - \sigma_w^2]\}\boldsymbol{U_s}^H \tag{4.5}$$

where $\boldsymbol{U_s}$ contains the columns of $\boldsymbol{U}$ corresponding to the P largest eigenvalues of $\boldsymbol{R}$. When a finite number of samples is used, then $\mu_{P+1} \neq \mu_{P+2} \neq \cdots \neq \mu_{MN} \neq \sigma^2$. To overcome it, we estimate the noise variance by $\hat{\sigma}_w^2 = (\mu_{P+1} + \mu_{P+2} + \cdots + \mu_{MN})/(MN - P)$.

Theoretically, $\breve{\boldsymbol{R}} = \boldsymbol{A}\,\boldsymbol{R_s}\,\boldsymbol{A}^H$ can be viewed as a block matrix with submatrices

$$\begin{aligned} \breve{\boldsymbol{R}}_{(m,m')} &= \mathrm{E}\{\breve{\boldsymbol{y}}_m(t)\,\breve{\boldsymbol{y}}_{m'}^H(t)\} \in \mathbb{C}^{N\times N} \\ &= \boldsymbol{A_r}\,\boldsymbol{D}_m\,\boldsymbol{R_s}\,\boldsymbol{D}_{m'}^*\,\boldsymbol{A_r}^H \end{aligned} \tag{4.6}$$

where $m' \in \{1, 2, \cdots, m_o, \cdots, M\}$. Because of the $N \times N$ dimension of $\breve{\boldsymbol{R}}_{(m,m')}$, the maximum number of targets this method can localize is N. When $m = m_o$, we have

$$\breve{\boldsymbol{R}}_{(m_o,m')} = \boldsymbol{A_r}\,\boldsymbol{R_s}\,\boldsymbol{D}_{m'}^*\,\boldsymbol{A_r}^H \tag{4.7}$$

because $\boldsymbol{D}_{m_o}$ is an identity matrix. Using (4.7), (4.6) can be rewritten as

$$\breve{\boldsymbol{R}}_{(m,m')} = \boldsymbol{A_r}\,\boldsymbol{D}_m\,\boldsymbol{A_r}^\dagger\,\breve{\boldsymbol{R}}_{(m_o,m')}. \tag{4.8}$$

On rearranging, we can get

$$\breve{\boldsymbol{R}}_{(m,m')}\,\breve{\boldsymbol{R}}^+_{(m_o,m')} = \boldsymbol{A_r}\,\boldsymbol{D}_m\,\boldsymbol{A_r}^\dagger \tag{4.9}$$

where $[\bullet]^+$ denotes the inverse operation using singular value decomposition which is

explained below.

As mentioned in [1], the inverse of $\check{\boldsymbol{R}}_{(m_o,m')}$ should be calculated by using the singular values and vectors corresponding to the P largest singular values to improve the robustness in a noisy environment. It is because, when $P < N$, $\check{\boldsymbol{R}}_{(m_o,m')}$ should theoretically be a non-invertible square matrix. Thus, we use the following method to obtain its inverse and use $\check{\boldsymbol{R}}^{+}_{(m_o,m')}$ to represent its inverse. Let $\check{\boldsymbol{R}}_{(m_o,m')} = \boldsymbol{U}_{m'}\,\boldsymbol{S}_{m'}\,\boldsymbol{V}^{H}_{m'}$ where $\boldsymbol{U}_{m'} \in \mathbb{C}^{N\times N}$, $\boldsymbol{S}_{m'} \in \mathbb{R}^{N\times N}$, and $\boldsymbol{V}_{m'} \in \mathbb{C}^{N\times N}$ are the matrices containing the left singular vectors, singular values, and right singular vectors respectively. Then, $\check{\boldsymbol{R}}^{+}_{(m_o,m')} = \check{\boldsymbol{V}}_{m'}\,\check{\boldsymbol{S}}^{-1}_{m'}\,\check{\boldsymbol{U}}^{H}_{m'}$ where $\check{\boldsymbol{U}}_{m'} \in \mathbb{C}^{N\times P}$, $\check{\boldsymbol{S}}_{m'} \in \mathbb{R}^{P\times P}$, and $\check{\boldsymbol{V}}_{m'} \in \mathbb{C}^{N\times P}$ are the matrices that contain the left singular vectors associated with the P largest singular values, the corresponding P singular values and right singular vectors respectively. In practice, the remaining $(N-P)$ singular values will be close to zero. Therefore, $\check{\boldsymbol{R}}_{(m_o,m')}$ will not be rank deficient and the conventional way of inverting a square matrix may introduce numerical accuracy. Thus, this step also improves the numerical accuracy of the calculation of pseudo-inverse.

The submatrices with the same index m have the same $\boldsymbol{D}_m$, thus we can add them together as

$$\overline{\boldsymbol{R}}_m = \frac{1}{M}\sum_{m'=1}^{M} \check{\boldsymbol{R}}_{(m,m')}\,\check{\boldsymbol{R}}^{+}_{(m_o,m')} = \boldsymbol{A}_{\boldsymbol{r}}\,\boldsymbol{D}_m\,\boldsymbol{A}^{\dagger}_{\boldsymbol{r}}. \tag{4.10}$$

(4.10) can also be expressed as

$$\overline{\boldsymbol{R}}_m\,\boldsymbol{A}_{\boldsymbol{r}} = \boldsymbol{A}_{\boldsymbol{r}}\,\boldsymbol{D}_m \tag{4.11}$$

where the columns of $\boldsymbol{A}_{\boldsymbol{r}}$ and diagonal elements of the diagonal matrix $\boldsymbol{D}_m$ (4.2) are, by definition, respectively the eigenvectors and eigenvalues of $\overline{\boldsymbol{R}}_m$. Let $\boldsymbol{u}_{(m,p)}$ and $\beta_{(m,p)}$ be respectively the pth eigenvector and eigenvalue of $\overline{\boldsymbol{R}}_m$ ($\beta_{(m,p)}$ is one of the P largest eigenvalues). Further, we can write $\boldsymbol{u}_{(m,p)} = \alpha_{(m,p)}\,e^{j\,\phi_{(m,p)}}\,\boldsymbol{a}_{\boldsymbol{r}_p}$ and $\beta_{(m,p)} = a_{e_{(m,p)}}$ where $\alpha_{(m,p)}$ and $\phi_{(m,p)}$ respectively represent the scaling factor and phase shift introduced during the eigendecomposition. Since the eigendecomposition of the $M-1$ matrices $\overline{\boldsymbol{R}}_m$ (with $m \neq m_o$) is performed independently, therefore an additional step is required to pair all the $M-1$ sets of the eigenvalues and eigenvectors. Classically, the pairing can be done by comparing the inner product of the eigenvectors from the fact that the inner product of two aligned vectors is greater than that of two nonaligned vectors [1].

ρ_{r_p} and θ_{r_p} can be estimated from the angular part of $\boldsymbol{u}_{(m,p)}$. The argument of a complex number can only be calculated in its principal form. Therefore, phase unwrapping is necessary [115]. Phase unwrapping also introduces phase shift. As we know that $\arg\{a_{r_{(p,n_o)}}\} = 0$, therefore the unwrapped phase at $n = n_o$ is the phase shift introduced during the eigendecomposition as well as unwrapping. Thus, subtracting this phase shift from all the remaining components of the unwrapped phase vector

gives an estimation of the true phases. The eigendecompositions of the $M-1$ $\overline{\boldsymbol{R}}_m$ matrices provide $M-1$ eigenvectors associated to the signal reflected by the pth target. Thus, $M-1$ estimates of the true phases can be obtained for each target. At high SNR each estimation will be the same, however, when SNR is low, it is better to combine them by averaging. Let $\hat{\delta}_{r_{(p,n)}}$ be the estimated value of $\delta_{r_{(p,n)}}$ obtained from the averaged estimate of the true phase by dividing it by $-2\pi/\lambda$. The estimated values of the range from the receiving array ($\hat{\rho}_{r_p}$) and DOA ($\hat{\theta}_{r_p}$) can be retrieved from $\hat{\delta}_{r_{(p,n)}}$ by using the procedure given in section 3.3.2.

The argument of the eigenvalue $\beta_{(m,p)} = e^{-j2\pi\delta_{e_{(m,p)}}/\lambda}$ can be used to estimate the transmitter side ranges and DODs of the targets. Being a complex entity, the unwrapped phase of $\beta_{(m,p)}$ should be estimated, which is followed by the phase shifting with respect to the phase of reference component like before to provide the true unwrapped phase vector. Since, (1.4) and (1.5) have the same expression, the similar steps are conducted as in the case of the estimation of the receiver side location parameters. The estimated value of $\delta_{e_{(m,p)}}$ is obtained from the true unwrapped phase and then used to build a system of linear equations whose mth equation is given by (3.25) in section 3.3.2. The estimated values of the range from the transmitting array ($\hat{\rho}_{e_p}$) and DOD ($\hat{\theta}_{e_p}$) can be retrieved from $\hat{\delta}_{e_{(m,p)}}$ by using the method used in section 3.3.2. Finally, $\hat{\boldsymbol{t}}_p$ can be estimated from $\hat{\rho}_{e_p}$, $\hat{\theta}_{e_p}$, $\hat{\rho}_{r_p}$, and $\hat{\theta}_{r_p}$ with the help of the method given in section 3.4. All the steps to implement this method is summarize in Algorithm 4.1.

Algorithm 4.1 Submatrix Based Method.

1: Estimate the covariance matrix $\boldsymbol{R}$ from the L samples of the received signal $\boldsymbol{y}(t)$.
2: Find the eigenvectors and eigenvalues of $\boldsymbol{R}$ and compute the mean of $MN-P$ smallest eigenvalues.
3: Subtract the above mean from the P largest eigenvalues and compute the reduced noise covariance matrix $\breve{\boldsymbol{R}}$ as mentioned in (4.5).
4: Break $\breve{\boldsymbol{R}}$ into M^2 submatrices $\breve{\boldsymbol{R}}_{(m,m')}$ of size $N \times N$.
5: Calculate $\overline{\boldsymbol{R}}_m$ for each $m \in \{1, 2, \ldots, M\}$ using the submatrices as given in (4.10).
6: Find the eigenvectors and eigenvalues of $\overline{\boldsymbol{R}}_m$ for all m and pair them using the inner product of the eigenvectors for different pairs of m.
7: Compute the principal values of the components of each eigenvector paired above and unwrap the phases followed by their normalization with respect to the reference component of each eigenvector.
8: Divide the mean of all the unwrapped and normalized phases calculated above by $-2\pi/\lambda$ to get $\hat{\delta}_{r_{(p,n)}}$.
9: Obtain $\hat{\rho}_{r_p}$ and $\hat{\theta}_{r_p}$ by applying TLS on (3.28) derived from (3.27) using $\hat{\delta}_{r_{(p,n)}}$.
10: Unwrap, normalize, and divide by $-2\pi/\lambda$ the principal values of the components of the paired eigenvalues along m for all m to get $\hat{\delta}_{e_{(m,p)}}$ in order to obtain $\hat{\rho}_{e_p}$ and $\hat{\theta}_{e_p}$ by using TLS on (3.26).
11: Finally, use the method given in section 3.4 to obtain $\hat{\boldsymbol{t}}_p$ from $\hat{\rho}_{e_p}$, $\hat{\theta}_{e_p}$, $\hat{\rho}_{r_p}$, and $\hat{\theta}_{r_p}$.

4.2 PARAFAC Based Method

For the L time samples, $\boldsymbol{y}(t)$ can be rewritten as [112]

$$\boldsymbol{Y_M} = (\boldsymbol{A_e} \boxdot \boldsymbol{A_r})\ \boldsymbol{S}^T + \boldsymbol{W_M} \in \mathbb{C}^{MN \times L} \tag{4.12}$$

where $\boldsymbol{S} \in \mathbb{C}^{L \times P}$ consists of $\boldsymbol{s}(t)$ at L different time instances. Every element of $\boldsymbol{Y_M}$ in (4.12) is associated with three parameters related, respectively, to the receiving antenna, transmitting antenna, and time sample. Therefore, $\boldsymbol{Y_M}$ can be rearranged like a three-way tensor $\boldsymbol{\mathcal{Y}} \in \mathbb{C}^{N \times M \times L}$, as shown in Figure 4.1. Creating a tensor out of lower dimensional data is known as tensorization [120].

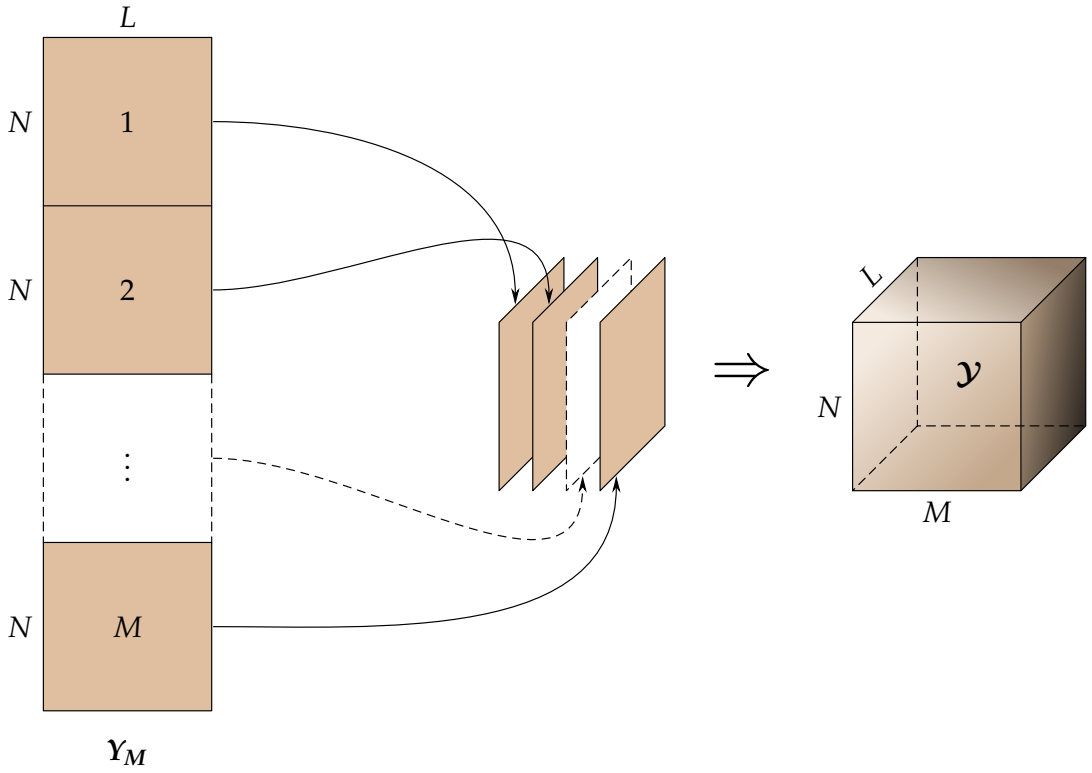

Figure 4.1 – Tensorization.

PARAFAC decomposition of tensor $\boldsymbol{\mathcal{Y}}$ is used to get the estimates of $\boldsymbol{A_r}$, $\boldsymbol{A_e}$, and $\boldsymbol{S}$ matrices [96]. Tensor operations are usually performed in its equivalent matrix form [65, 66, 96]. The process of creating a matrix out of a tensor is known as matricization [120]. Like $\boldsymbol{Y_M}$, $\boldsymbol{\mathcal{Y}}$ can be matricized into the following two additional matrices

$$\boldsymbol{Y_L} = (\boldsymbol{S} \boxdot \boldsymbol{A_e})\ \boldsymbol{A_r}^T + \boldsymbol{W_L} \in {}^{LM \times N} \tag{4.13}$$

and

$$\boldsymbol{Y_N} = (\boldsymbol{A_r} \boxdot \boldsymbol{S})\ \boldsymbol{A_e}^T + \boldsymbol{W_N} \in {}^{NL \times M}. \tag{4.14}$$

According to the least squares principle, the following objective functions can be

written from (4.12), (4.13), and (4.14)

$$\hat{\boldsymbol{S}} = \arg\min_{\boldsymbol{S}} \left\{ \left\| \boldsymbol{Y}_M - (\boldsymbol{A}_e \boxdot \boldsymbol{A}_r)\, \boldsymbol{S}^T \right\|_F^2 \right\}, \tag{4.15}$$

$$\hat{\boldsymbol{A}}_r = \arg\min_{\boldsymbol{A}_r} \left\{ \left\| \boldsymbol{Y}_L - (\boldsymbol{S} \boxdot \boldsymbol{A}_e)\, \boldsymbol{A}_r^T \right\|_F^2 \right\}, \tag{4.16}$$

and

$$\hat{\boldsymbol{A}}_e = \arg\min_{\boldsymbol{A}_e} \left\{ \left\| \boldsymbol{Y}_N - (\boldsymbol{A}_r \boxdot \boldsymbol{S})\, \boldsymbol{A}_e^T \right\|_F^2 \right\} \tag{4.17}$$

where $\hat{\boldsymbol{A}}_r$, $\hat{\boldsymbol{A}}_e$, and $\hat{\boldsymbol{S}}$ denote the estimated values of $\boldsymbol{A}_r$, $\boldsymbol{A}_e$, and $\boldsymbol{S}$ respectively.

The TALS algorithm is a classical method to minimize the above objective functions [65,66,96]. Least squares estimates of (4.15)–(4.17) are given by

$$\hat{\boldsymbol{S}} = \left[(\boldsymbol{A}_e \boxdot \boldsymbol{A}_r)^{\dagger}\, \boldsymbol{Y}_M \right]^T, \tag{4.18}$$

$$\hat{\boldsymbol{A}}_r = \left[(\boldsymbol{S} \boxdot \boldsymbol{A}_e)^{\dagger}\, \boldsymbol{Y}_L \right]^T, \tag{4.19}$$

and

$$\hat{\boldsymbol{A}}_e = \left[(\boldsymbol{A}_r \boxdot \boldsymbol{S})^{\dagger}\, \boldsymbol{Y}_N \right]^T. \tag{4.20}$$

In the TALS algorithm, (4.18)–(4.20) are alternatively updated with the new values of $\hat{\boldsymbol{A}}_r$, $\hat{\boldsymbol{A}}_e$, and $\hat{\boldsymbol{S}}$ until a stopping criteria is met. $\left\| \boldsymbol{Y}_M - (\boldsymbol{A}_e \boxdot \boldsymbol{A}_r)\, \boldsymbol{S}^T \right\|_F^2 < \epsilon_{\text{tol}}$ is often used as the stopping condition, where ϵ_{tol} is the tolerance. In practice, the algorithm given in [78] is used for PARAFAC decomposition, which uses compression, line search, normalization, etc. to accelerate the TALS method. The parameter identifiability of the PARAFAC decomposition is well studied in the existing literature [69,70,81,96]. It is clearly mentioned in [96] that the PARAFAC decomposition is unique when $\max(M, N) \geq 3$ and $P \leq MN - \min(M, N)$ for the non-coherent targets and Swerling model II which are fully satisfied by our assumptions.

According to [69], the matrices obtained by PARAFAC decomposition of a three-way tensor are scaled and permuted. The permutation has no impact because the columns of the matrices are paired. However, in the proposed method, the scaling factor must be removed by dividing all the elements of the directional vectors with their corresponding reference elements.

Then, a direct approach to estimate $\boldsymbol{t}_p$ could be the minimization of the following cost function

$$\hat{\boldsymbol{t}}_p = \arg\min_{\boldsymbol{t}_p} \left\{ \left\| \hat{\boldsymbol{a}}_{e_p} / \hat{a}_{e_{(m_o,\,p)}} - \boldsymbol{a}_e(\boldsymbol{t}_p) \right\|_F^2 + \left\| \hat{\boldsymbol{a}}_{r_p} / \hat{a}_{r_{(p,\,n_o)}} - \boldsymbol{a}_r(\boldsymbol{t}_p) \right\|_F^2 \right\} \tag{4.21}$$

where $\hat{\boldsymbol{a}}_{\boldsymbol{e}_p}$ and $\hat{\boldsymbol{a}}_{\boldsymbol{r}_p}$ are the estimated directional vectors obtained from the PARAFAC decomposition, and $\hat{a}_{e_{(m_o,p)}}$ and $\hat{a}_{r_{(p,n_o)}}$ are their respective reference elements used here to remove the scaling factor in the decomposition of the received signal tensor.

Even though a near-field region occupies a finite space, minimizing (4.21) by using grid search or Newton's method is computationally expensive. Therefore, we choose an indirect method in which we estimate the ranges and directional angles, followed by the estimation of the coordinates. Let $\hat{\delta}_{e_{(m,p)}}$ and $\hat{\delta}_{r_{(p,n)}}$ be the estimated path differences which are obtained from the estimated directional vectors as follows

$$\hat{\delta}_{e_{(m,p)}} = -\lambda \left[\arg\left\{\hat{a}_{e_{(m,p)}}\right\} - \arg\left\{\hat{a}_{e_{(m_o,p)}}\right\}\right] / (2\,\pi) \tag{4.22}$$

and

$$\hat{\delta}_{r_{(p,n)}} = -\lambda \left[\arg\left\{\hat{a}_{r_{(p,n)}}\right\} - \arg\left\{\hat{a}_{r_{(p,n_o)}}\right\}\right] / (2\,\pi) \tag{4.23}$$

where arg $\{\bullet\}$ represents the unwrapped phase value i.e. the estimated argument [115]. Equations (4.22) and (4.23) can be described as follows:

1. Get the directional vectors $\hat{\boldsymbol{a}}_{\boldsymbol{e}_p}$ and $\hat{\boldsymbol{a}}_{\boldsymbol{r}_p}$ from the PARAFAC decomposition.

2. Extract the arguments of all the components of $\hat{\boldsymbol{a}}_{\boldsymbol{e}_p}$ and $\hat{\boldsymbol{a}}_{\boldsymbol{r}_p}$.

3. Unwrap the phase vectors obtained from Step 2.

4. Subtract the unwrapped phase corresponding to $\hat{a}_{e_{(0,p)}}$ and $\hat{a}_{r_{(p,0)}}$ from all the components of the unwrapped phase vector of $\hat{\boldsymbol{a}}_{\boldsymbol{e}_p}$ and $\hat{\boldsymbol{a}}_{\boldsymbol{r}_p}$, respectively.

5. Divide each component of the normalized phase vectors obtained from the above step by $-2\,\pi/\lambda$ to get $\hat{\delta}_{e_{(m,p)}}$ and $\hat{\delta}_{r_{(p,n)}}$.

Once we have $\hat{\delta}_{e_{(m,p)}}$ and $\hat{\delta}_{r_{(p,n)}}$, the procedure in section 3.3.2 can be used to obtain $\hat{\rho}_{e_p}$, $\hat{\theta}_{e_p}$, $\hat{\rho}_{r_p}$, and $\hat{\theta}_{r_p}$. Finally, $\hat{\boldsymbol{t}}_p$ can be found by using (3.31) which is computationally less expensive and reliable than (4.21). Algorithm 4.2 provides a summary of this proposed method.

Algorithm 4.2 Tensor Decomposition Based Method.

1: Construct the three-way tensor $\boldsymbol{\mathcal{Y}}$ from the received data.
2: Estimate $\boldsymbol{A_e}$ and $\boldsymbol{A_r}$ from $\boldsymbol{\mathcal{Y}}$ using PARAFAC decomposition.
3: Use (4.22) and (4.23) to obtain $\hat{\delta}_{e_{(m,p)}}$ and $\hat{\delta}_{r_{(p,n)}}$ from the estimated $\boldsymbol{A_e}$ and $\boldsymbol{A_r}$, respectively.
4: Create the system of linear equations by substituting $\hat{\delta}_{e_{(m,p)}}$ and $\hat{\delta}_{r_{(p,n)}}$ in (3.25) and (3.27), respectively, for all the values of m and n for each target.
5: Separately solve each system of linear equations created in step 4 using the total least squares technique to obtain $\hat{\rho}_{e_p}$, $\hat{\theta}_{e_p}$, $\hat{\rho}_{r_p}$, and $\hat{\theta}_{r_p}$.
6: Substitute the four estimated location parameters in (1.37) and (1.38) to obtain the parametric equations of the circles, and minimize (3.31) to estimate $\hat{\varphi}_e$ and $\hat{\varphi}_r$.
7: Finally, substitute $\hat{\varphi}_e$ and $\hat{\varphi}_r$ along with $\hat{\rho}_{e_p}$, $\hat{\theta}_{e_p}$, $\hat{\rho}_{r_p}$, and $\hat{\theta}_{r_p}$ in (1.37) and (1.38) to get the estimated coordinates $\hat{\boldsymbol{t}}_p$ of the pth target.

4.3 Numerical Example

Consider a bistatic MIMO system as shown in Figure 1.11 with $M = 8$, $N = 9$, $m_o = 1$, $n_o = 1$ and $d_e = d_r = \lambda/2$. The values of $\boldsymbol{e_o}$, $\boldsymbol{r_o}$, $\boldsymbol{d_{c_e}}$ and $\boldsymbol{d_{c_r}}$ are kept the same as in section 3.5. Here, we use the accurate signal model in terms of Cartesian coordinates of the targets, therefore, we can use (3.32) to obtain the RMSE in the estimated position.

Figure 4.2 shows the RMSE in the estimated positions using the proposed methods elaborated in this chapter. To plot this figure, we have used $L = 10^3$ data samples, $K = 10^3$ Monte Carlo iterations. The position vectors of the two chosen near field targets are $[2\lambda, 7\lambda, 9\lambda]^T$ and $[3\lambda, -5\lambda, -8\lambda]^T$.

In Figure 4.2, we can see that the two proposed accurate model based methods have almost the same performance. Precisely, the PARAFAC decomposition based method has better performance than the proposed method in section 4.1. One of the reasons is that PARAFAC exploits all the available information together unlike the other method which uses sub-covariance matrices and process the information in chunks.

The proposed accurate model based methods is compared in Figure 4.3 with the proposed approximated model based method by using the same simulation parameters as used in section 3.5. From the figure, we can observe that at low SNR the approximated model based method surpasses the accurate model based methods. However, because of the Fresnel approximation, at high SNR the accurate model based methods show better performance.

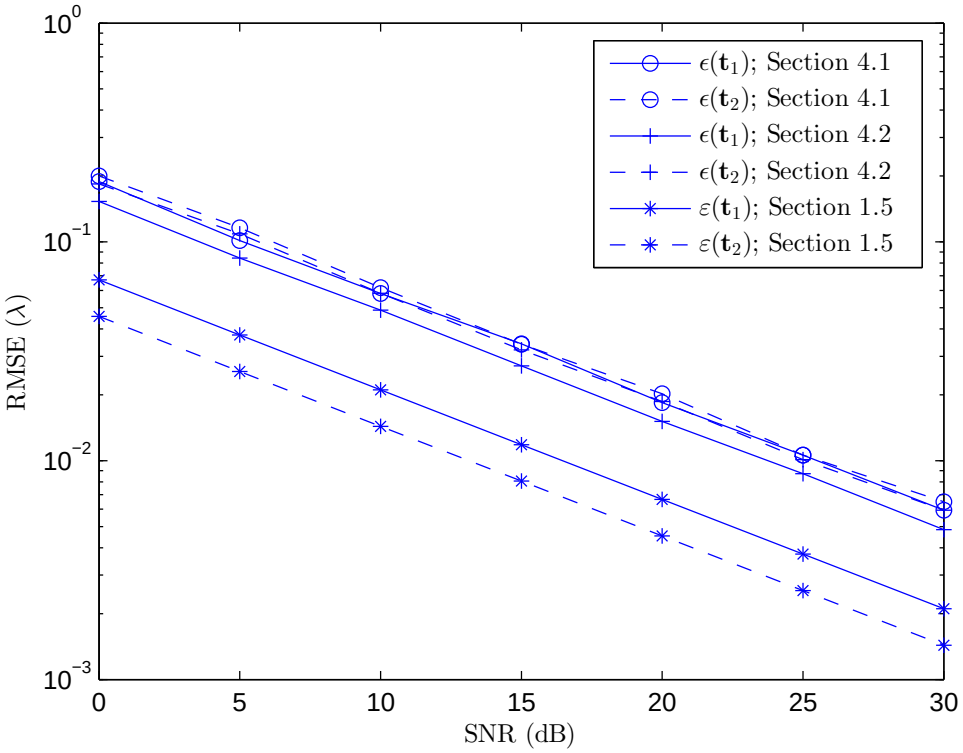

Figure 4.2 – RMSE in the position estimated by the proposed methods described in section 4.1 and section 4.2 versus SNR. $d_e = d_r = \lambda/2$, $K = 10^3$, $L = 10^3$, $M = 8$, $N = 9$, $m_o = 1$, $n_o = 1$, and $P = 2$. The CRLBs are calculated using (1.43) and (1.45).

4.4 Conclusion

From the simulation results it is clear that the accurate model based methods can easily surpass an extremely good approximated model based method because of the presence of bias due to the Fresnel approximation. Among the proposed accurate model based methods, the PARAFAC decomposition based method provides better estimates than the sub-covariance matrices based method at the cost of computation time because PARAFAC uses iterative TALS based method. The other advantage of an accurate model methods is that it can be used for a system which uses half wavelength inter element spacing to minimize mutual coupling between the array elements.

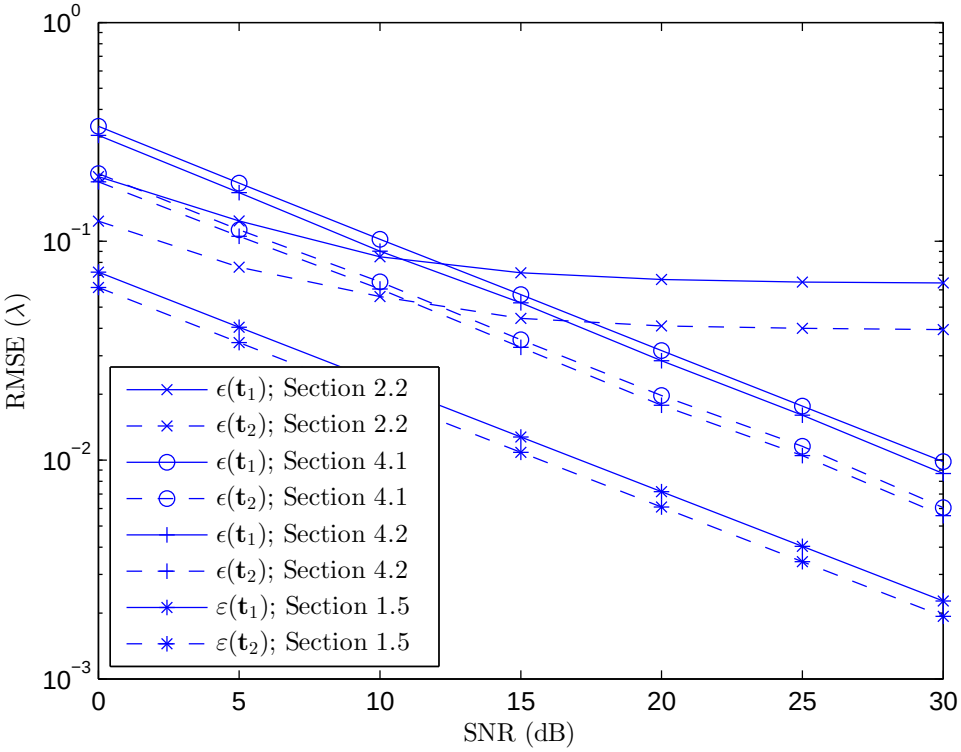

Figure 4.3 – RMSE in the position estimated by the proposed methods described in section 2.2, section 4.1, and section 4.2 versus SNR. $d_e = d_r = \lambda/4$, $K = 10^3$, $L = 10^3$, $M = 7$, $N = 9$, $m_o = 4$, $n_o = 5$, and $P = 2$. The CRLBs are calculated using (1.43) and (1.45).

Conclusion

1 Conclusions and Perspectives

The primary objective of the work in this thesis is to improve the localization performance of the targets in the near field regions of the transmitting and receiving arrays of a bistatic MIMO system. This thesis contains several proposed methods in this context for two different signal models with and without Fresnel approximation of the spherical wavefront.

The proposed methods are dedicated to the near field region of a bistatic MIMO radar with ULAs. Fresnel approximation is usually opted to locate the sources in the near field region of an array. Thus, we have proposed a localization method and compared it with an existing method and CRLB. The simulation results show that the performance of the proposed method is better in terms of RMSE and maximum number of localizable targets than the existing method. A drawback of the proposed method is its computational complexity. A flaw in the analysis of this proposed method is that the signal model used in its analysis is based on Fresnel approximation. However, for a point like target the wavefront is spherical. Hence, we can say that the analysis of an approximated model based method with an approximated model based signal data is biased.

When an approximated model based method is analyzed with the spherical wavefront based signal model, the location parameters show some biases. This bias can be considered as a function of the true location parameters and array parameters. If the array parameters, like number of antenna and inter element distance, are constant, the bias will be constant throughout the near field region. This property of the bias allows us to put it in the category of systematic error. This bais stands out at high SNR because at low SNR the additive noise dominates. At different locations, the bias has different values, therefore, the SNR at which the bias dominates the noise may vary with the location. We have proposed two methods to reduce the effect of the biases from location parameters. The first method is based on LUT. This proposed method can be subdivided into two steps. In the first step, we create the LUTs for the transmitting and receiving arrays. And in the second step, we reduce the biases in the location parameters by interpolation. This approach is effective, however, it is slow because find-

ing four nearest neighbors from two LUTs is time consuming. To overcome the space and time requirement of LUT based correction method, we have proposed the second method which estimates the accurate relative propagation path length vector and corrects the location parameters using TLS. The proposed methods add extra complexity to the localization process however greatly improves the estimation performance.

Beside the methods to reduce the effects of Fresnel approximation, we have proposed two methods which can directly process the spherical wavefront based signal model. The first method is based on subspaces whereas the second method is based on tensor decomposition. Principally in both the proposed methods, we estimate the directional vectors first and then the location parameters from them. Tensor decomposition usually uses iterative methods to find its components which makes it computationally costly. On the other hand, subspaces based proposed method processes submatrices which is faster than the tensor decomposition based method however the maximum number of localizable targets reduces to the number of receiving antennas. Because of the complete exploitation of the signal data all together by the tensor decomposition based proposed method, its performance surpasses the proposed subspace based method. Using the accurate model doesn't imply that the performance in terms of RMSE will always be better. This can be observed from the simulation results that if the proposed correction methods are applied on the proposed approximated model based method, it can surpass both the accurate model based methods. However, it is clear from this work that approximated model alone is not a great choice when we are looking for precision. It is better to correct the bias or to use the accurate model based methods in the near field region of a bistatic MIMO system. Additionally, the proposed accurate model based methods support interelement distance between $\lambda/4$ and $\lambda/2$ which can not be handled by most of the approximated model based methods.

2 Future Work

The performance of all the proposed methods in this thesis is analyzed only by computer simulations. However, the methods are proposed for real life applications. Therefore, the analysis is incomplete without testing the proposed methods with some real bistatic MIMO radar data.

In the near field region of an array, the fast moving target may not induce coherent Doppler shift. Thus, the model used in this study may not be suitable for such targets because in this study we have ignored the effects of Doppler shifts in the signal model. In the literature, we can find countless work on the point-like sources in the near field region of an array. However, we may come across large targets which can not be localized properly with the proposed methods. Thus, this work should be extended to the

fast moving distributed targets.

To handle the spherical wavefront based signal model, we have proposed to estimate directional vectors first and then extract the location parameters from them. The directional vectors are always in the complex form, therefore, the phases of these complex components can only be retrieved in their principal form. To extract the location parameter, we need unwrapped phases. There exists a working algorithm to unwrap theses principal valued phases. However, due to the estimation errors in the estimated directional vectors, the existing unwrapping algorithm induces a large error which can not be ignored. Thus, further research can be done to find an algorithm which can unwrap the phases without error.

The method in section 4.1 uses denoised covariance matrix. The used denoising method is not a best approach. Also, the advanced covariance estimators are not used. Therefore, the estimation accuracy of the proposed method in section 4.1 can further be improved by using an advanced covariance estimators and a better denoising technique.

The proposed approximated model based method in section 2.2 has high estimation accuracy, however it is slow because of the spectral search. If we try to convert the problem into a polynomial one, then we will get a sparse high order polynomial whose roots finding time will be very large because of the eigen decomposition in its background. Therefore, instead of decreasing, the computation time will increase. However, if we use a fast root finding algorithm which only looks for the P closest roots to the unity circle, then the polynomial rooting can be a useful approach.

A

Biased Location Parameters

As mentioned before, the propagation of the systematic error introduced by the Fresnel approximation may lead to different bias in the same location parameters. In the following, we show different possible approaches to obtain biased location parameters and the distribution of the bias attached to them in the Fresnel region of ULA. Like in section 1.3.2, we use the receiving array parameters here to elaborate the error distribution. In order to calculate the biased location parameters corresponding to the receiving array, we choose a location $(\rho_{r_p}, \theta_{r_p})$ in its near field region and construct $\delta_{\boldsymbol{r}}(\rho_{r_p}, \theta_{r_p})$ vector and extract the range and DOA from it using the methods given below. The same steps can be used for the transmitting ULA. To calculate the biased location parameters, there is not need to construct the directional vectors.

A.1 Biased Location Parameters Extraction Methods

A.1.1 Vector Flip

This biased location parameters extraction method is inspired by the method in [1], therefore it requires symmetric array described in section 1.3.3.

From (1.32), we can write

$$\boldsymbol{J}_N\, \widetilde{\delta}_{\boldsymbol{r}_p} - \widetilde{\delta}_{\boldsymbol{r}_p} = 2\,\omega_{r_p} \left[-\breve{N}, -\breve{N}+1, \ldots, 0, \ldots, \breve{N}-1, \breve{N}\right]^T \tag{A.1}$$

and

$$\boldsymbol{J}_N\, \widetilde{\delta}_{\boldsymbol{r}_p} + \widetilde{\delta}_{\boldsymbol{r}_p} = 2\,\phi_{r_p} \left[\breve{N}^2, (\breve{N}-1)^2, \ldots, 0, \ldots, (\breve{N}-1)^2, \breve{N}^2\right]^T. \tag{A.2}$$

Using the similar operations on δ_{r_p}, we can write

$$\grave{\delta}_{r_p} = J_N\, \delta_{r_p} - \delta_{r_p} \tag{A.3}$$

and

$$\acute{\delta}_{r_p} = J_N\, \delta_{r_p} + \delta_{r_p}. \tag{A.4}$$

Further, $\grave{\delta}_{r_p}$ can be expanded as

$$\grave{\delta}_{r_p} = 2\,\omega_{r_p} \begin{bmatrix} -\breve{N} \\ -\breve{N}+1 \\ \vdots \\ -1 \\ 0 \\ 1 \\ \vdots \\ \breve{N}-1 \\ \breve{N} \end{bmatrix} + \rho_{r_p} \begin{bmatrix} \gamma_{r_{(p,N)}} - \gamma_{r_{(p,1)}} \\ \gamma_{r_{(p,N-1)}} - \gamma_{r_{(p,2)}} \\ \vdots \\ \gamma_{r_{(p,n_o+1)}} - \gamma_{r_{(p,n_o-1)}} \\ 0 \\ \gamma_{r_{(p,n_o-1)}} - \gamma_{r_{(p,n_o+1)}} \\ \vdots \\ \gamma_{r_{(p,2)}} - \gamma_{r_{(p,N-1)}} \\ \gamma_{r_{(p,1)}} - \gamma_{r_{(p,N)}} \end{bmatrix} \approx 2\,\widetilde{\omega}_{r_p} \begin{bmatrix} -\breve{N} \\ -\breve{N}+1 \\ \vdots \\ -1 \\ 0 \\ 1 \\ \vdots \\ \breve{N}-1 \\ \breve{N} \end{bmatrix} \tag{A.5}$$

From (A.5), $\widetilde{\omega}_{r_p}$ can be estimated as

$$\widetilde{\omega}_{r_p} = \frac{1}{4\,\breve{N}} \sum_{i=1}^{2\breve{N}} \left\{ \left[\grave{\delta}_{r_p}\right]_{i+1} - \left[\grave{\delta}_{r_p}\right]_{i} \right\} = \omega_{r_p} + \frac{\rho_{r_p}}{2\,\breve{N}} \left(\gamma_{r_{(p,1)}} - \gamma_{r_{(p,N)}} \right) \tag{A.6}$$

which can be used to obtain the biased DOA using the following expression

$$\widetilde{\theta}_{r_p} = \arccos(\widetilde{\omega}_{r_p}/d_r). \tag{A.7}$$

As above, expanding $\acute{\delta}_{r_p}$ gives

$$\acute{\delta}_{r_p} = 2\,\phi_{r_p} \begin{bmatrix} -\breve{N}^2 \\ (\breve{N}-1)^2 \\ \vdots \\ 1 \\ 0 \\ 1 \\ \vdots \\ (\breve{N}-1)^2 \\ \breve{N}^2 \end{bmatrix} + \rho_{r_p} \begin{bmatrix} \gamma_{r_{(p,N)}} + \gamma_{r_{(p,1)}} \\ \gamma_{r_{(p,N-1)}} + \gamma_{r_{(p,2)}} \\ \vdots \\ \gamma_{r_{(p,n_o+1)}} + \gamma_{r_{(p,n_o-1)}} \\ 0 \\ \gamma_{r_{(p,n_o-1)}} + \gamma_{r_{(p,n_o+1)}} \\ \vdots \\ \gamma_{r_{(p,2)}} + \gamma_{r_{(p,N-1)}} \\ \gamma_{r_{(p,1)}} + \gamma_{r_{(p,N)}} \end{bmatrix} \approx 2\,\widetilde{\phi}_{r_p} \begin{bmatrix} -\breve{N}^2 \\ (\breve{N}-1)^2 \\ \vdots \\ 1 \\ 0 \\ 1 \\ \vdots \\ (\breve{N}-1)^2 \\ \breve{N}^2 \end{bmatrix}, \tag{A.8}$$

from which $\widetilde{\phi}_{r_p}$ can be calculated as follows

$$\widetilde{\phi}_{r_p} = \frac{1}{4\,\check{N}} \sum_{i=1}^{\check{N}} \frac{1}{i^2} \left\{ \left[\acute{\boldsymbol{\delta}}_{\boldsymbol{r}_p} \right]_{\check{N}-i+1} + \left[\acute{\boldsymbol{\delta}}_{\boldsymbol{r}_p} \right]_{\check{N}+i+1} \right\} \tag{A.9}$$

$$= \phi_{r_p} + \frac{\rho_{r_p}}{2\,\check{N}} \sum_{i=1}^{\check{N}} \frac{\gamma_{r_{(p,n_o+i)}} + \gamma_{r_{(p,n_o-i)}}}{i^2} \tag{A.10}$$

where $n_o = \check{N} + 1$. Finally, the biased range can be calculated as

$$\widetilde{\rho}_{r_p} = d_r^2 \, \sin^2(\widetilde{\theta}_{r_p}) / (2\,\widetilde{\phi}_{r_p}). \tag{A.11}$$

A.1.2 Double Difference

It can be observed in (1.25) that the coefficients of ω_{r_p} is linear. Therefore, taking difference between the consecutive elements of $\widetilde{\boldsymbol{\delta}}_{\boldsymbol{r}_p}$ make the coefficients of ω_{r_p} constant which can be eliminated by the second difference. This procedure also puts a constraint of $N \geq 3$ on this extraction method.

Difference between the consecutive elements of a vector of length N can be obtained by multiplying that vector with the following matrix

$$\boldsymbol{P}_N = \begin{bmatrix} -1 & 1 & 0 & \cdots & 0 & 0 \\ 0 & -1 & 1 & \cdots & 0 & 0 \\ \vdots & \vdots & \vdots & \ddots & \vdots & \vdots \\ 0 & 0 & 0 & \cdots & 1 & 0 \\ 0 & 0 & 0 & \cdots & -1 & 1 \end{bmatrix} \in \mathbb{R}^{(N-1)\times N}. \tag{A.12}$$

First difference of $\boldsymbol{\delta}_{\boldsymbol{r}_p}$ can be written as

$$\boldsymbol{P}_N \, \boldsymbol{\delta}_{\boldsymbol{r}_p} = \begin{bmatrix} -\omega_{r_p} + [2(1-n_o)+1]\ \phi_{r_p} \\ -\omega_{r_p} + [2(2-n_o)+1]\ \phi_{r_p} \\ \vdots \\ -\omega_{r_p} + [2(N-1-n_o)+1]\ \phi_{r_p} \end{bmatrix} + \rho_{r_p} \begin{bmatrix} \gamma_{r_{(p,2)}} - \gamma_{r_{(p,1)}} \\ \gamma_{r_{(p,3)}} - \gamma_{r_{(p,2)}} \\ \vdots \\ \gamma_{r_{(p,N)}} - \gamma_{r_{(p,N-1)}} \end{bmatrix} \tag{A.13}$$

$$\approx \begin{bmatrix} -\widetilde{\omega}_{r_p} + [2(1-n_o)+1]\ \widetilde{\phi}_{r_p} \\ -\widetilde{\omega}_{r_p} + [2(2-n_o)+1]\ \widetilde{\phi}_{r_p} \\ \vdots \\ -\widetilde{\omega}_{r_p} + [2(N-1-n_o)+1]\ \widetilde{\phi}_{r_p} \end{bmatrix} \in \mathbb{R}^{N-1} \tag{A.14}$$

because $(n+1-n_o)^2 - (n-n_o)^2 = 2\,(n-n_o)+1$.

Similarly, on multiplying (A.14) by $\boldsymbol{P}_{N-1} \in \mathbb{R}^{(N-2)\times(N-1)}$, we can obtain the second

difference as

$$\boldsymbol{P}_{N-1}\,\boldsymbol{P}_N\,\boldsymbol{\delta}_{\boldsymbol{r}_p} = \begin{bmatrix} 2\,\phi_{r_p} \\ 2\,\phi_{r_p} \\ \vdots \\ 2\,\phi_{r_p} \end{bmatrix} + \rho_{r_p} \begin{bmatrix} \gamma_{r_{(p,3)}} - 2\,\gamma_{r_{(p,2)}} + \gamma_{r_{(p,1)}} \\ \gamma_{r_{(p,4)}} - 2\,\gamma_{r_{(p,3)}} + \gamma_{r_{(p,2)}} \\ \vdots \\ \gamma_{r_{(p,N)}} - 2\,\gamma_{r_{(p,N-1)}} + \gamma_{r_{(p,N-2)}} \end{bmatrix} \tag{A.15}$$

$$\approx \begin{bmatrix} 2\,\widetilde{\phi}_{r_p} \\ 2\,\widetilde{\phi}_{r_p} \\ \vdots \\ 2\,\widetilde{\phi}_{r_p} \end{bmatrix} \in \mathbb{R}^{N-2}. \tag{A.16}$$

The $\widetilde{\phi}_{r_p}$ can be calculated by the half of the mean of the elements of $\boldsymbol{P}_{N-1}\,\boldsymbol{P}_N\,\boldsymbol{\delta}_{\boldsymbol{r}_p}$ as

$$\widetilde{\phi}_{r_p} = \frac{1}{2\,(N-2)} \sum_{i=1}^{N-2} \left[\boldsymbol{P}_{N-1}\,\boldsymbol{P}_N\,\boldsymbol{\delta}_{\boldsymbol{r}_p}\right]_i \tag{A.17}$$

$$= \phi_{r_p} + \frac{\rho_{r_p}}{2\,(N-2)} \sum_{i=1}^{N-2} \left(\gamma_{r_{(p,i+2)}} - 2\,\gamma_{r_{(p,i+1)}} + \gamma_{r_{(p,i)}}\right). \tag{A.18}$$

Furthermore, $\widetilde{\phi}_{r_p}$ can be used with (A.14) to get $\widetilde{\omega}_{r_p}$ as

$$\widetilde{\omega}_{r_p} = \frac{1}{N-1} \sum_{i=1}^{N-1} \left(\left[2\,(i-n_o)+1\right]\widetilde{\phi}_{r_p} - \left[\boldsymbol{P}_N\,\boldsymbol{\delta}_{\boldsymbol{r}_p}\right]_i\right) \tag{A.19}$$

$$= \omega_{r_p} + \rho_{r_p} \left[\frac{\gamma_{r_{(p,1)}} - \gamma_{r_{(p,N)}}}{N-1} + \frac{(N - 2\,n_o + 1)}{2\,(N-2)} \sum_{i=1}^{N-2} \left(\gamma_{r_{(p,i+2)}} - 2\,\gamma_{r_{(p,i+1)}} + \gamma_{r_{(p,i)}}\right)\right]. \tag{A.20}$$

Finally, $\widetilde{\theta}_{r_p}$ and $\widetilde{\rho}_{r_p}$ can be calculated from $\widetilde{\omega}_{r_p}$ and $\widetilde{\phi}_{r_p}$ by using (A.7) and (A.11) respectively.

A.1.3 Overdetermined System of Linear Equations

For $N \geq 3$, (1.34) can be considered an overdetermined system of linear equations with ω_{r_p} and ϕ_{r_p} as its two unknowns. This system of linear equations can be solved by using conventional LS estimator. Applying this concept on $\boldsymbol{\delta}_{\boldsymbol{r}_p}$ can provide the biased location parameters as

$$\begin{bmatrix} \widetilde{\omega}_{r_p} \\ \widetilde{\phi}_{r_p} \end{bmatrix} = \underline{\boldsymbol{N}}^{\dagger}\,\boldsymbol{\delta}_{\boldsymbol{r}_p} = \begin{bmatrix} \omega_{r_p} \\ \phi_{r_p} \end{bmatrix} + \rho_{r_p}\,\underline{\boldsymbol{N}}^{\dagger}\boldsymbol{\gamma}_{\boldsymbol{r}_p} \tag{A.21}$$

where $\boldsymbol{\gamma}_{r_p} = [\gamma_{r_{(p,1)}}, \gamma_{r_{(p,2)}}, \cdots, \gamma_{r_{(p,N)}}]^T$. As before, $\widetilde{\theta}_{r_p}$ and $\widetilde{\rho}_{r_p}$ can be calculated from $\widetilde{\omega}_{r_p}$ and $\widetilde{\phi}_{r_p}$ by using (A.7) and (A.11) respectively.

A.1.4 Least Squares Error

Like the above method in section A.1.3, this approach is also based on LS estimation. However, it directly estimates biased range and DOA by minimizing the following cost function

$$(\widetilde{\rho}_{r_p}, \widetilde{\theta}_{r_p}) = \arg\min_{(\rho,\theta)} \left\| \boldsymbol{\delta}_{r_p} - \widetilde{\boldsymbol{\delta}}_{\boldsymbol{r}}(\rho, \theta) \right\|_F^2 \tag{A.22}$$

with the help of a numerical method like Newton's minimization technique because closed form expression may not be easily found. The use of numerical methods to minimize the cost function makes this method slow because of the iterations; and unreliable due to the local minimums.

A.1.5 Vector Component Pairs

A pair of rows of $\widetilde{\boldsymbol{\delta}}_{r_p}$ makes a perfect system of linear equations in ω_{r_p} and ϕ_{r_p}. Using this fact, $\widetilde{\omega}_{r_p}$ and $\widetilde{\phi}_{r_p}$ can be calculated from $\boldsymbol{\delta}_{r_p}$.

The ith and i'th components of $\boldsymbol{\delta}_{r_p}$ can be used as follows

$$\begin{bmatrix} \widetilde{\omega}_{r_p} \\ \widetilde{\phi}_{r_p} \end{bmatrix} = \frac{1}{(i-i')(i-n_o)(i'-n_o)} \begin{bmatrix} (i'-n_o)^2 & -(i-n_o)^2 \\ (i'-n_o) & -(i-n_o) \end{bmatrix} \begin{bmatrix} \delta_{r_{(p,i)}} \\ \delta_{r_{(p,i')}} \end{bmatrix}. \tag{A.23}$$

Estimations from all the possible combinations of i and i' can be combined using mean which gives

$$\widetilde{\omega}_{r_p} = \omega_{r_p} + \frac{2\,\rho_{r_p}}{(N-2)(N-1)} \sum_{\substack{i=1 \\ i \neq n_o}}^{N-1} \sum_{\substack{i'=i+1 \\ i' \neq n_o}}^{N} \frac{(i'-n_o)^2\,\gamma_{r_{(p,i)}} - (i-n_o)^2\,\gamma_{r_{(p,i')}}}{(i-i')(i-n_o)(i'-n_o)} \tag{A.24}$$

and

$$\widetilde{\phi}_{r_p} = \phi_{r_p} + \frac{2\,\rho_{r_p}}{(N-2)(N-1)} \sum_{\substack{i=1 \\ i \neq n_o}}^{N-1} \sum_{\substack{i'=i+1 \\ i' \neq n_o}}^{N} \frac{(i'-n_o)\,\gamma_{r_{(p,i)}} - (i-n_o)\,\gamma_{r_{(p,i')}}}{(i-i')(i-n_o)(i'-n_o)}. \tag{A.25}$$

As above, $\widetilde{\theta}_{r_p}$ and $\widetilde{\rho}_{r_p}$ can be calculated by using (A.7) and (A.11) respectively.

A.1.6 Residue Vector Approximation

The residue can be approximated by the third order term of (1.12) as

$$\gamma_{r_{(p,n)}} \approx \frac{(n-n_o)^3\, d_r^3}{2\,\rho_{r_p}^3} \cos\left(\theta_{r_p}\right) \sin^2\left(\theta_{r_p}\right) \tag{A.26}$$

which can be used as

$$\begin{bmatrix} \widetilde{\omega}_{r_p} \\ \widetilde{\phi}_{r_p} \end{bmatrix} = \begin{bmatrix} \omega_{r_p} \\ \phi_{r_p} \end{bmatrix} + \rho_{r_p}\, \underline{\boldsymbol{N}}^{\dagger}\, \boldsymbol{\gamma}_{\boldsymbol{r}_p} \tag{A.27}$$

$$\approx \begin{bmatrix} \omega_{r_p} \\ \phi_{r_p} \end{bmatrix} + \underline{\boldsymbol{N}}^{\dagger} \begin{bmatrix} (1-n_o)^3 \\ (2-n_o)^3 \\ \vdots \\ 0 \\ \vdots \\ (N-n_o)^3 \end{bmatrix} \frac{d_r^3}{2\,\rho_{r_p}^2} \cos\left(\theta_{r_p}\right) \sin^2\left(\theta_{r_p}\right) \tag{A.28}$$

to obtain the biased range and DOA by using (A.11) and (A.7) respectively.

A.2 Numerical Example

In section A.1, we can see that different approaches lead to different biases in the location parameter. For a linear array, the range and DOA cover a 2D space. Thus, for easy visualization of the error distribution in the near field region, the Fresnel approximation error between the true and biased range and DOA is calculated in terms of Euclidean distance as

$$\begin{aligned} \widetilde{\xi}_{r_p} &= \sqrt{\left(\widetilde{\rho}_{r_p} \cos\left(\widetilde{\theta}_{r_p}\right) - \rho_{r_p} \cos\left(\theta_{r_p}\right)\right)^2 + \left(\widetilde{\rho}_{r_p} \sin\left(\widetilde{\theta}_{r_p}\right) - \rho_{r_p} \sin\left(\theta_{r_p}\right)\right)^2} \\ &= \sqrt{\widetilde{\rho}_{r_p}^2 + \rho_{r_p}^2 - 2\,\widetilde{\rho}_{r_p}\,\rho_{r_p} \cos\left(\widetilde{\theta}_{r_p} - \theta_{r_p}\right)}. \end{aligned} \tag{A.29}$$

Figure A.1, Figure A.2, Figure A.3, Figure A.4, Figure A.5, and Figure A.6 show the profile of this error $(\widetilde{\xi}_{r_p})$ for the biased location parameters extraction approaches briefed in section A.1.1, section A.1.2, section A.1.3, section A.1.4, section A.1.5, section A.1.6 respectively. The symmetric ULA used in this example is assumed to have $N = 9$ antennas and $d_r = \lambda/4$ inter element spacing. In the figures, the lower and upper limits of the Fresnel region are also drawn to show the near field region of the considered array.

From the error profiles of these methods, we can notice that the biases in the lo-

cation parameters due to the Fresnel approximation have significant variation with respect to DOA except for the method in section A.1.3. Additionally, as shown in Figure A.3, the error magnitude is also small and gradually decreases with the increase in range which is close to ideal behavior of a function inversely proportional to the range. Because of its closeness to the ideal error profile, we have used this method to construct LUT in section 3.2. And it has shown acceptable performance in the reduction of the biases in the location parameters due to the Fresnel approximation which can be backed up by the numerical examples in section 3.5. On analyzing Figure A.2 visually, we can say that the method in section A.1.2 can be accepted as the second choice to construct LUTs.

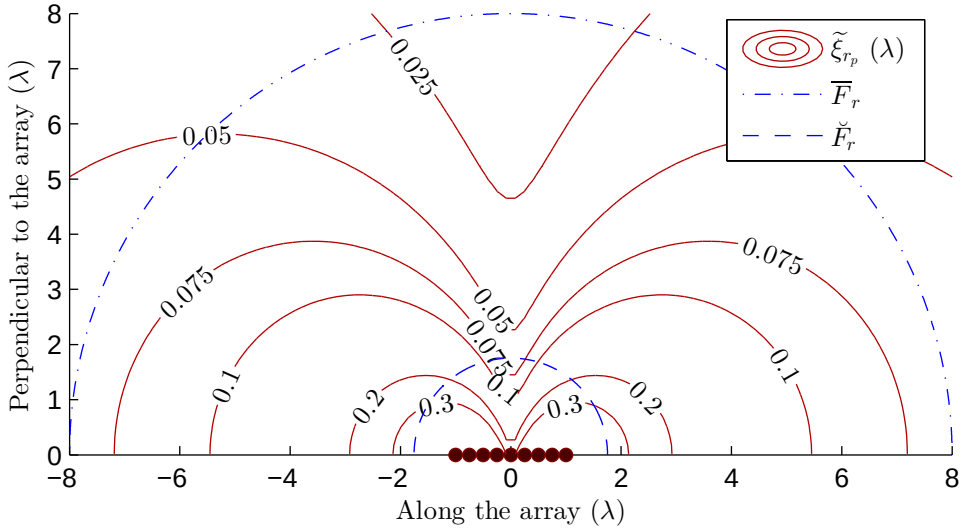

Figure A.1 – Approximation error ($\widetilde{\xi}_{r_p}$) profile of the extraction method in section A.1.1; $d_r = \lambda/4$, $N = 9$, and $n_o = 5$.

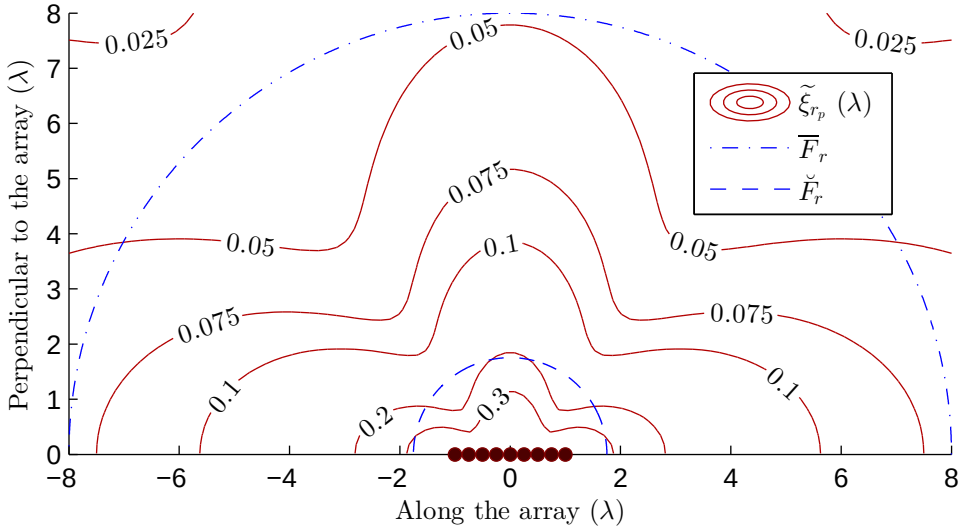

Figure A.2 – Approximation error ($\widetilde{\xi}_{r_p}$) profile of the extraction method in section A.1.2; $d_r = \lambda/4$, $N = 9$, and $n_o = 5$.

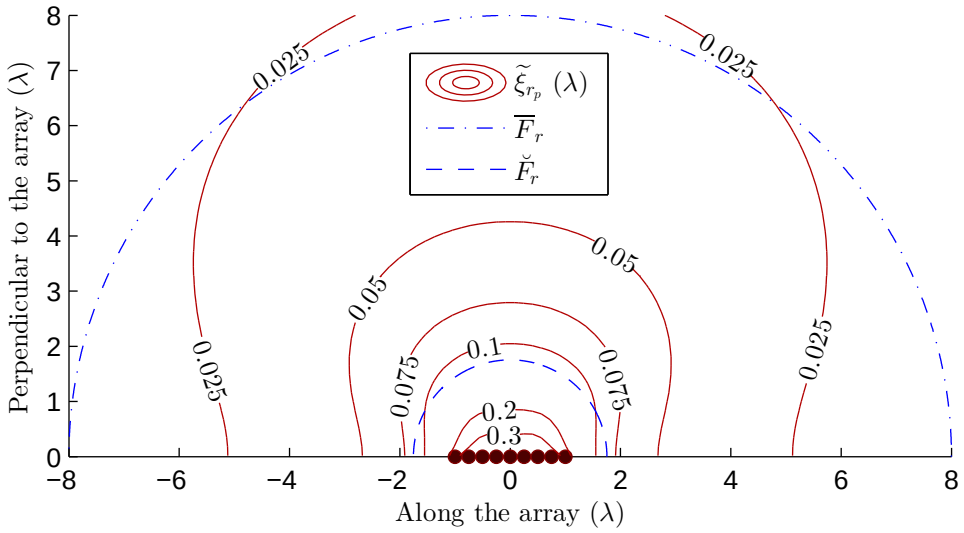

Figure A.3 – Approximation error ($\widetilde{\xi}_{r_p}$) profile of the extraction method in section A.1.3; $d_r = \lambda/4$, $N = 9$, and $n_o = 5$.

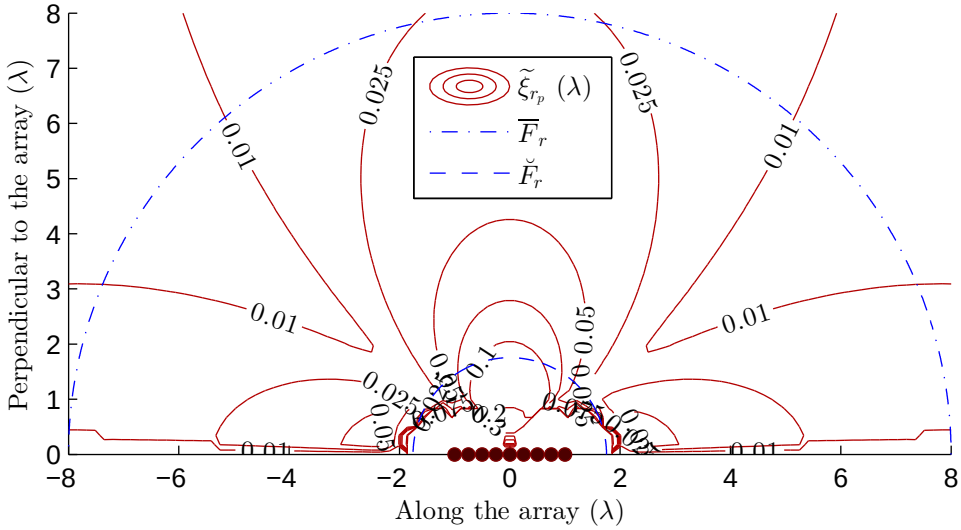

Figure A.4 – Approximation error ($\widetilde{\xi}_{r_p}$) profile of the extraction method in section A.1.4; $d_r = \lambda/4$, $N = 9$, and $n_o = 5$.

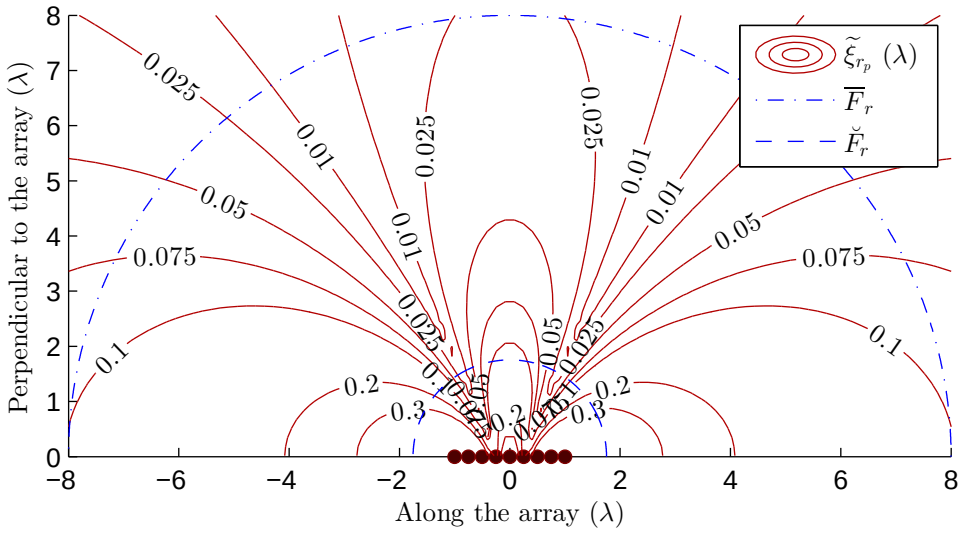

Figure A.5 – Approximation error ($\widetilde{\xi}_{r_p}$) profile of the extraction method in section A.1.5; $d_r = \lambda/4$, $N = 9$, and $n_o = 5$.

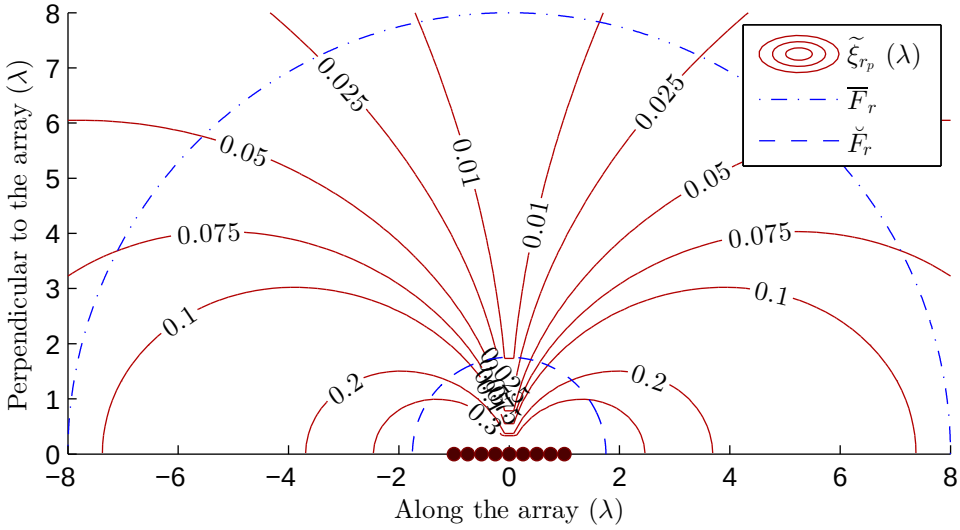

Figure A.6 – Approximation error ($\widetilde{\xi}_{r_p}$) profile of the extraction method in section A.1.6; $d_r = \lambda/4$, $N = 9$, and $n_o = 5$.

B

Correction Methods for Single Array

The two proposed correction methods in chapter 3 can be used for a single receiving array [105, 106]. In the following, we apply them to correct the biased location parameters estimated by the two existing approximated model based near field sources location methods in [2] and [3]. Consider a ULA with $N = 9$ receiving antennas and $d = \lambda/4$ inter element spacing. Since the methods in [2] and [3] require symmetric array, we take $n_o = 5$ which makes $\breve{N} = 4$. The received signals for the simulations are generated using the model based on spherical wavefront. The actual location parameters of the pth location is given by $(\rho_{r_p}, \theta_{r_p})$. As in Appendix A, $(\widetilde{\rho}_{r_p}, \widetilde{\theta}_{r_p})$ denotes the pair of biased location parameters estimated here by using [2] and [3]. And $(\hat{\rho}_{r_p}, \hat{\theta}_{r_p})$ denotes the corresponding pair of corrected location parameters. The estimation error $(\widetilde{\xi}_{r_p})$ between the actual and biased location parameters is calculated in terms of Euclidean distance using the expression in (A.29). By using the similar expression, we can calculate the estimation error $(\hat{\xi}_{r_p})$ between the actual and corrected location parameters as

$$\hat{\xi}_{r_p} = \sqrt{\hat{\rho}_{r_p}^2 + \rho_{r_p}^2 - 2\,\hat{\rho}_{r_p}\,\rho_{r_p}\,\cos\left(\hat{\theta}_{r_p} - \theta_{r_p}\right)}. \tag{B.1}$$

Figure B.1 and Figure B.2 show the contour plots of the Euclidean distances between the actual and biased locations estimated in noiseless situation by the methods in [2] and [3] respectively. The contours are generated by discretizing the near field region into a regular rectangular grid and then calculating $\widetilde{\xi}_{r_p}$ at each of these locations. Each location is handled separately, therefore the methods in [2] and [3] experience a single source situation. The upper and lower limits of the Fresnel region are also shown along with the contours to easily identify the near field region. $L = 10^3$ samples are

used to estimate the biased location parameters from both the methods to avoid the degradation in their performance due to the lack of samples, because both are based on subspace principle. The unit of the approximation error values shown on the contour lines is λ. These figures have similar meaning as the figures in section A.2. They also conclude that two different methods have different approximation error profiles.

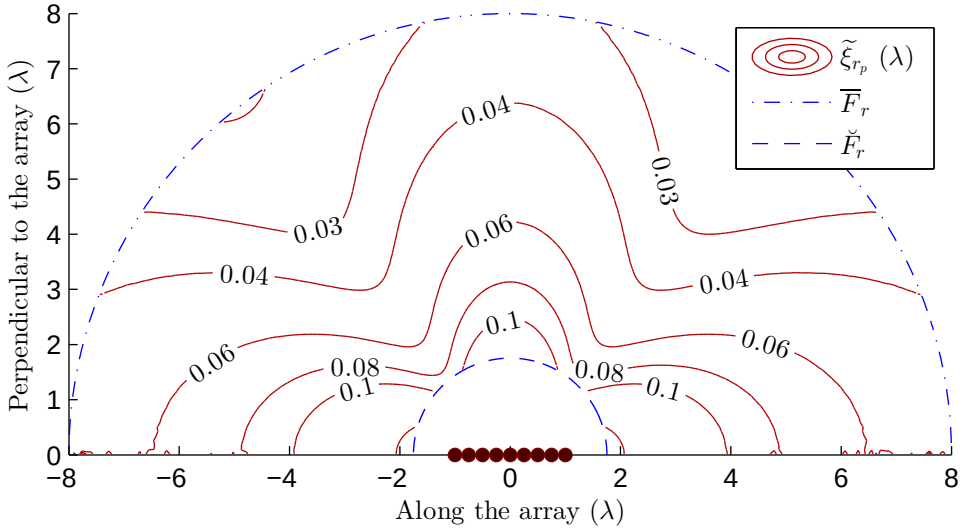

Figure B.1 – $\widetilde{\xi}_{r_p}$ of [2] in noiseless condition; $d = \lambda/4$, $L = 10^3$, and $\breve{N} = 4$.

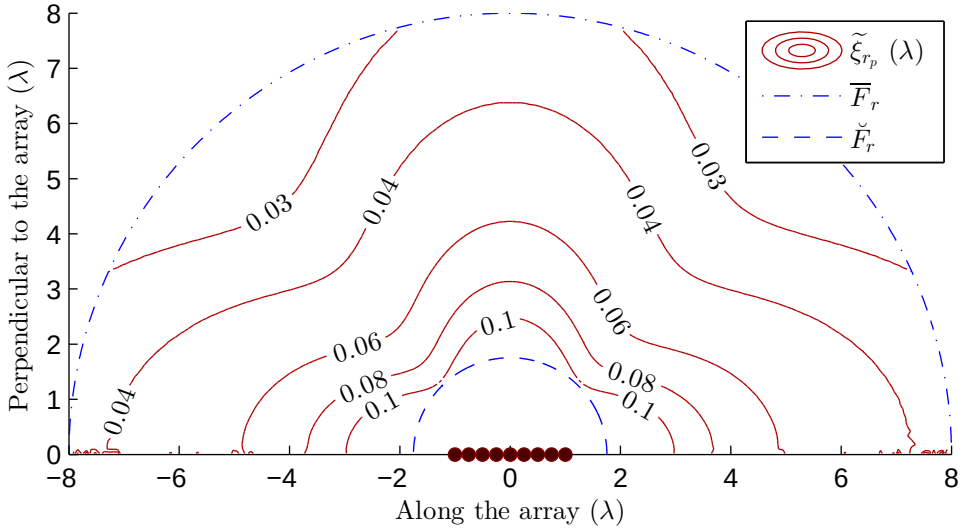

Figure B.2 – $\widetilde{\xi}_{r_p}$ of [3] in noiseless condition; $d = \lambda/4$, $L = 10^3$, and $\breve{N} = 4$.

Let $\xi_{r_p} = \widetilde{\xi}_{r_p}/\hat{\xi}_{r_p}$ be the ratio of the error in the location parameters at the pth location before correction to the error after correction. Figure B.3 and Figure B.4 respectively show this ratio for the near field region when the biased location parameters of

each location are estimated in noiseless condition by using the methods in [2] and [3] and corrected by our proposed method in section 3.2. The LUT is constructed by using 100 uniformly spaced discrete values of the ranges between $\breve{F}_r$ and $\overline{F}_r$; and 720 uniformly spaced discrete values of the DOA from 0.1° to 179.9°.

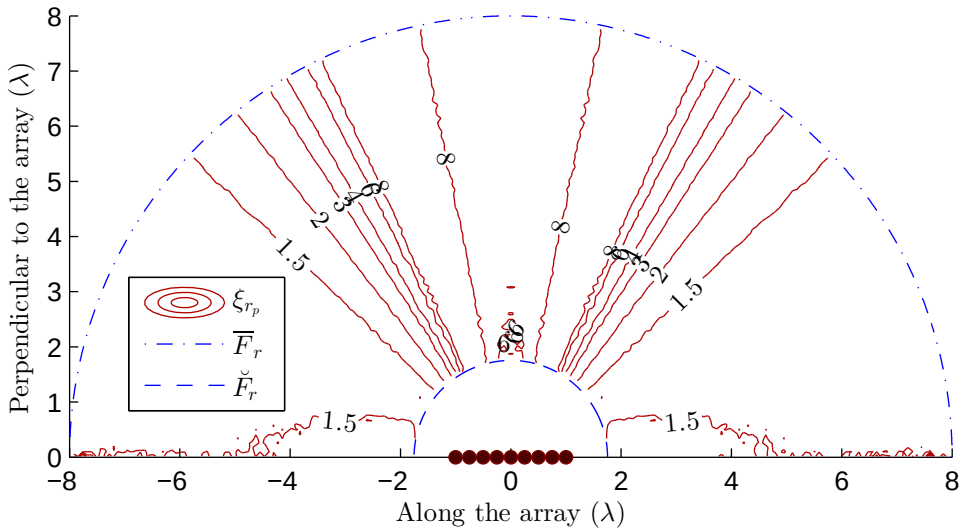

Figure B.3 – ξ_{r_p} of [2], corrected using section 3.2; $d = \lambda/4$, $L = 10^3$, and $\breve{N} = 4$.

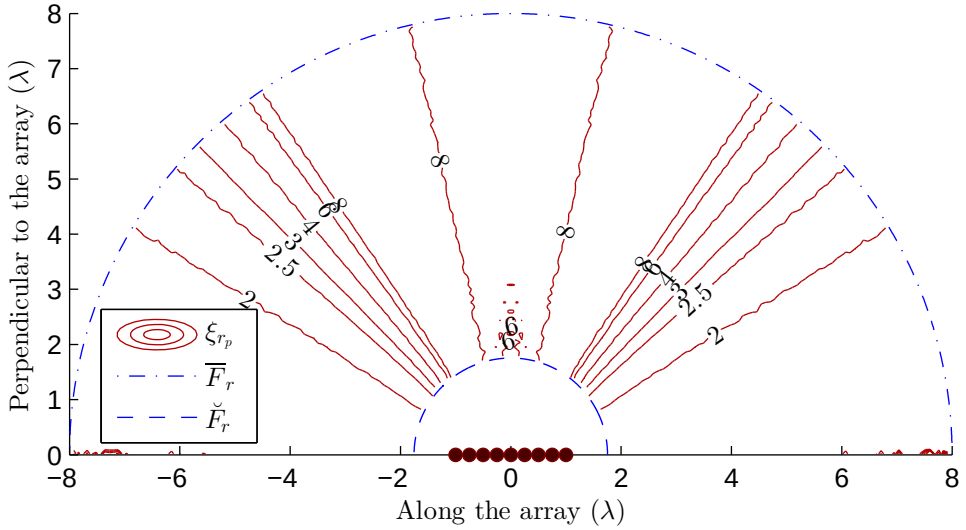

Figure B.4 – ξ_{r_p} of [3], corrected using section 3.2; $d = \lambda/4$, $L = 10^3$, and $\breve{N} = 4$.

Same as above, Figure B.5 and Figure B.6 respectively show the profile of ξ_{r_p} in the near field region when the biased location parameters of each location are estimated in noiseless condition by using the methods in [2] and [3] and corrected by our proposed method in section 3.3.

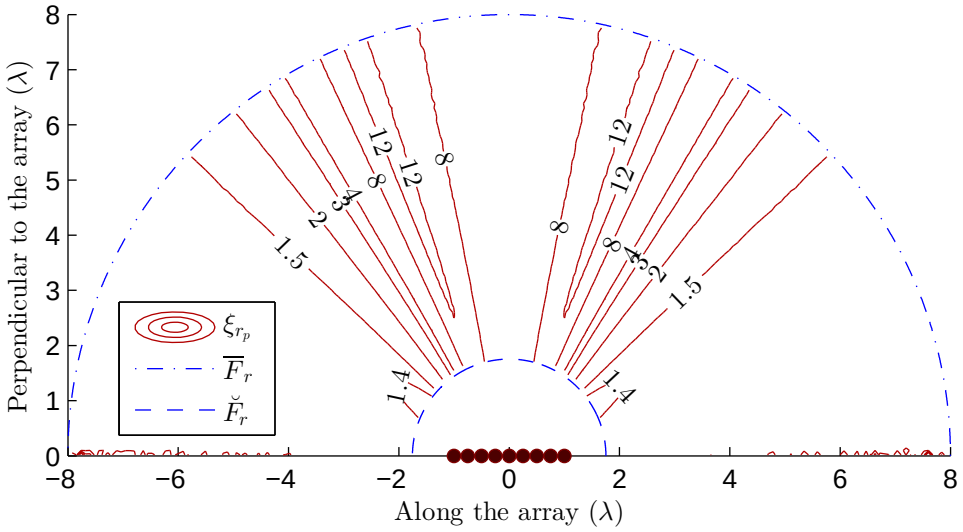

Figure B.5 – ξ_{r_p} of [2], corrected using section 3.3; $d = \lambda/4$, $L = 10^3$, and $\breve{N} = 4$.

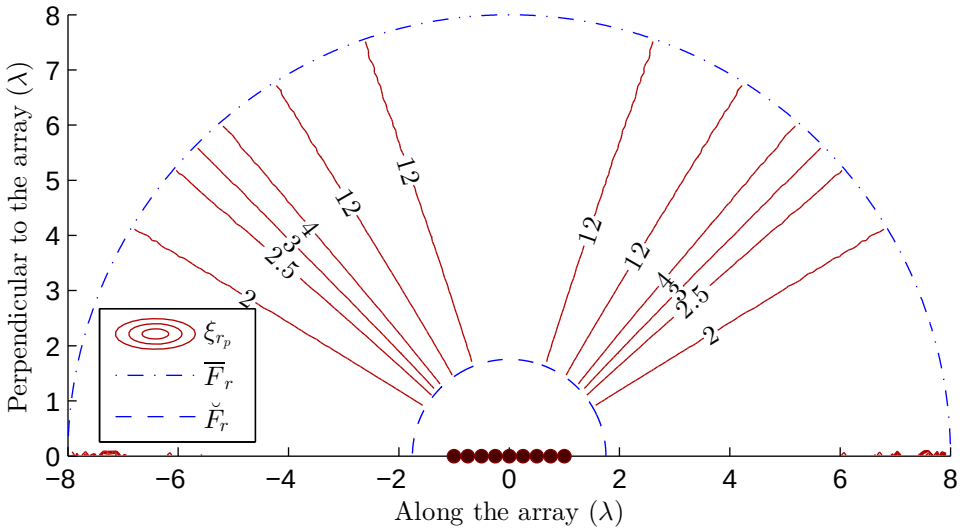

Figure B.6 – ξ_{r_p} of [3], corrected using section 3.3; $d = \lambda/4$, $L = 10^3$, and $\breve{N} = 4$.

In Figure B.3, Figure B.4 Figure B.5, and Figure B.6, the Fresnel region with $\xi_{r_p} > 1$ signifies that the proposed correction methods reduce the error due the approximated model. We can observe from these figures that the improvement of the proposed correction method varies inside the Fresnel region. The principal cause of this phenomenon is that the approximation error due to the higher order terms in (1.14) is a nonlinear function of range and DOA. In addition, the degree of the nonlinearity changes inside the Fresnel region. Large value of ξ_{r_p} implies better correction. From the patterns of contours in Figure B.3, Figure B.4 Figure B.5, and Figure B.6, we can observe that ξ_{r_p} does not have the same values in the same part of the near field region for the two methods. This illustrates that the correction methods have different performance for different methods.

Bibliography

[1] Erning Zhou, Hong Jiang, and Han Qi. 4-D parameter estimation in bistatic MIMO radar for near-field target localization. In *International Wireless Symposium (IWS)*, pages 1–4, Shenzhen, China, March 2015. IEEE. (Cited on pages 12, 15, 16, 31, 47, 51, 52, 53, 55, 57, 61, 62, 63, 64, 81, 83, and 95.)

[2] Wanjun Zhi and Michael Yan-Wah Chia. Near-field source localization via symmetric subarrays. *IEEE Signal Processing Letters*, 14(6):409–412, June 2007. (Cited on pages 12, 16, 26, 38, 39, 44, 45, 57, 58, 59, 60, 61, 62, 76, 105, 106, 107, and 108.)

[3] Jin He, MNS Swamy, and M Omair Ahmad. Efficient application of MUSIC algorithm under the coexistence of far-field and near-field sources. *IEEE Transactions on Signal Processing*, 60(4):2066–2070, April 2012. (Cited on pages 16, 26, 44, 45, 61, 76, 105, 106, 107, and 108.)

[4] Merrill Ivan Skolnik. *Introduction to Radar Systems*. Electrical engineering series. McGraw-Hill, 2001. (Cited on pages 24 and 36.)

[5] Merrill Ivan Skolnik. *Radar Handbook, Third Edition*. Electronics electrical engineering. McGraw-Hill Education, 2008. (Cited on pages 24 and 35.)

[6] David J. Daniels. *Ground Penetration Radar*. Radar. The institution of Electrical Engineers, 2004. (Cited on page 24.)

[7] Kai Luo. *MIMO RADAR: Target Localization*. PhD thesis, Imperial College, London, UK, March 2011. (Cited on page 24.)

[8] Jack Capon. High-resolution frequency-wavenumber spectrum analysis. *Proceedings of the IEEE*, 57(8):1408–1418, August 1969. (Cited on pages 25 and 28.)

[9] Harry L. Van Trees. *Optimum Array Processing: Part IV of Detection, Estimation, and Modulation theory*. John Wiley & Sons, 2004. (Cited on pages 25, 28, and 29.)

[10] V. F. Pisarenko. The retrieval of harmonics from a covariance function. *Geophysical Journal of the Royal Astronomical Society*, 33(3):347–366, 1973. (Cited on page 25.)

[11] Georges Bienvenu and Laurent Kopp. Optimality of high resolution array processing using the eigensystem approach. *IEEE Transactions on Acoustics, Speech and Signal Processing*, 31(5):1235–1248, 1983. (Cited on pages 25 and 28.)

[12] Ralph O Schmidt. Multiple emitter location and signal parameter estimation. *IEEE Transactions on Antennas and Propagation*, 34(3):276–280, March 1986. (Cited on pages 25 and 28.)

[13] A. Barabell. Improving the resolution performance of eigenstructure-based direction-finding algorithms. In *IEEE International Conference on Acoustics, Speech, and Signal Processing (ICASSP)*, volume 8, pages 336–339, April 1983. (Cited on pages 25 and 28.)

[14] Robert Roy, Arogyaswami Paulraj, and Thomas Kailath. ESPRIT–A subspace rotation approach to estimation of parameters of cisoids in noise. *IEEE Transactions on Acoustics, Speech and Signal Processing*, 34(5):1340–1342, 1986. (Cited on pages 25 and 28.)

[15] R Roy, A Paulraj, and T Kailath. Estimation of signal parameters via rotational invariance techniques-ESPRIT. In *30th Annual Technical Symposium*, pages 94–101. International Society for Optics and Photonics, 1986. (Cited on pages 25 and 28.)

[16] Richard Roy and Thomas Kailath. ESPRIT–Estimation of signal parameters via rotational invariance techniques. *IEEE Transactions on Acoustics, Speech and Signal Processing*, 37(7):984–995, 1989. (Cited on pages 25, 26, and 28.)

[17] Bhaskar D Rao and KVS Hari. Performance analysis of root-MUSIC. *IEEE Transactions on Acoustics, Speech and Signal Processing*, 37(12):1939–1949, 1989. (Cited on pages 26 and 28.)

[18] Sylvie Marcos, Alain Marsal, and Messaoud Benidir. The propagator method for source bearing estimation. *Signal processing*, 42(2):121–138, 1995. (Cited on pages 26 and 28.)

[19] Marius Pesavento, Alex B Gershman, and Kon Max Wong. Direction finding in partly calibrated sensor arrays composed of multiple subarrays. *IEEE Transactions on Signal Processing*, 50(9):2103–2115, September 2002. (Cited on pages 26 and 28.)

[20] S.S. Reddi. Multiple source location–A digital approach. *IEEE Transactions on Aerospace and Electronic Systems*, AES-15(1):95–105, January 1979. (Cited on pages 26 and 28.)

[21] Donald W Tufts and Ramdas Kumaresan. Estimation of frequencies of multiple sinusoids: Making linear prediction perform like maximum likelihood. *Proceedings of the IEEE*, 70(9):975–989, September 1982. (Cited on pages 26 and 28.)

[22] Ramdas Kumaresan and Donald W Tufts. Estimating the angles of arrival of multiple plane waves. *IEEE Transactions on Aerospace and Electronic Systems*, AES-19(1):134–139, January 1983. (Cited on pages 26 and 28.)

[23] A. L. Swindlehurst and T. Kailath. Passive direction-of-arrival and range estimation for near-field sources. In *Fourth Annual ASSP Workshop on Spectrum Estimation and Modeling*, pages 123–128, Minneapolis, Minnesota, August 1988. (Cited on pages 26, 31, 37, 39, 44, 45, and 61.)

[24] Emmanuèle Grosicki, Karim Abed-Meraim, and Yingbo Hua. A weighted linear prediction method for near-field source localization. *IEEE Transactions on Signal Processing*, 53(10):3651–3660, 2005. (Cited on pages 26, 39, 44, 45, 49, and 61.)

[25] Hongyang He, Yide Wang, and Joseph Saillard. A high resolution method of source localization in near-field by using focusing technique. In *European Signal Processing Conference*, pages 1–5, Lausanne, Switzerland, August 2008. IEEE. (Cited on pages 26 and 31.)

[26] Yi Duo Guo, Hui Xie, Yong Shun Zhang, Jian Gong, and Di Shen. Localization for near-field targets based on virtual array of MIMO radar. *Radar Science and Technology*, 10(1):82–87, February 2012. (Cited on pages 26 and 31.)

[27] Bo Wang, Yanping Zhao, and Juanjuan Liu. Mixed-order MUSIC algorithm for localization of far-field and near-field sources. *IEEE Signal Processing Letters*, 20(4):311–314, April 2013. (Cited on pages 26 and 31.)

[28] Jianzhong Li, Yide Wang, and Wei Gang. Signal reconstruction for near-field source localisation. *IET Signal Processing*, 9(3):201–205, 2015. (Cited on pages 26 and 31.)

[29] Gerard J Foschini. Layered space-time architecture for wireless communication in a fading environment when using multi-element antennas. *Bell labs technical journal*, 1(2):41–59, 1996. (Cited on page 27.)

[30] Daniel W Bliss, Keith W Forsythe, Alfred O Hero, and Ali F Yegulalp. Environmental issues for MIMO capacity. *IEEE Transactions on Signal Processing*, 50(9):2128–2142, September 2002. (Cited on page 27.)

[31] David Gesbert, Helmut Bolcskei, Dhananjay A Gore, and Arogyaswami J Paulraj. Outdoor MIMO wireless channels: Models and performance prediction. *IEEE Transactions on Communications*, 50(12):1926–1934, 2002. (Cited on page 27.)

[32] D.W. Bliss and K.W. Forsythe. Multiple-input multiple-output (MIMO) radar and imaging: Degrees of freedom and resolution. In *Conference Record of the Thirty-Seventh Asilomar Conference on Signals, Systems and Computers*, volume 1, pages 54–59. IEEE, November 2003. (Cited on pages 27 and 28.)

[33] Eran Fishler, Alex Haimovich, Rick Blum, Dmitry Chizhik, Len Cimini, and Reinaldo Valenzuela. MIMO radar: An idea whose time has come. In *Proceedings of the IEEE Radar Conference*, pages 71–78, April 2004. (Cited on page 27.)

[34] Alexander M. Haimovich, Rick S. Blum, and Leonard J. Cimini. MIMO radar with widely separated antennas. *Signal Processing Magazine, IEEE*, 25(1):116–129, 2008. (Cited on pages 27 and 36.)

[35] George Turin. An introduction to matched filters. *IRE transactions on Information theory*, 6(3):311–329, June 1960. (Cited on page 27.)

[36] Ilya Bekkerman and Joseph Tabrikian. Spatially coded signal model for active arrays. In *International Conference on Acoustics, Speech, and Signal Processing (ICASSP)*, volume 2, pages ii–209–12, Montreal, Que., Canada, May 2004. IEEE. (Cited on page 27.)

[37] Hugh Griffiths. Multistatic, MIMO and networked radar: the future of radar sensors? In *European Radar Conference (EuRAD)*, pages 81–84, Paris, France, September 2010. IEEE. (Cited on pages 27 and 28.)

[38] Jian Li and Petre Stoica. *MIMO radar signal processing*. John Wiley & Sons, Inc., Hoboken, New Jersey, 2009. (Cited on page 27.)

[39] MC Jackson. The geometry of bistatic radar systems. In *IEE Proceedings F (Communications, Radar and Signal Processing)*, volume 133, pages 604–612. IET, December 1986. (Cited on page 27.)

[40] Jian Li, Petre Stoica, Luzhou Xu, and William Roberts. On parameter identifiability of MIMO radar. *IEEE Signal Processing Letters*, 14(12):968–971, December 2007. (Cited on page 27.)

[41] Jian Li and Petre Stoica. MIMO radar with colocated antennas. *Signal Processing Magazine, IEEE*, 24(5):106–114, September 2007. (Cited on pages 27, 36, and 44.)

[42] Pier Francesco Sammartino. *A comparison of processing approaches for distributed radar sensing*. PhD thesis, University College London, 2009. (Cited on page 27.)

[43] Chen Chen and Xiaofei Zhang. A RD-ESPRIT algorithm for coherent DOA estimation in monostatic MIMO radar using a single pulse. *International Journal of Electronics*, 101(8):1074–1085, 2014. (Cited on page 28.)

[44] Ping Huanga, Hui Wang, and Cheng Yang. Non circular rootMUSIC algorithm for monostatic MIMO radar. *IEICE ELECTRONICS EXPRESS*, 11(13), 2014. (Cited on page 28.)

[45] Wei Wang, Xianpeng Wang, Hongru Song, and Yuehua Ma. Conjugate ESPRIT for DOA estimation in monostatic MIMO radar. *Signal Processing*, 93(7):2070–2075, 2013. (Cited on page 28.)

[46] X Zhang, Y Huang, C Chen, J Li, and D Xu. Reduced-complexity Capon for direction of arrival estimation in a monostatic multiple-input multiple-output radar. *IET Radar, Sonar & Navigation*, 6(8):796–801, 2012. (Cited on page 28.)

[47] Xiaofei Zhang and D Xu. Low-complexity ESPRIT-based DOA estimation for colocated MIMO radar using reduced-dimension transformation. *Electronics Letters*, 47(4):283–284, 2011. (Cited on page 28.)

[48] Rong Xie, Zheng Liu, and Zi-jing Zhang. DOA estimation for monostatic MIMO radar using polynomial rooting. *Signal processing*, 90(12):3284–3288, 2010. (Cited on page 28.)

[49] Rémy Boyer. Performance bounds and angular resolution limit for the moving colocated MIMO radar. *IEEE Transactions on Signal Processing*, 59(4):1539–1552, April 2011. (Cited on page 28.)

[50] Honglei Miao, Markku Juntti, and Kegen Yu. 2-D unitary ESPRIT based joint AOA and AOD estimation for MIMO system. In *IEEE 17th International Symposium on Personal, Indoor and Mobile Radio Communications*, pages 1–5. IEEE, 2006. (Cited on page 29.)

[51] Chen Duofang, Chen Baixiao, and Qin Guodong. Angle estimation using ESPRIT in MIMO radar. *Electronics Letters*, 44(12):770–771, 2008. (Cited on page 29.)

[52] Chen Jinli, Gu Hong, and Su Weimin. Angle estimation using ESPRIT without pairing in MIMO radar. *Electronics Letters*, 44(24):1422–1423, 2008. (Cited on page 29.)

[53] Ming Jin, Guisheng Liao, and Jun Li. Joint DOD and DOA estimation for bistatic MIMO radar. *Signal Processing*, 89(2):244–251, 2009. (Cited on page 29.)

[54] Jinli Chen, Hong Gu, and Weimin Su. A new method for joint DOD and DOA estimation in bistatic MIMO radar. *Signal Processing*, 90(2):714–718, 2010. (Cited on page 29.)

[55] Xiaofei Zhang, Lingyun Xu, Lei Xu, and Dazhuan Xu. Direction of departure (DOD) and direction of arrival (DOA) estimation in MIMO radar with reduced-dimension MUSIC. *Communications Letters, IEEE*, 14(12):1161–1163, 2010. (Cited on page 29.)

[56] Mohamed Laid Bencheikh, Yide Wang, and Hongyang He. Polynomial root finding technique for joint DOA DOD estimation in bistatic MIMO radar. *Signal Processing*, 90(9):2723–2730, 2010. (Cited on page 29.)

[57] Mohamed Laid Bencheikh and Yide Wang. Joint DOD-DOA estimation using combined ESPRIT-MUSIC approach in MIMO radar. *Electronics Letters*, 46(15):1081–1083, 2010. (Cited on page 29.)

[58] Mohamed Laid Bencheikh and Yide Wang. Combined ESPRIT-rootMUSIC for DOA-DOD estimation in polarimetric bistatic MIMO radar. *Progress In Electromagnetics Research Letters*, 22:109–117, 2011. (Cited on page 29.)

[59] Mohamed Laïd Bencheikh. *Exploitation des propriétiés des signaux dans les systèmes RADAR MIMO pour la détection et la localisation*. PhD thesis, Ecole polytechnique de l'université de Nantes, Nantes, France, Julliet 2011. (Cited on pages 29 and 59.)

[60] Raymond B Cattell. "Parallel proportional profiles" and other principles for determining the choice of factors by rotation. *Psychometrika*, 9(4):267–283, 1944. (Cited on page 29.)

[61] John B Carroll. An analytical solution for approximating simple structure in factor analysis. *Psychometrika*, 18(1):23–38, 1953. (Cited on page 29.)

[62] Henry F Kaiser. The varimax criterion for analytic rotation in factor analysis. *Psychometrika*, 23(3):187–200, 1958. (Cited on page 29.)

[63] Ledyard R Tucker. Some mathematical notes on three-mode factor analysis. *Psychometrika*, 31(3):279–311, 1966. (Cited on page 29.)

[64] George M Bergman. Ranks of tensors and change of base field. *Journal of Algebra*, 11(4):613–621, 1969. (Cited on page 29.)

[65] Richard A Harshman. Foundations of the PARAFAC procedure: models and conditions for an "explanatory" multimodal factor analysis. In *Working Papers in Phonetics (WPP)*, 16, pages 1–84. Department of Linguistics, University of California at Los Angeles (UCLA), December 1970. (Cited on pages 29, 30, 85, and 86.)

[66] J Douglas Carroll and Jih-Jie Chang. Analysis of individual differences in multidimensional scaling via an N-way generalization of "Eckart-Young" decomposition. *Psychometrika*, 35(3):283–319, 1970. (Cited on pages 29, 85, and 86.)

[67] Richard A Harshman. PARAFAC2: Mathematical and technical notes. *UCLA working papers in phonetics*, 22:30–44, 1972. (Cited on page 29.)

[68] Joseph B Kruskal. More factors than subjects, tests and treatments: an indeterminacy theorem for canonical decomposition and individual differences scaling. *Psychometrika*, 41(3):281–293, 1976. (Cited on page 30.)

[69] Joseph B Kruskal. Three-way arrays: rank and uniqueness of trilinear decompositions, with application to arithmetic complexity and statistics. *Linear algebra and its applications*, 18(2):95–138, 1977. (Cited on pages 30 and 86.)

[70] Joseph B Kruskal. Rank, decomposition, and uniqueness for 3-way and N-way arrays. *Multiway data analysis*, 33:7–18, 1989. (Cited on pages 30 and 86.)

[71] Richard A Harshman and Margaret E Lundy. PARAFAC: Parallel factor analysis. *Computational Statistics & Data Analysis*, 18(1):39–72, 1994. (Cited on page 30.)

[72] Rasmus Bro. PARAFAC. tutorial and applications. *Chemometrics and intelligent laboratory systems*, 38(2):149–171, 1997. (Cited on page 30.)

[73] Rasmus Bro. *Multi-way analysis in the food industry: models, algorithms, and applications*. PhD thesis, Universiteit van Amsterdam, Amsterdam, Netherlands, 1998. (Cited on page 30.)

[74] Henk AL Kiers, Jos MF Ten Berge, and Rasmus Bro. PARAFAC2-Part I. A direct fitting algorithm for the PARAFAC2 model. *Journal of Chemometrics*, 13(3-4):275–294, 1999. (Cited on page 30.)

[75] Rasmus Bro, Claus A Andersson, and Henk AL Kiers. PARAFAC2-Part II. Modeling chromatographic data with retention time shifts. *Journal of Chemometrics*, 13(3-4):295–309, 1999. (Cited on page 30.)

[76] R Bro, ND Sidiropoulos, and GB Giannakis. Optimal joint azimuth-elevation and signal-array response estimation using parallel factor analysis. In *Conference Record of the Thirty-Second Asilomar Conference on Signals, Systems & Computers*, volume 2, pages 1594–1598. IEEE, 1998. (Cited on page 30.)

[77] Nicholas D Sidiropoulos, Rasmus Bro, and Georgios B Giannakis. Parallel factor analysis in sensor array processing. *IEEE Transactions on Signal Processing*, 48(8):2377–2388, 2000. (Cited on page 30.)

[78] R Bro, N D Sidiropoulos, and G B Giannakis. A fast least squares algorithm for separating trilinear mixtures. In *International Workshop on Independent Component Analysis and Blind Separation*, pages 11–15, 1999. (Cited on pages 30 and 86.)

[79] Claus A Andersson and Rasmus Bro. The N-way toolbox for MATLAB. *Chemometrics and Intelligent Laboratory Systems*, 52(1):1–4, 2000. (Cited on page 30.)

[80] Henk AL Kiers. Towards a standardized notation and terminology in multiway analysis. *Journal of chemometrics*, 14(3):105–122, 2000. (Cited on page 30.)

[81] Nicholas D Sidiropoulos and Rasmus Bro. On the uniqueness of multilinear decomposition of N-way arrays. *Journal of chemometrics*, 14(3):229–239, 2000. (Cited on pages 30 and 86.)

[82] Tamara G Kolda and Brett W Bader. Tensor decompositions and applications. *SIAM review*, 51(3):455–500, 2009. (Cited on page 30.)

[83] Pierre Comon. Tensor decompositions, state of the art and applications. *arXiv preprint arXiv: 0905.0454*, 2009. (Cited on page 30.)

[84] Gilbert Strang. *Introduction to Linear Algebra*. Wellesley-Cambridge Press, 2003. (Cited on page 30.)

[85] Gilbert Strang. *Linear algebra and its applications*. Belmont, CA: Thomson, Brooks/Cole, 2006. (Cited on page 30.)

[86] Nicolaas Klaas M Faber, Rasmus Bro, and Philip K Hopke. Recent developments in CANDECOMP/PARAFAC algorithms: a critical review. *Chemometrics and Intelligent Laboratory Systems*, 65(1):119–137, 2003. (Cited on page 30.)

[87] Claus A Andersson and Rasmus Bro. Improving the speed of multi-way algorithms: Part I. Tucker3. *Chemometrics and intelligent laboratory systems*, 42(1):93–103, 1998. (Cited on page 30.)

[88] Rasmus Bro and Claus A Andersson. Improving the speed of multiway algorithms: Part II. Compression. *Chemometrics and Intelligent Laboratory Systems*, 42(1):105–113, 1998. (Cited on page 30.)

[89] CN Ho, GD Christian, and ER Davidson. Application of the method of rank annihilation to fluorescent multicomponent mixtures of polynuclear aromatic hydrocarbons. *Analytical Chemistry*, 52(7):1071–1079, 1980. (Cited on page 30.)

[90] Avraham Lorber. Quantifying chemical composition from two-dimensional data arrays. *Analytica chimica acta*, 164:293–297, 1984. (Cited on page 30.)

[91] Eugenio Sanchez and Bruce R Kowalski. Generalized rank annihilation factor analysis. *Analytical Chemistry*, 58(2):496–499, 1986. (Cited on page 30.)

[92] Eugenio Sanchez and Bruce R Kowalski. Tensorial resolution: a direct trilinear decomposition. *Journal of Chemometrics*, 4(1):29–45, 1990. (Cited on page 30.)

[93] Myriam Rajih, Pierre Comon, and Richard A Harshman. Enhanced line search: A novel method to accelerate PARAFAC. *SIAM Journal on Matrix Analysis and Applications*, 30(3):1128–1147, 2008. (Cited on page 30.)

[94] Dimitri Nion and Lieven De Lathauwer. An enhanced line search scheme for complex-valued tensor decompositions. Application in DS-CDMA. *Signal Processing*, 88(3):749–755, 2008. (Cited on page 30.)

[95] Anh-Huy Phan, Petr Tichavsky, and Andrzej Cichocki. Fast alternating LS algorithms for high order CANDECOMP/PARAFAC tensor factorizations. *IEEE Transactions on Signal Processing*, 61(19):4834–4846, 2013. (Cited on page 30.)

[96] Dimitri Nion and Nicholas D Sidiropoulos. A PARAFAC-based technique for detection and localization of multiple targets in a MIMO radar system. In *IEEE International Conference on Acoustics, Speech and Signal Processing (ICASSP)*, pages 2077–2080, Taipei, Taiwan, April 2009. (Cited on pages 31, 85, and 86.)

[97] Dimitri Nion and Nicholas D Sidiropoulos. Tensor algebra and multidimensional harmonic retrieval in signal processing for MIMO radar. *IEEE Transactions on Signal Processing*, 58(11):5693–5705, November 2010. (Cited on pages 31 and 44.)

[98] Jian-Yun Zhang, Zhi-Dong Zheng, and Xiao-Bo Li. An algorithm for DOD-DOA and Doppler frequency jointly estimating of bistatic MIMO radar. *Dianzi Yu Xinxi Xuebao(Journal of Electronics and Information Technology)*, 32(8):1843–1848, 2010. (Cited on page 31.)

[99] Nan Wang, Wenguang Wang, Fan Zhang, and Yunneng Yuan. The PARAFAC-MUSIC algorithm for DOA estimation with Doppler frequency in a MIMO radar system. *International Journal of Antennas and Propagation*, 2014, 2014. (Cited on page 31.)

[100] Renzheng Cao, Xiaofei Zhang, and Chenghua Wang. Reduced-dimensional PARAFAC-based algorithm for joint angle and Doppler frequency estimation in monostatic MIMO radar. *Wireless Personal Communications*, pages 1–19, 2014. (Cited on page 31.)

[101] Sebastian Miron, Song Yang, David Brie, and Kainam Wong. A multilinear approach of direction finding using a sensor-array with multiple scales of spatial invariance. *IEEE Transactions on Aerospace and Electronic Systems*, page 00, 2015. (Cited on page 31.)

[102] Youcef Begriche, Messaoud Thameri, and Karim Abed-Meraim. Exact conditional and unconditional Cramér–Rao bounds for near field localization. *Digital Signal Processing*, 31:45–58, 2014. (Cited on pages 31 and 38.)

[103] Parth Raj Singh, Yide Wang, and Pascal Chargé. Bistatic MIMO radar for near field source localisation using PARAFAC. *Electronics Letters*, 52(12):1060–1061, April 2016. (Cited on page 34.)

[104] Parth Raj Singh, Yide Wang, and Pascal Chargé. An exact model-based method for near-field sources localization with bistatic MIMO system. *Sensors*, 17(4):723, 2017. (Cited on page 34.)

[105] Parth Raj Singh, Yide Wang, and Pascal Chargé. A correction method for the near field approximated model based localization techniques. *Digital Signal Processing*, 67:76–80, 2017. (Cited on pages 34 and 105.)

[106] Parth Raj Singh, Yide Wang, and Pascal Chargé. Performance enhancement of approximated model based near field sources localisation techniques. *IET Signal Processing*, 11(7):825–829, 2017. (Cited on pages 34 and 105.)

[107] Parth Raj Singh, Yide Wang, and Pascal Chargé. Near field targets localization using bistatic MIMO system with symmetric arrays. In *25th European Signal Processing Conference (EUSIPCO)*, pages 2467–2471, Kos island, Greece, August 2017. EURASIP. (Cited on page 34.)

[108] Parth Raj Singh, Yide Wang, and Pascal Chargé. Near field targets localization using bistatic MIMO system with spherical wavefront based model. In *25th European Signal Processing Conference (EUSIPCO)*, pages 2472–2476, Kos island, Greece, August 2017. EURASIP. (Cited on page 34.)

[109] Peter Swerling. Probability of detection for fluctuating targets. *IRE Transactions on Information Theory*, 6(2):269–308, April 1960. (Cited on page 36.)

[110] Eran Fishler, Alexander M. Haimovich, Rick S. Blum, Leonard J. Cimini, Dmitry Chizhik, and Reinaldo A. Valenzuela. Spatial diversity in radars-models and detection performance. *IEEE Transactions on Signal Processing*, 54(3):823–838, March 2006. (Cited on page 36.)

[111] Peter Swerling. Radar probability of detection for some additional fluctuating target cases. *IEEE Transactions on Aerospace and Electronic Systems*, 33(2):698–709, April 1997. (Cited on page 36.)

[112] Haidong Yan, Jun Li, and Guisheng Liao. Multitarget identification and localization using bistatic MIMO radar systems. *EURASIP Journal on Advances in Signal Processing*, 2008(1):1–8, 2007. (Cited on pages 36 and 85.)

[113] Steven M Kay. *Fundamentals of Statistical Signal Processing: Estimation Theory*, chapter 3. Cramer-Rao Lower Bound, 15. Extensions for Complex Data and Parameters, pages 47, 565. PTR Prentice-Hall, Englewood Cliffs, New Jersey, 1993. (Cited on page 49.)

[114] Petre Stoica, E. G. Larsson, and A. B. Gershman. The stochastic CRB for array processing: A textbook derivation. *Signal Processing Letters, IEEE*, 8(5):148–150, May 2001. (Cited on page 49.)

[115] José Tribolet. A new phase unwrapping algorithm. *IEEE Transactions on Acoustics Speech and Signal Processing*, 25(2):170–177, April 1977. (Cited on pages 54, 83, and 87.)

[116] Feifei Gao and Alex B Gershman. A generalized ESPRIT approach to direction-of-arrival estimation. *IEEE Signal Processing Letters*, 12(3):254–257, March 2005. (Cited on page 59.)

[117] Donald Shepard. A two-dimensional interpolation function for irregularly-spaced data. In *23rd ACM national conference*, pages 517–524, New York, USA, August 1968. ACM. (Cited on page 68.)

[118] Gene H Golub and Charles Van Loan. Total least squares. In *Smoothing Techniques for Curve Estimation*, pages 69–76. Springer, 1979. (Cited on page 73.)

[119] Yariv Ephraim and Harry L. Van Trees. A signal subspace approach for speech enhancement. *IEEE Transactions on Speech and Audio Processing*, 3(4):251–266, July 1995. (Cited on page 82.)

[120] Andrzej Cichocki, Danilo P. Mandic, Anh Huy Phan, Cesar F. Caiafa, Guoxu Zhou, Qibin Zhao, and Lieven De Lathauwer. Tensor decompositions for signal processing applications: From two-way to multiway component analysis. *IEEE Signal Processing Magazine*, 32(2):145–163, 2015. (Cited on page 85.)

UNIVERSITE BRETAGNE LOIRE

UNIVERSITÉ DE NANTES

Thèse de Doctorat

Parth Raj SINGH

Localisation de Source par les Systèmes MIMO

Source Localization with MIMO Systems

Résumé

Dans cette thèse, nous considérons la dernière génération du radar. Il s'agit d'un radar MIMO bistatique qui est composé de plusieurs antennes d'émission et de réception. Pour ce système, les antennes émettrices transmettent des signaux linéairement indépendants afin qu'ils puissent être identifiés à l'aide d'un banc de filtres adaptés au niveau des antennes de réception. Les signaux filtrés sont alors traités pour extraire les paramètres des cibles, tels que les DOA, DOD, vitesse, etc. Un radar MIMO bistatique offre une grande diversité spatiale et une excellente identifiabilité des paramètres, etc., ce qui nous a incités à l'utiliser dans ce travail. La situation en champ lointain d'un radar MIMO bistatique est largement traitée dans la littérature. Mais, peu de travaux existe sur la situation en champ proche, c'est ce qui a motivé le travail de cette thèse. La localisation de cibles en champ proche est importante en raison de nombreuses applications à l'intérieur des constructions. A ce sujet, la plupart des méthodes actuelles utilisent l'approximation de Fresnel dans laquelle le front d'onde sphérique des signaux reçus est supposé quadrique plutôt que planaire comme en champ lointain. Dans ce travail de thèse, nous avons proposé une nouvelle méthode de localisation des cibles en champ proche qui utilise l'approximation de Fresnel. Celle-ci conduit à une estimation biaisée des paramètres de localisation car en réalité le front d'onde est sphérique. Nous avons proposé alors deux méthodes de correction pour réduire les effets de l'approximation de Fresnel et deux autres méthodes qui utilisent directement le modèle exacte basé sur le front d'onde sphérique.

Mots clés

Système MIMO bistatique, ULA, champ proche, approximation de Fresnel, distance, DOA, DOD.

Abstract

Sources localization is used in radar, sonar, and telecommunication. Radar has numerous civilian and military applications. Radar system has gone through many developments over the last few decades and reached the latest version known as MIMO radar. A MIMO radar is composed of multiple transmitting and receiving antennas like a conventional phased array radar. However, its transmitting antennas transmit linearly independent signals so that they can be easily identified by the matched filters bank at its receiving end. The matched filtered signals are then processed to extract the ranges, DOAs, DODs, velocities, etc. of the targets. A bistatic MIMO radar system provides high resolution, spatial diversity, parameter identifiability, etc. which inspired us to use it in this work. There are many existing methods to deal with the far field region of MIMO radar system. However, little work can be found on the near field region of a bistatic MIMO radar which motivated the work in this thesis. Near field targets localization is also important because of many indoor applications. Most of the existing near field sources localization techniques use Fresnel approximation in which the real spherical wavefront is assumed quadric unlike planar in far field situation. In this work we have proposed a novel near field targets localization method using Fresnel approximation. The Fresnel approximation leads to a biased estimation of the location parameters because the true wavefront is spherical. Consequently, we have proposed two correction methods to reduce the effects of Fresnel approximation and other two methods which directly use the exact signal model based on spherical wavefront.

Key Words

Bistatic MIMO system, ULA, near field, Fresnel approximation, range, DOA, DOD.